UNIVERSITÀ DEGLI STUDI DI PADOVA

Dipartimento di Agronomia Animali Alimenti Risorse Naturali e Ambiente

Dipartimento di Geoscienze

Corso di laurea magistrale in Scienze e Tecnologie per l'Ambiente e il Territorio

High performance stabilisation/solidification (HPSS) system to stabilise Pb-contaminated soils and municipal solid waste incinerator (MSWI) fly ash using alternative binder formulations

Relatore: Prof. Gilberto Artioli

Correlatori: Prof. Maria Chiara Dalconi

Dott. ssa Silvia Contessi

Laureando: Cristian Bano

Matricola n. 1179985

ANNO ACCADEMICO 2018/2019

ABSTRACT

In this thesis an innovative Solidification/Stabilisation (S/S) method was applied to treat two different contaminated matrixes, that is, a lead-contaminated soil and a Municipal Solid Waste Incinerator Fly Ash (MSWIFA). The soil was stabilised using a Calcium Aluminate Cement (CAC) cured at two different temperatures, 20 °C and 40 °C respectively, to assess the effects that the conversion reaction, transforming hexagonal hydrates towards cubic hydrates in the CAC cements, might have on the system. XRPD analyses were conducted to ascertain the mineralogical phases being formed during curing time, and SEM-EDX analysis was performed to investigate the internal microstructure. Mechanical strength tests were also carried out to assess whether the conversion reaction had a detrimental effect upon the mechanical properties of the considered specimens. Leaching tests at three different pH values were conducted to verify the effectiveness of CAC in binding the heavy metals in the soil. Conversion reaction occurred just in the sample containing only CAC, whereas in the contaminated soil the presence of gypsum promoted the formation of ettringite. Presence of calcite in the soil prevented the conversion reaction to occur. The stabilised soil developed good mechanical properties (25- 31 MPa). Both SEM-EDX and SEM-WDS analyses ascertained that ettringite bound lead, probably during the early stages of hydration of the cement. Leaching test outcomes showed good retention capacities of the stabilised soil at high pH values (pH > 11.4), highlighting the key role of pH in regulating the leaching behaviour.

Mineralogical characterization of untreated MSWIFA was ascertained via XRPD analyses. The material was characterized by presenting heavy metals and chloride salts at remarkable concentrations. XRPD analyses revealed that MSWIFA were prone to hydrate under ambient conditions and the formation of new phases was observed. The stabilisation of the MSWIFA was attempted using three different binders, that is, Ordinary Portland Cement (OPC), CAC and ground granulated blast furnace slag (GGBS). The results showed that the presence of MSWIFA in OPC and CAC had detrimental effect on both setting and hardening processes, probably due to the presence of both heavy metals and chlorides in the ashes working as retarders in both systems. The results showed that MSWIFA had some cementitious activities, but the reaction rate was low. Formations of thaumasite in the first case, and probably carbonation reaction in the second one were observed. The sample stabilised using GGBS developed a well hardened structure and XRPD analyses revealed that this might be due to the formation of both ettringite and Friedel's salt in the system. MSWIFA reacts thus differently depending on the binder being used.

SOMMARIO

La tesi riporta lo studio di un innovativo sistema di solidificazione/stabilizzazione (S/S) applicato a due diverse matrici, rispettivamente, un suolo contaminato da piombo, e ceneri leggere da termovalorizzatore di rifiuti solidi.

Per ciò che concerne il suolo, esso è stato stabilizzato utilizzando un cemento alluminoso (CAC 70) lasciato reagire a 20 °C e 40 °C per valutare quale fosse l'effetto della reazione di conversione che trasforma gli idrati esagonali a idrati cubici, nelle prestazioni finali del sistema. Analisi in diffrazione sono state eseguite al fine di verificare l'evoluzione delle varie fasi mineralogiche nel sistema, mentre analisi al SEM-EDX sono state effettuate per investigare la microstruttura interna. Test di resistenza meccanica sono stati eseguiti per determinare se la reazione di conversione determinasse un peggioramento delle proprietà meccaniche del suolo stabilizzato e per verificare le resistenze meccaniche dei vari sistemi considerati. Test di cessione sono stati effettuati esponendo il suolo stabilizzato a 3 diversi pH (4.5, 5.5 e 7) per analizzare l'efficacia del cemento CAC aveva nel trattenere i metalli presenti nel sistema. La reazione di conversione è stata osservata solo nel sistema contenente CAC, in quanto nel suolo contaminato, sia la presenza di gesso, che quella di calcite hanno prevenuto la reazione, spostando il sistema verso la formazione di ettringite. Analisi condotte al SEM-EDX e SEM-WDS hanno verificato la presenza di piombo associato ad ettringite. I test di cessione dimostrano che il suolo stabilizzato con CAC ha buone capacità di ritenzione a pH basici (pH> 11.4) verso elementi caratterizzati dall'avere un comportamento anfotero. Diminuendo il pH, la capacità di ritenzione del sistema diminuisce con un aumento delle concentrazioni di metalli ceduti. Questo è probabilmente dato dalla destabilizzazione dell'ettringite a pH acidi.

Le ceneri leggere da termovalorizzatore non trattate sono state analizzate al fine di determinare la loro composizione mineralogica di partenza. In generale, il materiale è caratterizzato dalla presenza di metalli pesanti e cloruri ad alte concentrazioni. Le ceneri idratano facilmente quando esposte a condizioni ambientali con formazione di nuove fasi idrate. La stabilizzazione con tre diversi leganti è stata studiata. Questi erano: cemento portland (OPC), CAC 70 e loppe d'altoforno. I risultati dimostrano anche che le ceneri hanno un basso potere cementizio nonché una cinetica di reazione lenta. Riguardo ai primi due leganti, è stato osservato un effetto negativo sulla loro presa e indurimento, probabilmente dovuto alla presenza di elementi considerati ritardanti per i due sistemi. Nel sistema portland

è stata osservata la formazione di thaumasite, mentre il sistema CAC probabilmente è stato interessato da un fenomeno di carbonatazione. L'uso di loppe invece ha dato risultati positivi in quanto il campione ha fatto presa ed ha indurito probabilmente grazie alla formazione di sale di Friedel ed ettringite.

TABLE OF CONTENTS

ABSTRACT I

SOMMARIO II

LIST OF FIGURES VII

LIST OF TABLES X

ABBREVIATIONS XI

ACKNOWLEDGEMENTS XII

1. INTRODUCTION 1

1.1 HEAVY METALS CONTAMINATION 1

1.1.1 HEAVY METALS SOURCES IN SOIL AND TOXICITY 2

1.1.2 CHEMISTRY OF HEAVY METALS IN SOILS 4

1.1.3 CONTAMINATED SITES AND ITALIAN LEGISLATION FRAMEWORK 6

1.2 THE CONTAMINATED SITE OF BAGNOLO MELLA 10

1.3 CLEAN- UP STRATEGIES 11

1.3.1 IMMOBILISATION TECHNIQUES 13

1.3.2 VITRIFICATION TECHNOLOGY 14

1.3.3 PHYTOEXTRACTION TREATMENT 14

1.3.4 ELECTROKINETIC PROCESS 15

1.3.5 PHYSICAL METHODS FOR METAL REMOVALS TREATMENT 15

1.3.6 LEACHING PROCESSING FOR THE SOLUBILISATION OF HEAVY METALS 16

1.3.7 THERMAL DESORPTION 16

1.4 THE HPSS SYSTEM 17

1.5 CALCIUM ALUMINATE CEMENT (HYDRATION MECHANISMS AND REACTIONS) 19

1.5.1 CAC + CALCIUM SULPHATE BINARY SYSTEM 22

1.5.2 CAC + CALCITE BINARY SYSTEM 23

1.6 ORDINARY PORTLAND CEMENT (OPC) 24

1.7 GROUND GRANULATED BLASTFURNACE SLAG (GGBS) 26

1.8 MUNICIPAL SOLID WASTE INCINERATOR (MSWI) AND FLY ASH GENERATION 27

1.9 TREATMENT METHODS APPLIED TO MSWIFA 31

1.9.1 WASHING PROCESS 31

1.9.2 Leaching process 31
1.9.3 Stabilisation/solidification method 32
1.9.4 Vitrification 32
1.10 Instrumental analysis theory 32
1.10.1 X-ray Powder Diffraction Analysis (XRPD) 32
1.10.2 Scanning Electron Microscopy coupled with Energy Dispersed X-ray spectroscopy (SEM-EDX) 33
1.10.3 Inductively Coupled Plasma Mass Spectrometry (ICP-MS) 34
2 Purpose of the study 37
3 Materials and Methods 39
3.1 Bagnolo Mella 39
3.1.1 Materials 39
3.1.2 Inductively coupled plasma mass spectrometry (ICP-MS) 42
3.1.2 Sem analysis 42
3.1.3 XRPD Analysis 44
3.1.4 Compressive strength test 47
3.1.5 Leaching tests 49
3.2 Municipal Waste Incinerator Fly Ash (MWIFA) 49
3.2.1 Materials 49
4. Results & Discussion 51
4.1 Bagnolo Mella 51
4.1.1 The contaminated soil of Bagnolo Mella 51
4.1.2 Solidification/stabilisation of lead contaminated soil using CAC 70 54
4.1.2.1 Samples cured at 20 °C for 35 days 54
4.1.2.2 Samples cured at 40°C for 35 days 72
4.1.2 Compressive strength analysis 82
4.1.3 Leaching Tests 85
4.2 Municipal solid waste incinerator fly ash (MSWIFA) 92
4.2.1 Untreated MSWIFA 92
4.2.1 Hydration of OPC-MSWIFA 99
4.2.2 Hydration of CAC-MSWIFA 102

4.2.3 BINARY HYDRATION OF GGBS-MSWIFA 105
5. CONCLUSIONS AND FUTURE RESEARCH 107
6. REFERENCES 111
7. APPENDIX 125
7.1 APPENDIX A: CHEMICAL ANALYSIS OF THE SOIL 125
7.2 APPENDIX B: SEM IMAGES OF THE SOIL 126
7.2 APPENDIX C: XRPD ANALYSIS 128

LIST OF FIGURES

FIG. 1: COMPLEXATION REACTION OF METAL IONS BY ORGANIC MATTER. FROM THRUMAN (1985). *5*
FIG. 2: REMEDIATED, IDENTIFIED, ESTIMATED CONTAMINATED SITES IN EUROPE *7*
FIG. 3: S.I.N IN ITALY. SOURCE: ISPRA, 2019 ..... *9*
FIG. 4: 2018 SATELLITE IMAGE OF THE AREA OF INTEREST *11*
FIG. 5: COMPARISON OF DIFFERENT SOIL CLEAN-UP TECHNOLOGIES.(GONG ET AL., 2018). *12*
FIG. 6: SCHEME OF THE HPSS GRANULATION PROCESS. *18*
FIG. 7: FINAL PRODUCT AFTER THE PELLETIZATION PROCESS *19*
FIG.8: STRUCTURAL MODEL OF THE CAH10 ..... *21*
FIG.9: STRUCTURAL MODEL OF THE C3AH6 ..... *21*
FIG.10: ETTRINGITE TRIGONAL CRYSTAL STRUCTURE *23*
FIG.11: MONOSULFATE HEXAGONAL CRYSTAL STRUCTURE *23*
FIG. 12: MONOCARBOALUMINATE TRIGONAL STRUCTURE *24*
FIG.13: TYPICAL PROCEDURES APPLIED IN A MSWI *28*
FIG. 14: CLASSICAL XRPD SETUP *33*
FIG. 15: ICP-MS COMPONENTS SET -UP *35*
FIG. 16: DEMOULDED CYLINDRICAL SAMPLES. *41*
FIG. 17: SEM-EDX UTILISED FOR THE ANALYSIS. *43*
FIG.18: CRASHED CYLINDRICAL SAMPLES IMPREGNED WITH EPOXY RESIN *43*
FIG. 19: MICRONIZED SAMPLES LEFT TO DRY IN GLASS WATCHES. *45*
FIG. 20: XRPD SAMPLES *45*
FIG. 21: SAMPLE HOLDER USED FOR KINETIC ANALYSIS *47*

FIG. 22: DIFFRACTOMETER USED TO PERFORM THE KINETIC ANALYSES. 47
FIG. 23: MATERIAL TESTING MACHINE USED DURING THE COMPRESSIVE STRENGTH TESTS. 48
FIG. 24: FLY ASH MIXED WITH ZINCITE IN THE MORTAR 50
FIG. 25: SIZE DISTRIBUTION OF THE SOIL PARTICLES ASSUMING PARTICLES AS SPHERES. 53
FIG. 26: ELEMENTAL X-RAY COMPOSITIONAL MAP OF THE CONTAMINATED SOIL 54
FIG. 27: DIFFRACTION PATTERNS OF CAC 70 RECORDED DURING THE EARLY 24 HOURS OF HYDRATION. 57
FIG. 28: TEMPORAL TREND OF THE MINERALOGICAL PHASES IN SAMPLE 4-20 °C. 58
FIG. 29: XRPD PATTERNS FOR SAMPLE 4 ATTAINED AS A FUNCTION OF THE CURING TIME- 20°C. 58
FIG. 30: COMPARISON BETWEEN THE PORTION OF THE DIFFRACTOGRAMS AT HIGH D-SPACING VALUES OBTAINED AFTER 14 AND 28 DAYS OF CURING AT 20 °C FOR SAMPLE 4. 59
FIG. 31: SEM IMAGE OF CAC 70 CEMENT CURED AT 20 °C FOR 7 DAYS. 59
FIG. 32: TEMPORAL TREND OF THE MINERALOGICAL PHASES IN SAMPLE 3 CURED AT 20 °C. 61
FIG. 33: XRPD PATTERNS FOR SAMPLE 3 ATTAINED AS A FUNCTION OF THE CURING TIME 61
FIG. 34: SEM IMAGE OF AN ETTRINGITE PARTICLE IN SAMPLE 3 62
FIG. 35: TEMPORAL TREND OF THE MINERALOGICAL PHASES IN SAMPLE 3 CURED AT 20 °C. 64
FIG. 36: XRPD PROFILES FOR SAMPLE 2 ATTAINED AS A FUNCTION OF THE CURING TIME. 64
FIG. 37: SEM IMAGES OF SAMPLE 2 65
FIG. 38: SEM-EDX ANALYSIS ON SAMPLE 2 65
FIG. 39: TEMPORAL TREND OF THE MINERALOGICAL PHASES IN SAMPLE 1 CURED AT 20°C 66
FIG. 40: XRPD PATTERN FOR SAMPLE 1 ATTAINED AS A FUNCTION OF THE CURING TIME 68
FIG. 41: SEM IMAGE OF A DOLOMITE PARTICLE RIMMED WITH A REACTING HYDRATE BEARING METALS 69
FIG. 42: SEM-EDX IMAGE OF SAMPLE 1 70
FIG. 43:SEM-WDS IMAGE OF AN ETTRINGITE PARTICLE IN SAMPLE 1 70
FIG. 44: DIFFRACTOGRAMS OF THE SAMPLE 4 CURED AT 40 °C ANALYSED FROM 14 TO 35 DAYS. 73
FIG. 45: TEMPORAL TREND OF THE MINERALOGICAL PHASES IN SAMPLE 4 CURED AT THE 40 °C. 74
FIG. 46: SEM IMAGE CARRIED OUT ON SAMPLE 4. 74
FIG. 47: TEMPORAL TREND OF THE MINERALOGICAL PHASES IN SAMPLE 3 TREATED AT 40 °C 75
FIG. 48: XRPD PATTERNS OF SAMPLE 1 CURED AT 40 °C. 76
FIG. 49: TEMPORAL TREND OF THE SAMPLE 2 CURED AT 40 °C FOR 35 DAYS. 77
FIG. 50: XRPD PATTERNS OF SAMPLE 2 CURED AT 40°C FROM 14 TO 35 DAYS. 78
FIG. 51: XRPD PATTERNS OBTAINED ANALYSING SAMPLE 1 CURED AT 40 °C EACH WEEK FOR 35 DAYS 79
FIG. 52: XRPD TRENDS OF THE OBSERVED PHASES IN SAMPLE 1 TREATED AT 40 °C FOR 35 DAYS. 80

Fig. 53: SEM image of sample 1 obtained at 20X magnification. 80
Fig 54: Sem-edx analysis on an hematite particle in sample 1 cured at 40 °C.....81
Fig. 55: Ettringite formation between two gypsum particles. 82
Fig. 56: Box plot illustrating the compressive strengths obtained for each sample under the two different curing conditions. 85
Fig. 57: leaching of the main elements in the soil as a function of pH. 91
Fig. 58: Solubility of hydroxide metals showing amphoteric behaviour 91
Fig. 59: XRPD diffractograms performed on the untreated MSWIFA sample 93
Fig. 60: Sample of fly ash exposed to ambient conditions for 3 days.. 95
Fig. 61: Sem image of a MSWIFA.....97
Fig. 62: Boundaries of the MSWIFA particles used for the dimensional distribution analysis..97
Fig 63: Dimensional distribution analysis of MSWIFA.....97
Fig. 64: Sem-edx images of MSWIFA.....98
Fig. 65: Sem-edx images of MSWIFA.....99
Fig. 66: Kinetic XRPD analysis of the system - 80 % MSWIFA and 20 % OPC..... 101
Fig. 67: Demoulded OPC-MSWIFA sample after 60 days of curing. 102
Fig. 68: Diffraction patterns of CAC+MWIFA system at different curing time. 104
Fig. 69: Demoulded CAC70-MSWIFA sample after 55 days of curing. 104
Fig. 70: Demoulded CAC70-MSWIFA sample after 55 days...... 106
Fig. 71: Demoulded GGBS-MSWIFA cylindrical sample after 48 days.....107
Figure B.1: BEI-SEM image of the contaminated soil. 126
Figure B.2: BEI-SEM image of a spot having a high presence of Anglesite. 126
Figure B.3: BEI-SEM image of a portion of the contaminated soil sample..... 127
Figure B.4: SEM-EDX analysis realized on the particle 12 of the Fig. B.3... 127
Figure C.1: XRPD pattern of both contaminated and uncontaminated (blank) soils. 128

LIST OF TABLES

TABLE 1: SOURCE AND TOXICITY OF HEAVY METALS. 2

TABLE. 2: COMPARISON OF DIFFERENT CLEAN-UP STRATEGIES 17

TABLE 3: TYPES OF CALCIUM ALUMINATE CEMENTS 20

TABLE 4: MINERALOGICAL COMPOSITION OF AN OPC CLINKER 24

TABLE 5: MINERALOGICAL COMPOSITION OF A HYDRATED OPC [BENSTED AND BARNES, 2008]. 25

TABLE 6: TYPICAL COMPOSITION OF GGBS (WANG ET AL., 2019) 26

TABLE 7: SOURCES, SPECIATION AND DISTRIBUTION OF HEAVY METALS IN MSWI (CHANDLER ET AL.1997) 30

TABLE 8: MINERALOGICAL COMPOSITION OF CAC 70. 39

TABLE 9: ENRICHMENT FACTOR CLASSIFICATION (QINGJIE ET AL., 2008) 40

TABLE 10: MIX PROPORTION OF DESIGNED SAMPLES OF BAGNOLO MELLA. 41

TABLE 11: ICP-MS INSTRUMENTAL SETTING 42

TABLE 12: XRPD INSTRUMENTAL SETTINGS. 46

TABLE 13: MIX PROPORTION OF DESIGNED MATRIXES OF MSWIFA 50

TABLE 14 CALCULATION OF THE ENRICHMENT FACTOR FOR THE SOIL 52

TABLE 15: SEM-WDS CARRIED OUT ON A ETTRINGITE PARTICLE. 71

TABLE 16: INITIAL AND FINAL PH OF THE SOIL ONCE TREATED WITH ACID SOLUTIONS 86

TABLE 17: TOTAL CONTENT CONCENTRATIONS OF DIFFERENT MSWIFA SAMPLES 92

TABLE 18: MSWFA XRPD QUANTITATIVE ANALYSIS 96

TABLE A.1: ICP-MS ANALYSIS OF THE CONTAMINATED SOIL OF BAGNOLO MELLA.. 125

TABLE A.2: ICP-MS ANALYSIS OF THE UNCONTAMINATED SOIL OF BAGNOLO MELLA 125

TABLE C.1: QUANTIFICATION OF THE MINERAL PHASES IN THE CONTAMINATED SOIL. 128

TABLE C.2: QUANTIFICATION OF THE MINERAL PHASES IN THE UNCONTAMINATED SOIL. 129

TABLE C.3: WEIGHT FRACTIONS (WT. %) OF MINERAL PHASES IN SAMPLE 4 CURED AT 20 °C. 129

TABLE C.4: WEIGHT FRACTIONS (WT. %) OF MINERAL PHASES IN SAMPLE 3 CURED AT 20 °C. 129

TABLE C.5: WEIGHT FRACTIONS (WT. %) OF MINERAL PHASES IN SAMPLE 2 CURED AT 20 °C. 129

TABLE C.6: WEIGHT FRACTIONS (WT%) OF MINERAL PHASES IN SAMPLE 1 CURED AT 20 °C. 130

TABLE C.7: WEIGHT FRACTIONS (WT. %) OF MINERAL PHASES IN SAMPLE 4 CURED AT 40 °C. 130

TABLE C.8: WEIGHT FRACTIONS (WT. %) OF MINERAL PHASES IN SAMPLE 3 CURED AT 40 °C. 130

TABLE C.9: WEIGHT FRACTIONS (WT. %) OF MINERAL PHASES IN SAMPLE 2 CURED AT 40 °C 131

TABLE C.10: WEIGHT FRACTIONS (WT. %) OF MINERAL PHASES IN SAMPLE 1 CURED AT 40 °C. 131

ABBREVIATIONS

% wt: weight percent

AFm-14: Monosulphate

ANC: Acid Neutralizing Capacity

APC: Air Pollution Control

BA: Bottom Ash

BDATs: Best demonstrated available technologies

CAC: Calcium aluminate cement

CEC: Cation-exchange capacity

EDX: Energy dispersive x-ray spectroscopy

EPA: Environmental Protection Agency

FA: Fly Ash

GGBS: Ground granulated blast furnace slag

HPSS: High Performance Solidification/Stabilisation

ICP-MS: Induced coupled plasma mass spectrometry

MSWIFA: Municipal Solid Waste Incinerator Fly Ash

OPC: Ordinary Portland cement

S/S: Solidification/Stabilisation

SEM: Scanning electron microscopy

S.I.N: Site of National Interest

SOM: Soil Organic Matter

W/C: water/cement ratio

WDS: Wavelength-dispersive spectroscopy

XRPD: X-ray powder diffraction

ACKNOWLEDGEMENTS

Hereby, I would like to acknowledge the contributions of many people who have supported me throughout this project.

First, I wish to thank my supervisor Prof. Gilberto Artioli who gave me full faith permitting me to have a chance to work at this project and get knowledge about the huge world of cements and S/S at which I was very interested on. A huge thank to Prof. Maria Chiara Dalconi who supported me during this long period in laboratory sharing her expertise in mineralogy and filling all the gap that I had at the beginning of this experience, replying always with extreme patience and professionalism at my endless questions, and sharing with me her passion to science. I wish to thank Dr. Silvia Contessi for having convinced me from the beginning to undertake this path, and for transmitting me the passion for the topic I have dealt with in this thesis. I' ve very appreciated the time she dedicated on me even though completely full of tasks! I am a better scientist for the guidance, assistance, and support that they afforded me. I am extremely grateful to them also for introducing me to a love of chemistry/mineralogy and starting me on this journey.

Alongside my supervisors, I wish to thank Dr. Loris Calgaro for his educational explanations of chemistry, and for the suggestions He gave me during the thesis writing. Thanks also for his time at the train station trying to understand how LeachXS works, unfortunately we did not even use it. I'd like to thank Dr. Giorgio Ferrari for having provided the materials and, for all the meetings we have arranged in which I had the possibility to resolve my doubts and get his priceless information about the cement field.

I had the pleasure of working with a number of other researchers and support staff at CIRCe with whom I have shared this priceless experience.

1. INTRODUCTION

1.1 HEAVY METALS CONTAMINATION

The term “heavy metals” is largely used to define the group of naturally occurring elements having a relative high density (> 5 g/cm^3). A small part of heavy metals contains among the most harmful elemental pollutants, and these are of concern because of their toxicity to humans. They are ubiquitously present in all the environmental matrix (ATSDR, 2000). These elements, that are in general the transition metals and some of the representative elements such as lead and tin, are placed in the lower righthand corner of the periodic table. However, the “heavy metals” definition is somewhat ambiguous and, it would make more sense considering the difference between essential metals and non-essential metals. The first ones play a relevant role in regulating the physiologic function of the living being, whereas the second ones have no roles in biologic functions and may exhibit toxicity even at low concentrations. Many metals like Zn, Fe, Cu, etc. carry out a key role on the enzymatic processes in plants and animals working as co-factor and play important roles in various oxidation-reduction reactions (WHO, FAO, IAEA, 1996), i.e iron is the haemoglobin co-factor and play the fundamental role of binding and carrying oxygen. Copper serves as an essential co-factor for several oxidative stress-related enzymes, such as catalase, superoxide dismutase, cytochrome c oxidases (Stern, 2010). Regardless, at high concentrations they may manifest toxicity. For non-essential elements case, like arsenic (As), lead (Pb), mercury (Hg) and cadmium (Cd), the story is different as they do not play biological roles and for this reasons they may exhibit toxicity even at low concentrations if they are available, and in a form that organisms may assume.

The relevant characteristic of the metals is that they are totally non-degradable towards the formation of non-toxic forms and this makes challenging the site restorations when contamination occurs (Adriano, 2003). Although we commonly think of heavy metals as water or soil pollutants, they are for the most part transported from place to place via the air, either as gases or as species adsorbed on, or absorbed in, suspended particulate matter (Baird and Cann, 2012). They ultimately may be transformed into insoluble forms, which therefore are biologically unavailable unless they are again converted into more soluble substances. The ultimate sinks for heavy metals are soils and sediments. The most important factor drastically impinging upon the toxicity of heavy metals is their speciation i.e chemical

form of the element. The speciation depends upon temperature, phase association, adsorption and sequestration, chemical factors and biological factors (Hamelink et al., 1994; Verkleji, 1993).

1.1.1 HEAVY METALS SOURCES IN SOIL AND TOXICITY

From a geochemical viewpoint, all soils contain a large spectrum of heavy metals, but the concentrations vary widely, and some may be below the limit of detection (LOD) for certain analytical procedures. Indeed, they normally occur in trace amounts (usually <1,000 ppm) in rocks and soils. Heavy metals and metalloids in soils naturally come from the soil parent material by weathering (lithogenic source), but various anthropogenic sources contribute to the input of heavy metals into the soil. Kuo et al. (1983) reported that heavy metals coming from anthropogenic sources tend to be more mobile than pedogenic or lithogenic ones. Soils may be contaminated by accumulation of heavy metals from the rapidly expanding industrial areas, mine tailings, land application of fertilizers, coal combustion residues, spillage of petrochemicals and atmospheric deposition (Khan et al., 2008; Zhang et al., 2010). There are many different anthropogenic sources of heavy metals contamination affecting both agricultural and urban soils. In **table 1** both anthropogenic sources and the related health effects for some heavy metals are reported. As mentioned, the toxicity of the heavy metals depends upon their speciation, and as they may have an effect on an organism, a metal must first be bioavailable. Heavy metals contamination of soil may pose risks and hazards to humans and the ecosystem through: direct ingestion or contact with the contaminated soil, the food chain, drinking of contaminated groundwater, reduction of food quality via phytotoxicity, reduction in land availability caused by pollution, and tenure problems (McLaughlin et al., 2000; Ling et al., 2007).

Table 1: *Source and toxicity of different heavy metals cited in this thesis.*

Element	**Sources** (Manahn, 2010)	**Toxic effect on human beings** (Manahn, 2010)
Arsenic (As)	Metal smelting, burning of fossil fuels, timber treatment, agricultural chemicals, mining by-product	The toxic +3 oxide, As_2O_3, is absorbed through the lungs and intestines. Biochemically, arsenic acts to coagulate proteins, forms complexes with coenzymes, and inhibits the production of adenosine triphosphate (ATP) in

		essential metabolic processes involving the utilization of energy.
Beryllium (Be)	Coal, industrial waste	Its most serious toxic effect is berylliosis, a condition manifested by lung fibrosis and pneumonitis, which may develop after a latency period of 5–20 years. Beryllium is a hypersensitizing agent and exposure to it causes skin granulomas and ulcerated skin.
Boron (B)	Coal, detergents, wastes	Toxic at high concentrations
Mercury (Hg)	Metal mining, coal, industrial waste	Elemental mercury vapor can enter the body through inhalation and be carried by the bloodstream to the brain where it penetrates the blood–brain barrier. It disrupts metabolic processes in the brain causing tremor and psychopathological symptoms such as shyness, insomnia, depression, and irritability. Divalent ionic mercury, Hg^{2+}, damages the kidney. Organometallic mercury compounds are also very toxic.
Lead (Pb)	Fertilizers, leaded fossil fuels. Lead-based paints, lead smelters, lead-acid batteries, mining, industrial waste	Inhibition of the synthesis of haemoglobin. It also adversely affects the central and peripheral nervous systems and the kidneys.
Chromium (Cr)	Metal plating, paints and pigments, tannery, wood preservation, pulp and paper production.	It is hemotoxic, genotoxic, and carcinogenic. When hexavelent chromium enters the bloodstream, it damages blood cells by causing oxidation reactions. This oxidative damage can lead to hemolysis and, ultimately, kidney and liver failure (Dayan and Paine, 2001)
Cadmium (Cd)	p-fertilizers, sewage sludge, cement production	It adversely affects several important enzymes; it can also cause painful osteomalacia (bone disease) and kidney damage. Inhalation of cadmium oxide dusts and fumes results in cadmium pneumonitis characterized by edema and

		pulmonary epithelium necrosis (death of tissue lining lungs).
Copper (Cu)	Fertilizers, pesticides, mining, industrial wastes	Essential trace element, toxic to plants and algae at higher levels
Zinc (Zn)	Industrial waste, metal plating, plumbing	Essential element, toxic to plants at higher levels
Selenium (Se)	Natural sources, coal	Essential at lower levels, toxic at higher levels
Iron (Fe)	Industrial wastes, corrosion, acid mine water, microbial action	Essential nutrient
Molybdenum (Mo)	Industrial waste, natural sources	Essential to plants, toxic to animals
Manganese (Mn)	Industrial wastes, acid mine water microbial action	Essential nutrient

1.1.2 CHEMISTRY OF HEAVY METALS IN SOILS

When present in the soil matrix, heavy metals may be strongly bound to both the organic and inorganic fractions naturally present as colloidal compounds in soil. Particularly, they may be adsorbed by amorphous materials, clay surfaces or iron/manganese oxyhydroxides, in lattice of secondary minerals like carbonates, sulphates or oxides, organic matter, or lattice of primary minerals such as silicates (Tessier et al., 1979). Soil is composed by 50 % of solid, and just 5 % thereof is composed by organic matter. However, soil organic matter (SOM) is probably the most important component playing a role on the sorption of contaminants in the soil because of its high micro porosity containing voids of different dimensions that can trap and bind organics, and inorganic components and water. The complexation of metal ions by SOM is extremely important in affecting the retention and mobility of metal contaminants in soils, sediments and waters. Several different types of SOM-metal reactions can occur (**Fig.1**). The capacity of performing such a binding capacity by SOM is due to the presence of enolate, amine, azo compounds, N rings, carboxylate groups in its structure. The complexations of SOM with metals can beneficially as well as deleteriously affect the fate of metals in soils and water. For instance, humic acid present in SOM can act as a reducing agent and reduce Cr (VI), the more toxic form of Cr, to Cr (III) (Wittbrodt and Palmer, 2005). Because of the presence of functional groups, SOM has a great cation exchange capacity (CEC) and it has been estimated that up to 80 % of the CEC of soils is due to organic matter (Parfitt et al., 2008).

Also, evidence on the sorption of heavy metals on microorganisms has been reported as cell surfaces of all bacteria are largely negatively charged thus sorbing cations (Gadd, 1990). Sorption-desorption reactions are the predominant processes controlling the bioavailability of metals and metalloids in soils (Caporale and Violante, 2016). Soil is a very complex matrix as both microbiological and soil component are present, playing a role on the reactions affecting the heavy metals solubility. Indeed, if present in a bioavailable form, heavy metals may be taken by plant's roots or interact with microorganisms. Heavy metal's solubility depends upon several factors, among which: type of soil, soil properties (pH, redox potential, water content, temperature etc,) presence of determinant compound such as phyllosilicates, SOM, metal oxides, carbonates, and organo-mineral complexes, soil-metal interaction time, and affinity of the specific heavy metals toward the soil adsorption surface. The study and the modelling of this interaction is particularly challenging as several factors contribute to it. Heavy metal solubility is regulated by the following processes:

- Adsorption/desorption
- Soil complexation
- Oxidation/reduction
- Precipitation/dissolution

Soil components different greatly in their sorption capacities, their cation and anion exchange capacities, and the binding energies of the sorption sites (Violante et al., 2012).

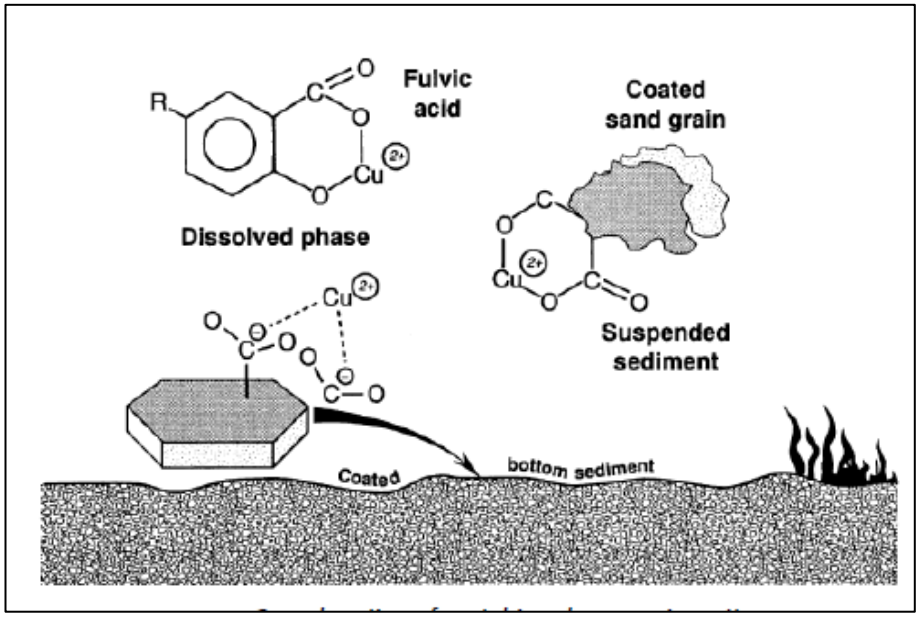

Fig. 1: *Complexation of metal ions by organic matter in suspended sediment, bottom sediment, colloidal, and dissolved phases. From Thruman (1985).*

These includes inner- and outer sphere surface complexes (Borda et al., 2008). Even in this case, speciation fulfils a key role on the behaviour of the element. Presence of complex-

forming ligands severely modulates the metals solubility. Organic compounds such as fulvic and humic acids as well as inorganic ligands like SO_4^{2-}, F^-, NO_3^-, Cl^- may increase the metal solubility. Changing of the soil redox potential due to occurrence of anaerobic/aerobic conditions may permit also changes in metal valence. For instance, the conversion between arsenate and arsenite is well known to occur when mildly anaerobic conditions are present in the environment (Kirk, 2004). By considering a Pourbaix diagram, it is also possible to understand that pH and Eh must be considered together when one deals with heavy metal speciation. The diagram gives information about the precipitation of insoluble compounds as well as the redox state of the species. The Oxidation Reduction Potential (ORP) (ASTM 200-09) of a determinant compound must also be considered. Probably, the most important factor influencing solubility of the heavy metals is the pH value. Indeed, the variation of concentration of leaching elements with pH follows three different patterns including cationic, oxoanionic, and amphoteric patterns (Komonweeraket et al., 2015). The pH affects the sorption of metal cations on variable charge minerals either by changing the number of sites available for sorption (sorption increases by increasing pH) or by changing the concentration of cation species [Me^{2+}, $MeOH^+$, $Me(OH)_2$] (Caporale and Violante, 2016). By increasing solution pH, leads to a rapid increase in net negative surface charge and, thus, increases the affinity of the soil for metal cations (Wu et al., 2013). Humic substances have a great affinity for heavy metal cations and extract them from the water that passes through them by the process of ion exchange. The binding of metal cations occurs largely because of the formation of complexes with the metal ions by —COOH groups in the humic and fulvic acids (Baird and Cann, 2012).

On the other hand, sorption of anions decreases with increasing pH, and thus anionic ions (i.e selenite, arsenate, molybdate) are specifically sorbed replacing the $-OH^-$ or $-OH_2$ groups present in variable charge minerals. In particular, with pH decreasing, the competition between H^+ and the dissolved metals for ligands (e.g. OH^-, CO_3^{2-}, SO_4^{2-}, Cl^-, S^{2-} and phosphates) become more significant (Peng et al., 2008). To further complicate the dynamic, it has been demonstrated that inorganic and organic anions (e.g. root exudates at the soil/root interface) strongly prevent the sorption of toxic anions onto different sorbents (Violante, 2013).

1.1.3 CONTAMINATED SITES AND ITALIAN LEGISLATION FRAMEWORK

The key message presented by the Joint Research Centre (JRC) technical report about the status of local soil contamination in Europe (2018) is that the prevention of soil

contamination in the European Union has strong links with policies on industrial activities and chemical substances use, e.g. the Industrial Emission Directive (IED), the registration, evaluation, authorisation and restriction of chemicals (REACH), plant-protection products, fertilisers and biocides regulations, and with environmental-protection policies for water and air (e.g. the ELD). It has also strong links with policies concerning certain land uses, for instance agriculture. However, none of these regulations include guidelines to identify and deal with soil contamination (Ecologic Institute, 2017). Also, the commitments to which the European Union has signed up are fragmentary: it is essential to develop a generic framework that encompasses the uses and functions of the soil-(ground)water-sediment system in order to achieve effective protection of soil resources. The European environmental agency (EEA,2019) reported that the number of potentially contaminated sites in Europe is around 2.5 million, of which 45% have been identified to date. The estimated contaminated sites are instead 342'000, and just the 15 % of them have been remediated (**Fig.2**).

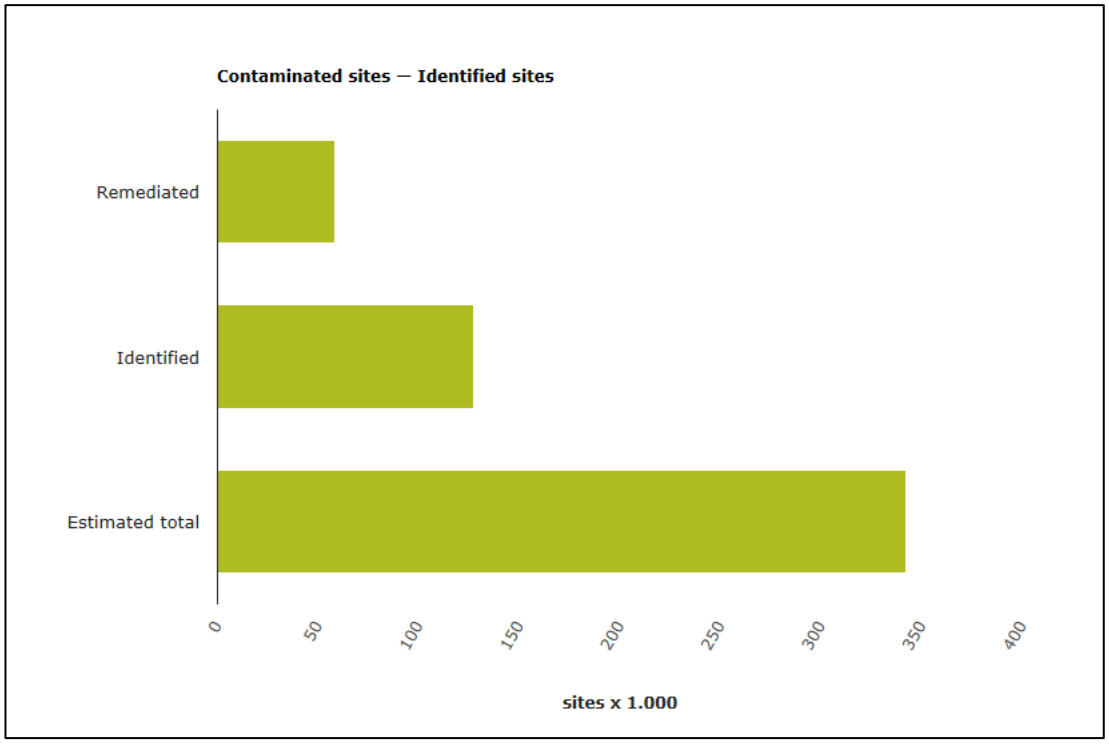

Fig. 2: *Remediated, Identified, Estimated contaminated sites in Europe*

In Italy, contaminated sites of national interest (S.I.N) are those sites heavily contaminated and considered as dangerous for the public health. In 2019, 41 (**Fig. 3**) S.I.N were reported in the national territory (Ispra, 2019). They are characterized by remarkable extent and its management is employed by the Ministry of the environment, land and sea.

These sites are defined as S.I.N since it was proved that they are characterized by qualitative alterations of the soil, groundwater and superficial waters properties. The contaminations were derived from anthropogenic sources such as: industrial activities, asbestos manufacturing, ports, accidents due to chemicals realising, landfill, and former mines.

Historical contamination is defined as that contamination episode occurred before the introduction of a specific law on soil contamination. The criteria for addressing historical contamination are based on the application of risk-based approaches. It is under responsibility of national, regional or local authorities to manage the remediation of such orphan sites in order to reduce the risk they pose to human health and the environment.

Additionally, other contaminated sites are present in the Italian territory even though not considered as S.I.N. A particular type of contaminated sites are the so-called brownfields. These are defined by the US EPA (Environmental Protection agency) as real properties, the expansion, redevelopment or reuse of which may be complicated by the presence or potential presence of a hazardous substance, pollutant or contaminant. Several projects around the world demonstrated that recovery of brownfield sites can ensure not only the acquiring of a more available space but also, increase environment liveability, create new jobs, preserve green spaces, and prevent urban expansion. Brownfield sites may be revitalized and be reused in a way that generate greatest local benefit. For instance, in Chicago a former illegal landfill area has been recovered by building the Chicago centre for green technology, meeting the highest standard for green building.

The Italian law that deals with the restoration of contaminated sites is the legislative decree 152/06 fourth part, title V. This law substitutes, and radically modifies the D.M 471/99 previously dealing with contaminated sites. The decree has the purpose to regulate the restoration actions, and the environmental recovery of the contaminated sites carrying out the necessary actions for eliminating the pollution sources as well as reducing the concentrations of the pollutants, in accordance to the “polluter must pay” principle. This principle is sometimes not applicable though, in particular, when one deals with historical contamination cases. The decree is hinged on the risk analysis approach to define a site as contaminated or not. Article 242 ratifies that in case of occurrence of episodes able to contaminate a site, the responsible of the contamination must activate emergency measures to mitigate the effects given by the events, as well as draw up a preliminary investigation of the pollution parameters. If the concentrations of the considered parameters exceed the reported threshold concentrations (reported in Column A and column B), then the site is defined as potentially contaminated. The responsible must start a characterization process based on a risk assessment analysis. Thus, a site is defined as “contaminated” when the so-

called Risk Threshold concentrations (RTC), determined by applying the risk analysis procedure, are exceed. When the site is defined as contaminated, it must undergo to a remediation action in order to remove the pollution sources or reduce the concentration at a level lower than the RTC.

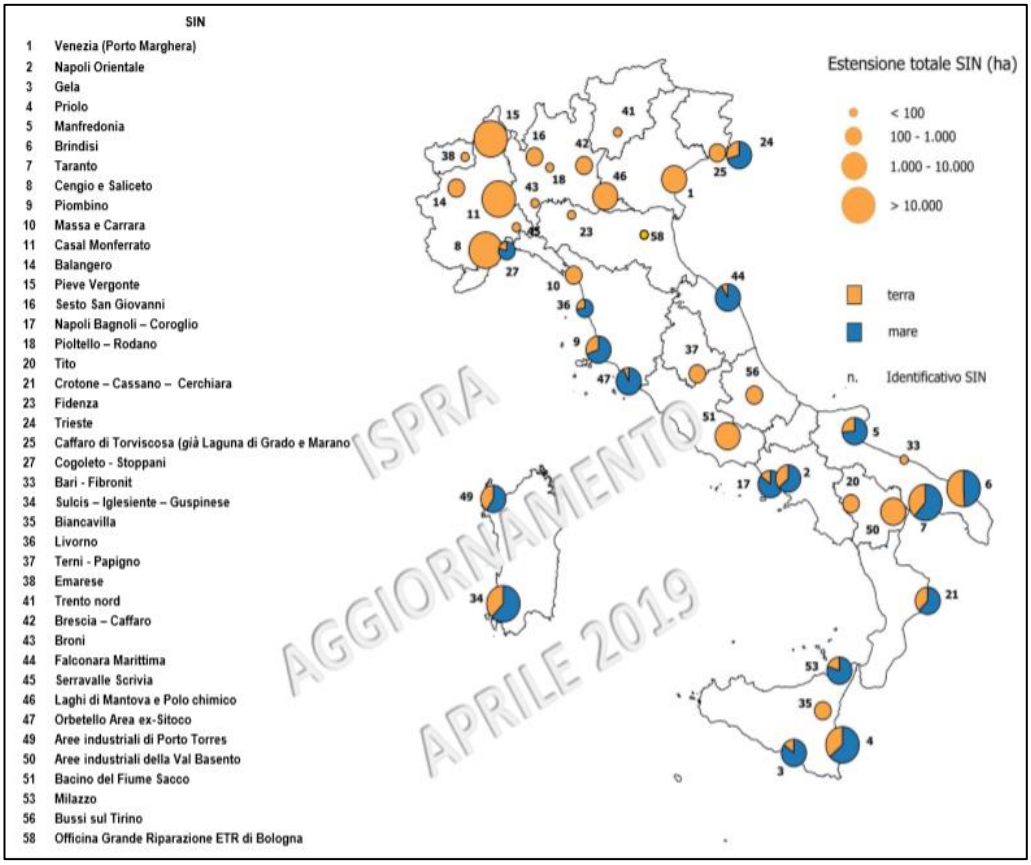

***Fig. 3**: S.I.N (Siti interesse Nazionale- Contaminated sites of national interest) individuated in Italy. Source: ISPRA, 2019*

Additionally, an operative project must be carried out with the purpose of finding the solution for achieving an acceptable level based on the risk assessment.

A contaminated site must be also characterized according to the following phases:

1) Collection of available data and creation of a preliminary conceptual model
2) Processing of an initial investigation plan (through sampling and analysis)
3) Further analysis
4) Outcomes analysis and elaboration of a definitive conceptual model.

The purpose of the definitive conceptual model is to obtain information about the contamination source, the pathway that the contaminant does through the environmental matrixes and, the final receptors. Then, the approbation of a site-specific risk analysis may be made, and the recovery of the contaminated site may be approved and executed.

1.2 THE CONTAMINATED SITE OF BAGNOLO MELLA

The area that is object of this study (**Fig. 4**) is an orphan brownfield in Bagnolo Mella, a small town located in the North of Italy. In the site, recently subjected by a restoration HPSS project performed by In.T.Ec s.r.l, an agrarian consortium producing and packaging fertilizers was present. The agrarian consortium had been operating since the 1898 until the 1985, year of its closure. The area has an extension of approximately 27,000 m^2 with an industrial/commercial land use. The characterization plan performed by In.T.Ec revealed that the site was dedicated to the production and packaging of superphosphate fertilisers. The first step of the production process consisted on grounding the phosphorite containing 70-80 % of insoluble tricalcium phosphate. The grounded product was then treated with sulphuric acid giving monocalcium phosphate and calcium sulphate as products (**Reaction 1**).

$Ca_3(PO_4)_2 + 2H_2SO_4 \rightarrow 2CaSO_4 + Ca(H_2PO_4)_2$ (**1**)

The process consisted in producing sulphuric acid by pyrite roasting to produce solid oxide and gaseous sulphur dioxide at temperature of 600 °C- 1000 °C (Gabarròn et al., 2018). Then the sulphur dioxide is furtherly processed to form sulphuric acid (Lòpez et al., 2009). The roasting process leaves a ash residue consisting of hematite, a considerable amount of heavy metals and a small amount of sulphur (Pèrez-Lòpez et al.,2009). Thus, in this site the roasted pyrite ashes were probably not correctly managed and buried in the nearby soil. The oxidation conditions furthermore promoted the oxidation of sulfide minerals leading to acid sulphate water production (Bigham and Nordstrom, 2011). When pyrite is exposed to oxygen and water, it is oxidized, resulting in hydrogen- ion release, creating acidity, sulfate ions, and soluble metal ions. This so produced acidic water solubilized the heavy metals contained in the ash leading to the formation of mineral phases like jarosite [$KFe^{3+}_3(OH)_6(SO_4)_2$] which normally forms in a pH range of 1-3 (Stoffregen et al., 2011). The pH of soil was neutralized (pH 7.5) by the presence of calcite. The anglesite ($PbSO_4$) presence is instead justified by the oxidation of galena normally present in pyrite ores. Finally, a significant amount of hematite is given by the oxidation of ferrous iron forming ferric acid, that then can precipitate at higher pH as exactly hematite.

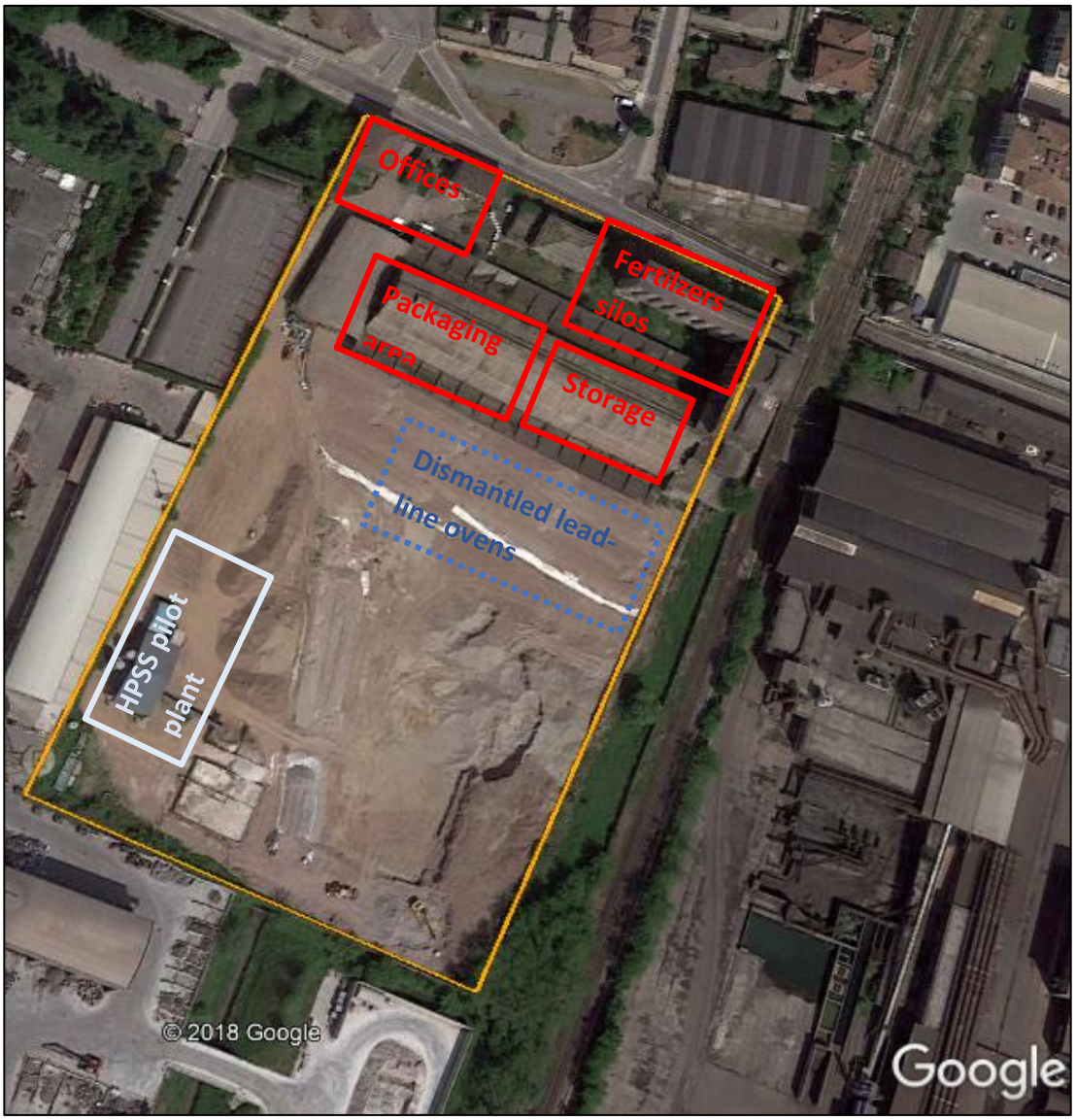

Fig. 4: *2018 satellite image of the area of interest (yellow rectangular). The total area is approximately 27,000 m^2. As it may be observed, the restoration of the site is still occurring. Also, oven area, fuel storage area, and lead-line oven were dismantled. The HPSS pilot plant is also visible.*

1.3 CLEAN- UP STRATEGIES

Several methods are available to manage contaminated soils. Unfortunately, the most widely used method to manage them is excavation followed by disposal in an appropriate secure landfill site (Guemiza et al., 2017). Clearly, this latter method is no longer sustainable because of both the consumption of land by landfills and the fact that the waste is not treated and are subjected to release contaminants over time. Furthermore, even diluting the contaminated soil adding a clean one does not resolve the leaching problems. Clean-up remediation strategies may be subdivided in 3 large groups: chemical methods, biological

methods and physical methods (**Fig.5**). Additionally, these techniques may be applied either ex-situ, treating the contaminated matrix in other sites, different than the contaminated one, or in-situ, in which the remediation techniques is applied directly on the contaminated site. Among the clean-up strategies, immobilization, soil washing, and phytoremediation techniques are frequently listed among the best demonstrated available technologies (BDATs) for remediation of heavy-metals-contaminated sites (GWRTAC, 1997). Determination of the best remediation technology is a site-dependent decision as several factors impinge upon this choice. As the number of contaminated-site cases grew up in the last decades, more awareness was dedicated by governments and the public on finding solutions to handle them in order to reduce the risk associated with their presence. The section will deal with the available techniques usable to manage sites contaminated by heavy metals.

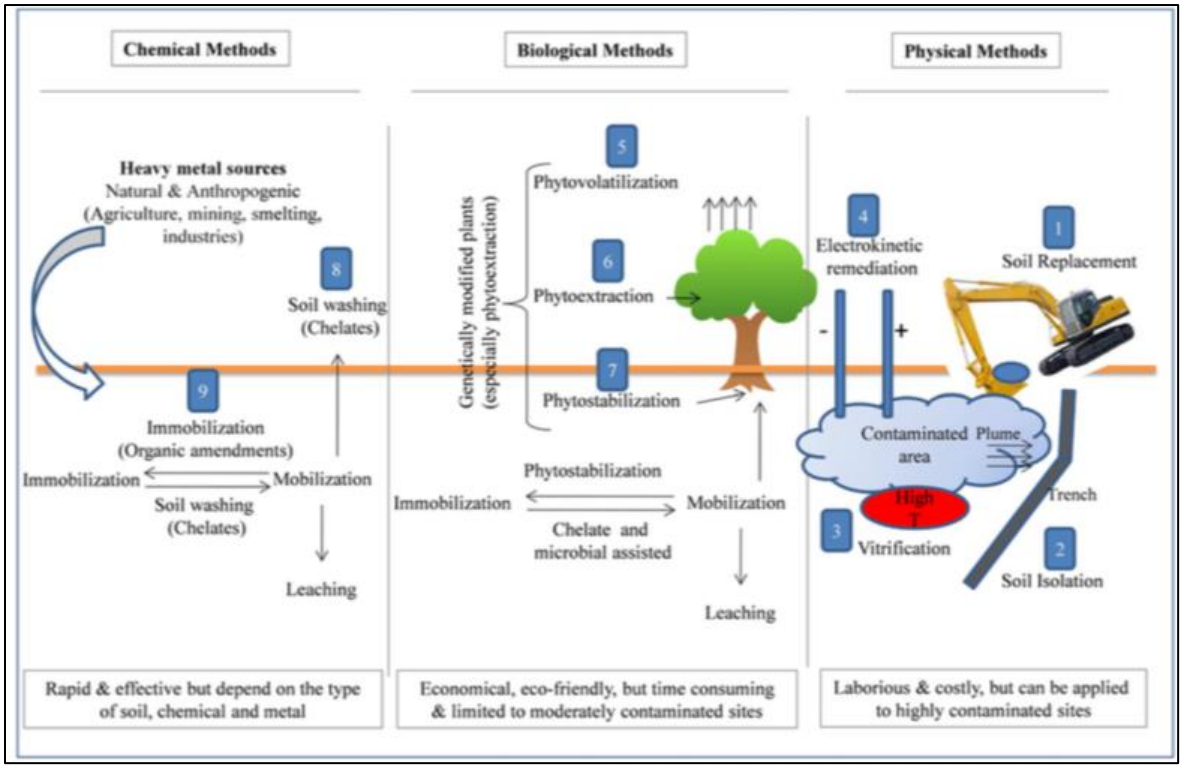

***Fig. 5**: Comparison of different soil clean-up technologies. The available techniques may be divided into 3 categories: physical, chemical and biological treatments (Gong et al., 2018).*

One of the key limitations of traditional heavy metals restoration sites is that they are extremely time consuming (Peng et al., 2018). In choosing a kind of method, a multiple-criteria decision analysis must be carried out, considering technical implications and finances, field-scale application, pollutant type, stakeholder liability, future use of the remediated site, available time. In **table 2** a comparison of different soil clean-up strategies is reported.

1.3.1 IMMOBILISATION TECHNIQUES

These techniques are widely applied to treat heavy metal contaminated soils. It may be either in-situ or ex-situ methods. The in-situ one is based on the utilization of geomembranes, and composite clay membranes to cover the contaminated sites. Even phytostabilisation process can be used by using plants capable to take up metals (Arthur et al., 2005). Among the ex-situ strategies, the most important is the stabilisation/solidification (S/S) technique, consisting on reducing the solubility and mobility of the contaminants by the addition of binding agents (FRTR, 2012). Particularly, the waste material is encapsulated in a monolithic solid showing good mechanical properties (Kahn et al., 2014). Heavy metals may be stabilized by complexation, precipitation, and adsorption reaction that redistribute the heavy metals from the soil solution to solid particles, decreasing their leachability, thus staving off that chemicals harm the environment. Several binders may be used such as: cements (OPC, CAC, CSC), fly ash, lime and portlandite, aluminosilcates. Industrial by products are also used, such as: ground granulated blast furnace slag (GGBS), red mud, and industrial eggshells (Soares et al.,2015). Spuller et al. (2007) reported good Pb-leaching reduction outcomes using iron (hydro) oxide to stabilize a Pb-bearing soil.

Despite several binders were tested (as above mentioned), cement is preferred one in S/S method as its availability, versatility, and cost effectiveness (Pandey et al., 2012). Cocke and Mollah (1993) reported the possible mechanisms involved in the incorporation of ions. An ion may chemisorb, precipitate, form a surface compound to any of several cement component surfaces, form inclusions or be chemically incorporated into the cement structures. Although OPC has been commonly used, other binders such as CAC (Navarro et al., 2013) has been studied. This latter, in particular, has shown high efficiency on metal retainment. Encapsulation with lime and concrete has also been reported to effectively immobilise heavy metals bearing soils. The major drawback of these methods is an instant market for the final product, that should be reused (Mulligan et al., 2001). Metallic nanoparticles (NPs) has also been deeply studied to be used to treat wastewater (Zhang et al., 2010). However, application of nanoparticles to remove of heavy metals is very limited.

Long-term studies conducted by Antemir et al. (2014) in stabilised soils, revealed that after 4 years of the remediation of a treated soil contaminated by Pb, Zn, and Cu, these elements were adequately stabilized.

The principle drawback of this technique is that sometimes some contaminants are not well stabilized remaining accessible. This phenomenon is particularly observed when the matrix to be treated is contaminated by different elements/compounds, particularly, heavy metals presenting soluble phases in the stabilised matrix. For this reason, sometimes combining more binders together could be a solution, but this increases irremediably the final cost. In addition, a continued monitoring program is needed to assess the system integrity in long-term period. Another problem of this technique is that it is matrix-dependent, and a case-by-case approach must be considered. The success of solidification with OPC strongly depends upon whether or not the waste adversely affects the strength and stability of the concrete product. A number of substances i.e salts of arsenate, borate, phosphate, iodate, and salts of copper, lead, magnesium, tin, and zinc are incompatible with OPC as they interfere with its setting and hardening, producing a mechanically weak product and resulting in deterioration of the cement matrix with time. Moreover, the method does not remove the heavy metals from the contaminated matrix but just cage them in the structure changing their physicochemical properties. Finally, the environment in which the stabilised material is placed, impinges on the properties thereof. Indeed, the combination of wet/dry, freeze/thaw cycling carbonation, alkali-aggregate reaction sulfate attack and other environmentally induced stresses may cause structural degradation of the material (Malviya and Chaudhary, 2006).

1.3.2 VITRIFICATION TECHNOLOGY

The method foresees to heat up the matrix at temperatures between 1400 and 2000 °C. Indeed, the mobility of heavy metal(loids) inside soil can be reduced by applying a high temperature treatment at the contaminated site (Mallampati et al.,2015) leading to the formation of a vitreous material. It may be also carried out in-situ by inserting array of electrodes into the contaminated area. The mechanical strength of this final material is reported to be 10 folds higher than that of the concrete (Yao et al., 2012). However, the great disadvantage of this technique is its high cost required for achieving the needed temperature.

1.3.3 PHYTOEXTRACTION TREATMENT

This technique is based on the use of tolerant and accumulating plants to phytoextract metals and metalloids such as Cu, As and Cr from a matrix (Cooper et al., 1999; Raskin et al., 1997). Bizily et al., (1999) engineered a transgenic plant to express the gene merBe able to degrade methylmercury. Although the transgenic plants were able to resist at high concentration of methylmercury, they did not show a great uptake capacity. Although the technique is safe, least destructive, eco-friendly and cost-efficient, the process is time-consuming, and the sorption of heavy metals carried out by the roots may not achieve high capacities. Additionally, it cannot be applied in soils contaminated by heavy metals present at a toxic concentration.

1.3.4 ELECTROKINETIC PROCESS

This method consists on applying a low intensity electric current between a cathode and an anode inserted into the contaminated soil. This makes possible that the ions and small charged particles are carried to the two poles according to their charges through electromigration, electroosmosis flow or electrophoresis and then treated (Swartzbaugh et al., 1990). The principle disadvantage of this method is that is only suitable for low-permeable soils as well as not control the pH value, the treatment efficiency results to be low as metals may be bound with the soil component. Additionally, soil having a high alkali content (1.4 wt%) is not feasible for this technique as not a good conductor (Buelt and Thompson, 1992).

1.3.5 PHYSICAL METHODS FOR METAL REMOVALS TREATMENT

The physical process may be helpful when the purpose is to reduce the volume of the treated material or to separate uncontaminated to contaminated particles (Mercier et al., 2000). Among the physical methods the density, and the gravimetric separation including spiral, hydro cyclone, Jig or shaking table are the most used. The efficiency of this technique depends on the contaminant to be treated as well as the soil characteristics. Regardless, several authors reported that these techniques applied particularly to Pb-bearing soils, show good outcomes (Laporte-Saumure et al., 2010) in particular, when more techniques are combined.

1.3.6 LEACHING PROCESSING FOR THE SOLUBILISATION OF HEAVY METALS

The method is based on using chemical agents to transfer metals from contaminated matrix to the aqueous solution. The contaminant is removed via ion exchange, precipitation, adsorption and chelation. If combined with physical separation processes, the method shows good treatment performances (Mercier et al., 2000; Laporte-Saumure et al., 2010). As for the other techniques, even in this case the performances of the method are matrix dependent. The use of chelating agents such as EDTA, EDDS, ADA, DTPA, citric acid and tartaric acid are reported to be efficient on removing As, Cd, Cu, Pb and Zn with removal yields ranging between 65 to 99 % (Wasay et al., 1998).

Additionally, as chemical agents even surfactants and oxidizing or reducing agents have been tested. However, both have resulted to little influence the removal efficiency. Using of phosphoric acid has been proved to be efficient on removing arsenic with a yield of 99 % after 6-hour extraction (Tokunage and Hakuta, 2002). Yao et al. (2012) reported that the results are frequently unsatisfactory using single extractor, in particular when many pollutants are present in the soil. Furthermore, they need more washing steps to show some effectiveness. Furthermore, the chelation agent EDTA is expensive and its biodegradability is bad. Hong et al. (2002) reported that the use of saponin was effective for the heavy metal removal, accomplishing 90-100% of Cd and 85-98 % of Zn extraction.

1.3.7 THERMAL DESORPTION

This technique is based upon the heavy metal's volatility. The matrix is heated using different sources (Microwave, infrared radiations) to volatilize the element. These are then removed by a carrier gas. The drawback of this technique is that is costly, time-consuming, and not all the heavy metals present high penchant to volatilize.

Table 2: *Comparison of different clean-up strategies, reporting their advantages and drawbacks. [Gong et al., 2018]*

Remediation technology		Description	Advantages	Disadvantages
Physical remediation	Soil replacement	Use of non-contaminated soil to replace or partly replace contaminated soil	Feasible for small volumes of heavily polluted shallow soil in small area	Costly, the removed contaminated soil may need further handling and disposal, may not be applicable to agricultural sites due to the associated high cost and potential loss of soil fertility
	Vitrification	Use of high temperature to melt the soil and to stabilize heavy metals after cooling within a solidified vitreous mass	Permanent remedy with good long-term effectiveness, potential volume reduction of materials, products with potential reuse options, wide application range	Costly, big power loss, off gases may be created and must be treated, not suitable for large area repair
	Electrokinetic remediation	Application of electrical current on two sides of the electrolytic tank containing saturated contaminated soil	Applicable for saturated soils with low groundwater flow, short repair time, low energy consumption, complete repair	Limited treatment depth, any heterogeneity of the soil body decreases the effectiveness of the method
	Thermal treatment	Heating of the contaminated soil via steam, microwave, and infrared radiation to volatize the pollutant without combustion of the media or contaminants	Simple process, devices with mobility, effective extraction and recovery of mercury, and safety	High capital costs, effectiveness only at rather high total soil mercury contents, requires gas emission control and specialized facilities, easy damage of soil structure
Chemical remediation	Chemical stabilization	Addition of immobilizing agents to the contaminated soil to decrease the mobility, bioavailability, and bioaccessibility of heavy metals in soil	Relatively cost effective, simple, and rapid remediation approach	Cannot remove heavy metals from soil, change the physicochemical properties of soil
	Solidification/ stabilization	Stabilization refers to a process of adding reagents to the contaminated soil to convert a toxic waste to a physically and chemically more stable form. Solidification is a process that encapsulates the waste materials in a monolithic solid of high structural integrity.	Relatively low cost, easy use, comprehensive strength, and high resistance to biodegradation, good engineering applicability	Increased volume of the treated material, long-term monitoring is needed
	Soil washing	Leaching of heavy metals from soil matrix with various reagents and extractants	Permanently removes metal contaminants from soil, a rapid method, highly effective method for cleaning up strongly contaminated soil	Soil structure deterioration and high cost, nutrients can be released simultaneously from soil during the remediation process, high costs and arduous working processes
Biological remediation	Phytostabilization	Use of plants with ability to decrease the mobility or/and bioavailability of a metal via certain mechanisms including adsorption by roots, precipitation, and complexation in the root zone	Cost effective, non-invasive, no secondary pollution	Limited repair capacity and treatment depth, long repairing cycle, plants and soil require long-term monitoring
	Phytoextraction	Uptake of contaminants from soil by plant roots and their translocation and accumulation in aboveground biomass		
	Phytovolatalization	Uptake and transpiration of metal into volatile form and its release into the atmosphere through stomata		
	Microbial remediation	Process of using microorganisms (i.e., bacteria, fungi, and algae) to induce adsorption, precipitation, oxidation, and reduction of heavy metals in soil		
	Microbial assisted phytoremediation	Assistance of plant growth promoting bacteria together with phytoremediation		

1.4 THE HPSS SYSTEM

As above stated, the S/S method presents several drawbacks when used to stabilise contaminated matrices. This is principally due to its unreliability to maintain the binder starting conditions with time, basically due to the natural damages occurring, which may reduce its effectiveness in a long-term period (Al-Tabbaa and Evans, 1996). MAPEI has engineered this method developing an ex-situ High Performance Solidification/Stabilisation Technology (HPSS). The ex-situ method permits to overcome the problems related to excess moisture, soil inhomogeneity, presence of debris, and deep contamination (Mulligan et al.,

2001). The method entails to transform the contaminated matrix in a durable and eco-friendly granular material having excellent mechanical features among which high density, low porosity and high mechanical strength. These properties considerably lower the heavy metal leaching. Surico et al. (2003) performed a 100-year period model, demonstrating that the cumulative leaching was far below the reported limits of the Dutch Building Material Decree (VROM, 1999). As the final product is conceived to be reused, the method permits to limiting waste soil dumping, supporting soil reclamation and reuse as well as reduce contaminated brownfield remediation costs. (Scanferla et al., 2009). The granules production phase scheme is reported in **Fig.6.**

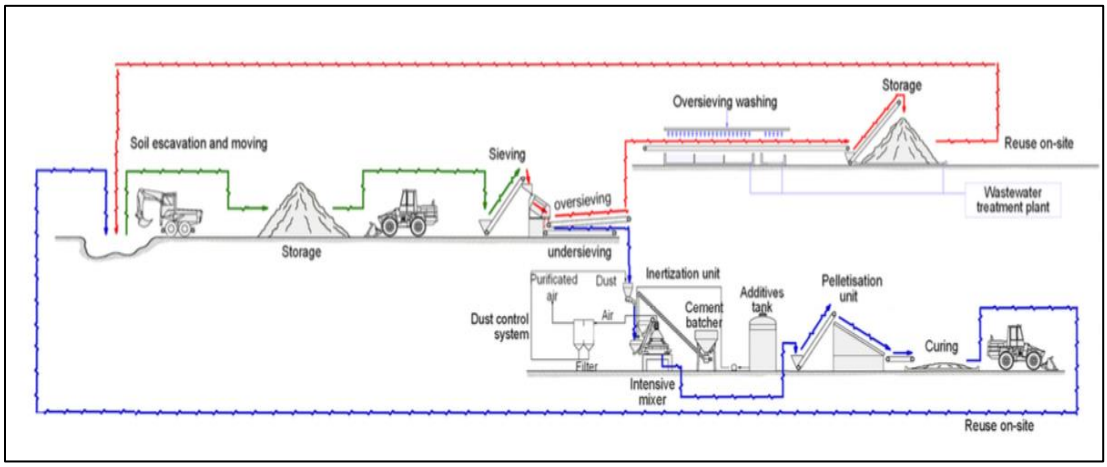

Fig. 6: *Scheme of the HPSS granulation process. [http://www.mapintec.it/pdf/brochure.pdf]*

The process basically consists in the following steps:

1) Sieving of the excavated material. The contaminated material is excavated and sieved using 4 mm as diameter threshold value. Then, two fractions are obtained, having a diameter > 4 mm and < 4 mm, respectively. The former is just washed with tap water and immediately reused. The wastewater produced is as well treated to be reused thereafter. The latter fraction undergoes to further steps of treatment as it is formed by contaminated fine particles of silt and clay.
2) Treatment of the fine material using the Mapei HPSS Process. The material is sent to a rolling-plate system in which the pellets are formed mixing together contaminated soil with Portland cement, water and two superplasticizers. The typical used formulation is: 73 % of soil, 27 % of Portland cement, 2 % of superplasticizers, and 3-5% of water (Contessi et al., 2019). The two superplasticizers are called: Mapeplast ECO 1-A and Mapeplast ECO 1-B. The first one is a hydrophobic additive that is used to decrease

water adsorption (usually in concrete), the second one is an acrylic-based superplasticizer that is used to better disperse cement particles (Contessi et al., 2019). Together they permit to lower the W/C (Water-Cement) ratio to values < 0.4. Modulating the rolling-plate inclination and speed, the diameter of the particles may be changed. The final product (**Fig. 7**) is than cured for 28 days and thereafter reused as excavation filler.

Application of this method to two sites contaminated by heavy metals revealed that the system gave pellitized materials having mechanical strength comparable with those of mixed gravel (Surico etl al., 2013). Moreover, the stabilised material showed a drastic effectiveness on reducing the concentrations of leached heavy metals. Also, Scanferla et al. (2009) observed several physicochemical, mechanical, ecotoxicological advantages in a contaminated soil stabilised with HPSS method. Indeed, leaching tests never exceeded regulatory limits for As, Cd, Hg or Pb.

Contessi et al. (2019) observed a drastic reduction on the concentration of leached lead from the Bagnolo Mella soil pelletized with CAC and OPC, obtaining better results in the first case.

***Fig. 7**: Final product after the pelletization process.*

1.5 CALCIUM ALUMINATE CEMENT (HYDRATION MECHANISMS AND REACTIONS)

Calcium aluminate cements (CACs) are produced by using limestone and bauxite. This latter is the principle source for its alumina content. The clinker is obtained by charging bauxite and limestone in an open-hearth furnace and heating it at 1450 °C. The fused material is placed in moulds and cooled. After cooling, the moulds are crushed and ground in ball mills. Scrivener and Campas (1998) divided them in four types, depending on their alumina content (**Table 3**).

Table 3: *Types of Calcium Aluminate Cements [Scrivener and Campas, 1998]*

	Composition (%)			
Grade	**Al_2O_3**	**CaO**	**SiO_2**	**Fe_2O_3 + FeO**
Standard/low alumina	36-42	63-42	3-8	12-20
Low alumina/low iron	48-60	36-42	3-8	1-3
Medium alumina	65-75	25-35	<0.5	<0.5
High alumina	>80	<20	<0.2	<0.2

The main anhydrous phase of all types of CAC is monocalcium aluminate (CA), following by CA_2 (grossite). A high alumina CAC cement contains approximately 60 % of CA and 40 % of CA_2. This type of cement is mainly used in refractory concretes, since their capacity to support high temperatures, but they may be also used in combination with other binders for obtaining rapid setting and drying properties (Scrivener and Capmas, 1998).

Contrary to other cements, the hydration process of the CAC depends upon the temperature at which it occurs. The hydration reaction is based on two reactions, that is, the dissolution of the anhydrous phases, that is, CA and CA_2, and the precipitation of the hydrates. The hydration products strongly depend on the temperature at which the reaction happens as well as, the type of other minerals present in the sample. Gosselin (2009) reported the different hydration reactions occurring at different temperatures. At temperature below 15 °C, CAH_{10} (**Fig.8**) is formed (**reaction 2**), whilst between 15 and 27 °C, CAH_{10} and C_2AH_8 coexist. When the system is exposed to temperature higher than 27 °C, C_2AH_8 and AH_3 (this latter formed in a gel form) dominate (**reaction 3**). If the hydration temperature is increased above 40 °C, the conversion reaction (**reaction 4**) may take place. This reaction consists on the conversion between the hexagonal phases (i.e. C_2AH_8 and CAH_{10}) to a cubic phase, called C_3AH_6, having a structure ascribable to that of hydrogarnet (**Fig. 9**).

$CA + 10\ H \rightarrow CAH_{10}$ (**2**)

$2CA + 11\,H \rightarrow C_2AH_8 + AH_3$ **(3)**

$3CA + 12\,H \rightarrow C_3AH_6 + 2\,AH_3$ **(4)**

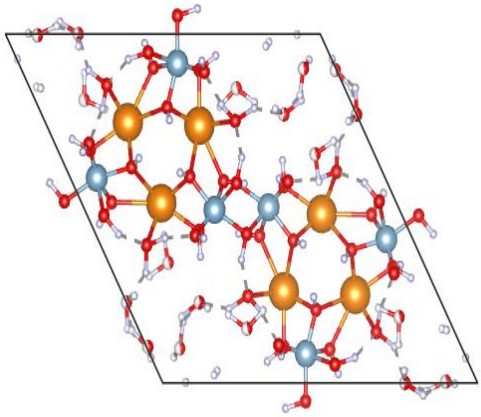

Fig.8: *Structural model of the CAH_{10}. It has a hexagonal crystal system having a= 1.63 nm and b= 0.83 nm. Ca atoms: blue, Al atoms: orange, O: red, H: white. The visualisation is achieved with VESTA package.*

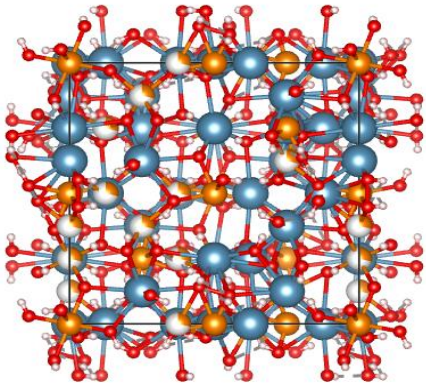

Fig.9: *Structural model of the C_3AH_6. It has a cubic crystal system having a= 1.245 nm. Ca atoms: blue, Al atoms: orange, O: red, H: white. The visualisation is achieved with VESTA package.*

C_2AH_8 and CAH_{10} are metastable products, and they may transform in C_3AH_6 even at room temperature after several years (**reaction 5, 6,7**) (Guirado et al, 1998). Concerning **reaction 6,** Rashid et al. (1994) reported that C_2AH_8, formed from CAH_{10}, acts as nucleating agent for C_3AH_6 growth.

$3CAH_{10} \rightarrow C_3AH_6 + 2AH_3 + 18\,H$ **(5)**

$2CAH_{10} \rightarrow C_2AH_8 + AH_3 + 9H$ **(6)**

$3C_2AH_8 \rightarrow 2\,C_3AH_6 + AH_3$ (gibbsite)$+ 9H$ **(7)**

The AH_3 (alumina gel) is formed together with C_2AH_8 and changes with time, and with temperature rise, from amorphous state to form hexagonal crystals of gibbsite (Taylor et al., 1997).

The conversion reactions produce more porosity and permeability, decreasing the strength of the final product (Bendsted, 1993). Indeed, the two hexagonal phases and AH_3 are the main phases giving strength to the material at ordinary temperatures. Regardless, conversion effects may be counterbalanced keeping the water/ratio as low as possible (indicatively 0.4). As observed in **reaction 7**, the conversion reaction produces a water release that may enhance the hydration of more anhydrous phases producing more alumina gel that might again decrease the porosity, lowered by C_3AH_6 formation. Regardless, Bendsted (1993)

reported volume decreases of 47 and 75 % when hydrogarnet is formed from CAH_{10} and C_2AH_8, respectively. It is important to specify that C_3AH_6 is not a weak binder as when directly formed it may give good mechanical strength to the final material (Taylor, 1997). The real issue in the conversion case is due to the porosity increase.

With a S/S insight, CAC cement may be used to stabilise contaminated soils (Contessi et al., 2019; Navarro et al., 2013).

1.5.1 CAC + CALCIUM SULPHATE BINARY SYSTEM

This admixture is well documented as well as largely used in the field of building chemistry. The system hydration promotes the formation of ettringite ($3CaO \cdot Al_2O_3 \cdot 3CaSO_4 \cdot 32\ H_2O$) (**Fig. 10**) and calcium monosulfoaluminate hydrate ($3CaO \cdot Al_2O_3 \cdot CaSO_4 \cdot 14\ H_2O$) (**Fig. 11**). The first one is characterized by having a trigonal crystal structure composed by columns and channels. Columns consists of $[Ca_6Al_2(OH)_{12} \cdot 24H_2O]^{6+}$ groups, and channels of $[(SO_4)_3 \cdot 2H_2O]^{6-}$ groups, resulting in a needle-like crystal. The second one is an AFm product with one sulfate group in the interlayer of a platy structure (Chrysochoou et al., 2006). Ettringite is generated when gypsum reacts with CAC anhydrous phases according to **reactions 8** and **9**.

$3CA + 3CaSO_4 \cdot 2H_2O + 32\ H_2O \rightarrow 3CaO \cdot Al_2O_3 \cdot 3CaSO_4 \cdot 32\ H_2O + 2\ AH_3$ (**8**)

$3CA_2 + 3CaSO_4 \cdot 2H_2O + 41\ H_2O \rightarrow 3CaO \cdot Al_2O_3 \cdot 3CaSO_4 \cdot 32\ H_2O + 5\ AH_3$ (**9**)

The ettringite is important as heavy metal binder in the S/S method. It possesses a great stability when the temperature is below 60 °C and pH higher than 10.7. Its capacity to take up trivalent cations, such as Cr^{3+}, Ni^{3+}, and Co^{3+} in place of Al is well documented (Gougar et al., 1996). Furthermore, it can be exploited for immobilization of anions such as Cl^-, NO^{3-}, and metalloid oxyanions, like AsO^{3-}, CrO_4^{2-}, MoO_4^{2-}, VO_4^{2-}. Sulfate ions in ettringite may easily be replaced by anions of similar geometry and charge (Chrysochoou and Dermatas, 2006). Monosulfate as ettringite, may host oxyanions by replacement of the sulfate groups.

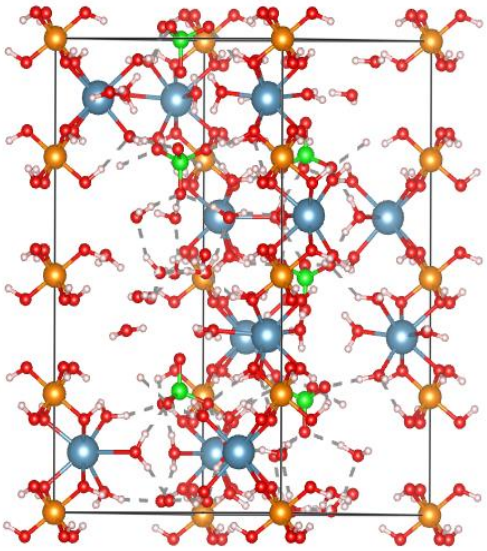

***Fig.10**: Ettringite trigonal crystal structure. Ettringite is composed by the columns that consists of $[Ca_6Al_2(OH)_{12} \cdot 24H_2O]^{6+}$ groups, and channels with $[(SO_4)_3 \cdot 2H_2O]^{6-}$. Ca atoms: blue, Al atoms: orange, O: red, H: white, S atoms: green*

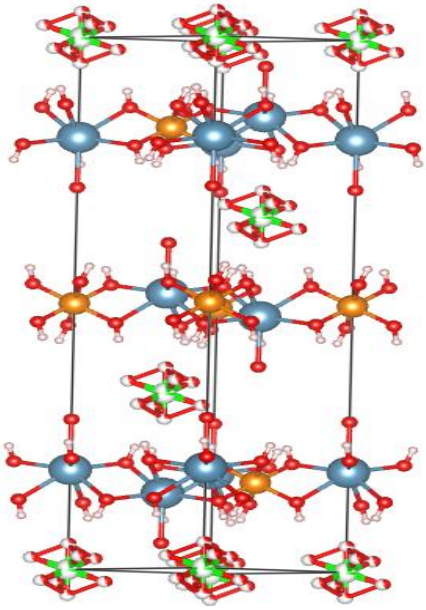

***Fig. 11**: Monosulphate (AFm-14) hexagonal crystal structure.*
Ca atoms: blue, Al atoms: orange, O: red, H: white, S atoms: green

1.5.2 CAC – CALCITE BINARY SYSTEM

This binary system is reported to be efficient in staving the conversion reaction off to occurring, thus preventing the theorical loss of strength (Cussino and Negro, 1980). Indeed, the preferential reaction is that forming monocarboaluminate ($3CaO \cdot Al_2O_3 \cdot CaCO_3 \cdot 11H_2O$). This phase belongs to the AFm family and it is characterized by a trigonal crystal structure based on distorted main $[Ca_2Al(OH)_6]^+$ layers containing $[0.5\ CO_3 \cdot 2.5\ H_2O]^-$ groups inserted between them (**Fig. 12**). The reactions forming monocarboaluminate are reported (**reactions 10** and **11**).

$CaCO_3 + 3CA + 17\ H \rightarrow C_3A \cdot CaCO_3 \cdot 11\ H + 2AH_3$ _____(**10**)

$CaCO_3 + 3CA_2 + 26\ H \rightarrow C_3A \cdot CaCO_3 \cdot 11\ H + 5AH_3$ _____(**11**)

The conversion reaction is prevented as monocarboaluminate is formed at the expenses of C_2AH_8 within a temperature range of 25-60 °C. However, CAH_{10} is still formed. The strength of the system is thus due to the presence of hydrated cement phases (alumina gel (AH_3) and CAH_{10}) as well as the presence of the monocarboaluminate phase.

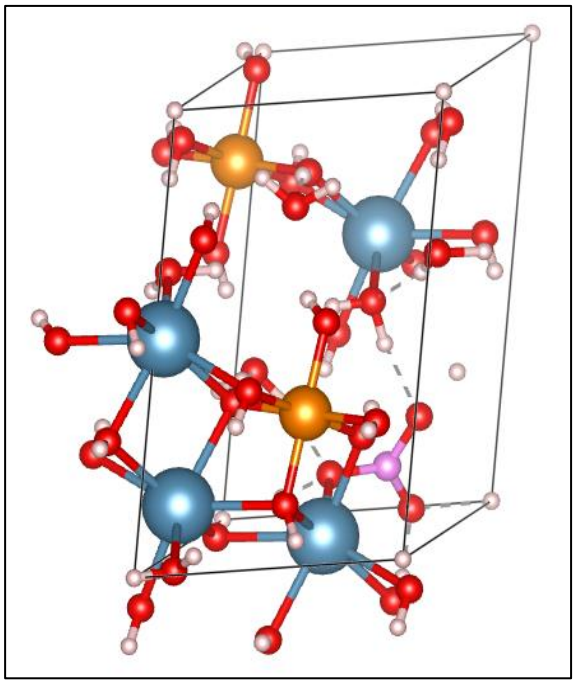

Fig. 12: *Monocarboaluminate trigonal structure. Ca atoms: blue, Al atoms: orange, O: red, H: white, C atoms: pink*

1.6 Ordinary Portland Cement (OPC)

Ordinary Portland Cement (OPC) is surely the most widely used cement worldwide because of its low cost and high availability. It is made by heating at 1450 °C the raw materials in a rotary kiln, forming the clinker phase. Once the cooling process takes place, the clinker is grounded with gypsum addition. The main components of the clinker are: alite ($3CaO \cdot SiO_2$), belite ($2\ CaO \cdot SiO_2$), tricalcium aluminate ($3\ CaO \cdot Al_2O_3$) and tetracalcium aluminoferrite ($4CaO \cdot Al_2O_3 \cdot Fe_2O_3$). The mineralogical composition of the clinker is reported in **table 4.**

Table 4: *Mineralogical composition of an OPC clinker*

Mineralogical phase	**Wt. % (Kurdowski, 2002)**
Alite (C_3S)	55-65%
Belite (C_2S)	15-25 %
$3\ CaO \cdot Al_2O_3$ (C_3A)	8-14 %
$4CaO \cdot Al_2O_3 \cdot Fe_2O_3$ (C_4AF)	8-12 %

The OPC hydration process consists in dissolution of anhydrous phases and precipitation of hydrates to form microcrystalline phases that give strength to the system because of their low solubility. The addition of water to the clinker permits to alite and belite to undergo hydration, forming calcium silicate hydrate gel (C-S-H gel) and portlandite ($Ca(OH)_2$)

according to **reaction 12** and **13**. In presence of gypsum, the reaction with C_3A forms ettringite (**reaction 14**) or monosulfate (**reaction 15**). In absence of gypsum instead, the hydration of C_3A forms tetracalcium aluminate hydrate [3 $CaO \cdot Al_2O_3 \cdot Ca(OH)_2 \cdot 12\ H_2O$] (**reaction 16**).

$3C_3S + 6\ H_2O \rightarrow 3\ C\text{-}S\text{-}H + 3\ CH$ (**12**)

$2C_2S + 4\ H_2O \rightarrow 3\ C\text{-}S\text{-}H + CH$ (**13**)

$C_3A + 3C\hat{S} + 26\ H \rightarrow 3C_6A\hat{S}_3H_{32}$ (**14**)

$2C_3A + C_6A\hat{S}_3H_{32} + 4\ H \rightarrow C_4A\hat{S}H_{12}$ (**15**)

$3\ C_3A + 12\ H + CH \rightarrow C_4AH_{13}$ (**16**)

Table 5 reports the mineralogical composition of a hardened hydrated OPC.

Table 5: *Mineralogical composition of a hydrated OPC [Bensted and Barnes, 2008].*

Mineralogical phase	**Wt. %**
C-S-H	50-60%
CH	20-25%
$C_6A\hat{S}_3H_{32}$	15-20 %

To enhance the C-S-H production and thus ameliorate the hardening of the cement, pozzolanic materials may be used. These class of materials are defined by the STM Standard Specification C618 as, “Siliceous or siliceous and aluminous materials which in themselves possess little or no cementitious value but will, in finely divided form and in presence of moisture, chemically react with portlandite at ordinary temperatures to form compounds possessing cementitious properties”. Pozzolanas may be either natural or artificial materials capable to harden in water when mixed with portlandite or with materials that can release it (Lea, 204).

Many pozzolanas materials are available and used to substitute OPC. Taylor (1997) reported that the most important are fly ash, ground granulated blast furnace slag (GGBS), natural pozzolanas and silica fume. Many of these are by-product materials of industrial activities as fly ashes and GGBS. Their utilisation is thus advantageous as the final product may have similar properties of a hardened OPC. When pozzolanic reaction (**17-18**) takes place, a consumption of portlandite is observed.

$CH + SiO_2 + H_2O \rightarrow$ C-S-H_____(**17**)

$CH + Al_2O_3 + H_2O \rightarrow$ C-A-H _____(**18**)

The increase of C-S-H fosters the final mechanical strength of the material. The main drawback on using pozzolanas as cement substituent is that kinetic of the pozzolanic reaction is slow and may take place even after some weeks after hydration starts. Regardless, when pozzolanic reaction occurs, beneficial effects on the final mechanical strength are reported because of the higher production of C-S-H gel. Furthermore, in the case of industrial by-products used as pozzolanas, releasing of contaminants may happen if treatment process does not take place.

1.7 Ground Granulated Blast-furnace Slag (GGBS)

GGBS is considered a latent hydraulic cement as it needs an activator (typically alkali) for employing its cementitious properties. It is a by-product of iron and steelmaking obtained by quenching the iron-slag. It is formed by quenching of molten GGBS at 1350 °C lowering the temperature to 800 °C. In this condition a glassy material is produced. Taylor (1997) reported that the glass structure is a continuous anionic network composed of Si and other electronegative elements, with the net charge balanced by Ca ions. The typical composition is reported in **table 6**, even though it may vary depending on the ores and the operating conditions.

***Table 6**: Typical composition of GGBS (Wang et al., 2019)*

Compound	**Wt %**
CaO	35 – 50 %
SiO_2	28-38 %
Al_2O_3	5-24 %
MgO	1-18%
S	0.4-2.5 %
Fe_2O_3	0.3-3 %
MnO	0.2- 3 %

Dewar and Anderson (1992) reported the potential benefits of using the GGBS as cement substituent. These include cost reduction, temperature reduction, improved resistance to

sulphate attack and other durability threats and the inhibition of expansion caused by alkali-reactivity.

GGBS was reported having some beneficial effects even when used in S /S method. For instance, Spence and Shi (2004) reported that it decreases the pH value of the initial pore solution at a value of approximately 11, which foster the precipitation of some heavy metals as sulphides. Sulphides are more insoluble than the corresponding hydroxides. Langton (1989) observed that the reducing conditions created by GGBS in a OPC-GGBS system utilised to stabilised radioactive alkaline salt solutions, promotes the reduction of Cr(VI) to Cr (III) precipitating it as $Cr(OH)_3$. Shi and Kan (2009) comparing different mineral admixtures added to MSWIFA, observed that GGBS showed better performances for improving the compressive strength and immobilizing heavy metals.

1.8 Municipal Solid Waste Incinerator (MSWI) and Fly Ash generation

With the world population that is expected to growth up to 9 billion in the next 30 years (UN, 2019), more and more wastes will be produced worldwide. Landfills may not be a good solution to treat these wastes as available land is not endless, and because of the environmental threats that the landfill brings. In the last years, more and more countries adopted Municipal Solid Waste Incinerators (MSWI) as a method to reduce the waste volumes (by up to 90 %) as well as to produce thermal energy by burning the wastes. Hazardous waste incineration entails a process involving exposure of the waste materials to oxidizing conditions at a high temperature, usually higher than 900 °C. A similar temperature is fundamental to oxidise all the organic matter not producing unwanted toxic by-products such as dioxins and furans. As a result of these conditions though, two main types of residues are produced, called Bottom ash (BA) and Fly ash (FA). Huber et al. (2018) estimated that Europe produces about 2.1 million Mg of FA each year, that is, 4.2 Kg/y per capita.

Whereas bottom ash (BA) consists on the non-combustible materials (i.e metals and glass) that remain as solid collected at the outlet of the combustion chamber in a quenching tank, Fly ash (FA) are all types of finely-sized ash and sorbent material collected in APC system (Chandler et al., 1997). In particular, fly ash consists in the particulate matter transported from the combustion chamber and removed from the flue gas stream prior to the addition of any type of sorbent material. These are characterized by presenting great amounts of volatile compounds (i.e. heavy metals and salts) due to volatilisation and subsequent condensations as well as concentration phenomena acting during combustion (Chandler et

al., 1997). Studies reveal that these ashes are managed in two different ways: either disposed in landfills or salt mines (In China more than 80 % of MSWI residues ends up in landfills (Li et al.,2004)), or be reused as raw materials. As regards to the first option, Jacob et al. (1995) stated that the chemical reactions taking place over residence times of years of MSWIFA in a landfill cannot be controlled or predicted accurately.

Concerning the reuse option, several studies reported that treated and stabilised MSWIFA and BA may be used as:

1) Road-pavement (Ma et al., 2007; Nishida et al.,2001; Mulder, 1996)
2) Glasses, Glass-ceramic and ceramics (Haiying et al.,2007; Rawlings et al., 2006; Kim et al., 2003)
3) Adsorbent for removing dyes from wastewater ((Gupta et al.,2005; Shim et al., 2003)

Fig. 13 illustrates a scheme of the incineration processes taking place in a MSWI. It typically consists in 6 different sections:

1) A waste receiving and storage area
2) A waste feed system to charge the incinerator
3) A boiler which convert the heat of combustion to usable energy by transferring heat from gases to water, then used to produce electricity by means of steam driven turbines.
4) An air pollution control (APC) system
5) An ash handling system

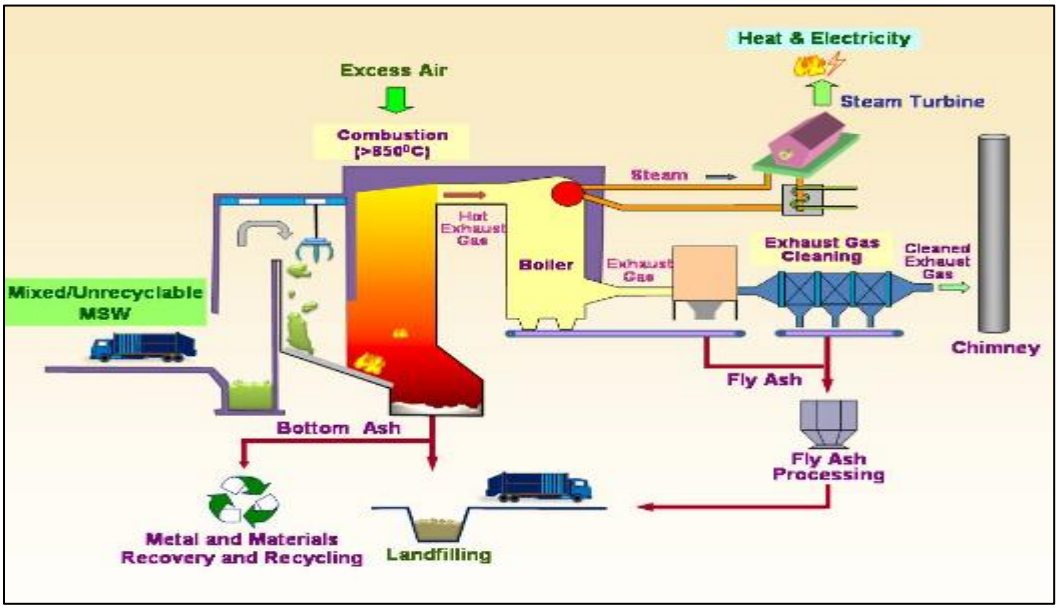

***Fig.13**: Typical procedures applied in a MSWI (source: Environmental Protection department of Hong Kong)*

In a MSWI the wastes are continually loaded into the furnace characterized by having a temperature of at least 850°C to up 2000 °C, and the wastes have a residence time of approximately 2 seconds. For preventing both furan and dioxin production, the oxidating condition are maintained with an air flow. Bottom ash are produced in the combustion unit whereas the fly ashes are produced in both the APC systems and in the boiler. In this latter case, the fly ashes are particularly enriched by heavy metals that volatilise from the burned waste and condense in the boiler's surface. This ash is periodically removed as it acts as an insulator reducing the heat transfer rates (Chandler et al., 1997). The material leaving the heat recovery system consists on solid particulate matter, vapour forms of metals and organics and gaseous products of combustion. These are then treated with APC. Modern incinerators adopt three types of APC, that is:

- Wet systems are usually employed downstream of a dry system. They consist in a vessel containing a bed of granular or fibrous materials which trap the particles in the gas, then washed using water, lime slurry and caustic for removing soluble salts. The method produces a stream of fly ash (that are those not intercepted by the bed) which is collected upstream of the acid gas cleaning process (generally by an ESP unit) and a stream of acid scrubber effluent which is enriched by salts and heavy metals (Chandler et al., 1997). The method is not largely used as produces a wastewater enriched in salts and heavy metals difficult to handle.
- Dry system which may be made with an electrostatic precipitator or fabric filter. Powdered lime is injected in a reactor chamber into the flue gas stream before the particles be separated in a different collection unit that may be either an electrostatic precipitator or fabric filter.

  Concerning the electrostatic precipitators (ESP), the process consists of a series of highly charged electrodes through which the gas passes. The electrodes impart a negative charge to the particles present in the gas that are then attracted by a collector electrode placed adjacent to the electrodes. Thereafter, the particles are gathered into a hopper by rapping the collectors.

  The fabric filter consists instead of a woven bag filter system to handle the particulate matter and dust particles. They are basically a set of bags which allow the passage of gases, adsorbing particulate matter present in the gas. The performances are usually better that that of the ESP (Chandler et al., 1997).
- Semi-dry systems are similar to the dry systems, but lime is mixed with water and injected into the flue-gas as a slurry.

These clean-up processes collect fly ashes produced during the waste incineration. The ashes being generated present a great variability that depends on the composition of the burnt waste, the operational conditions and type of incinerator (He et al., 2004). Leaching tests performed on untreated semi dry and dry fly ash revealed that soluble salts (e.g. chlorides and hydroxides of calcium, sodium and potassium) and metals (in particular, lead) can easily be released. Chandler et al. (1997) reports that lead can form complexes with chlorides increasing its solubility. The leachability of fly ash is strongly affected by the APC being used in the MSWI plant. In fact, the residues from wet scrubbing process contain less soluble salts than that derived from dry and semi dry processes as the former underwent to a washing process. Thus, wet scrubbling fly ash are less prone to release contaminants.

Fly ashes are enriched by many volatile heavy metals such as Zn, Cd, Cr, Cu, Hg, Ni and Pb as well as chlorides salts (Eighmy et al., 1995). This is due to the vaporization of these elements during the combustion together with their adsorption on the fly ashes surface. The concentration of these elements in the sample varies seasonally and deeply depends on the type of waste be incinerated (Eighmy et al., 1995). **Table 7** reports the conditions at which the metals are produced during the incinerator process as well as them partition between bottom ash and fly ash.

Table 7: *Sources, speciation and distribution of heavy metals in MSWI. [Chandler et al., 1997]*

Element	**Source in waste**	**Speciation after incinerator**	**Partition FA/BA**
Mercury	Thermometers, barometers, diffusion pumps, batteries, fluorescent light tubes, dental alloys, dyes.	$HgCl_2$	BA: 2%; FA: 13%, 75% vapour form (removed from gas steam after APC with activated carbon)
Cadmium	Rechargeable Ni-Cd, dyes and plastic dyes, screws	$CdCl_2$	BA: 20%, FA: 80%
Zinc	Paper, plastic, wood	$Zn(OH)_2$, $ZnCl_2$	BA: 65%, FA: 35%
Lead	Lead acid batteries, pigments, plastics.	$PbCl_2$	BA: 70 %; FA: 30 %
Arsenic	Wood, alloy, special semiconductor.	$AsCl_3$ or oxides	BA: 60%; FA: 40%

Antimony	Special alloys, btteries, cable sheathing, glass, paints	Sb_2O_3, $SbCl_3$	BA: 50%; FA: 50%

The main problem associated with the FA production is that heavy metals are leached easily and the concentrations in the leachate solution usually exceed the regulatory limits (Shim et al., 2005) Bottom ash instead does not contain volatile heavy metals in great concentrations.

1.9 TREATMENT METHODS APPLIED TO MSWIFA

Different treatment methods have been reported as useful to treat MSWIFA. Quina et al. (2008) classified them as: separation process, solidification/stabilisation and thermal methods. All the three method have been defined previously, thus in the following section the reported outcomes using the different methods, based on the literature review, are reported.

1.9.1 WASHING PROCESS

As previously reported, MSWIFA resulted associated with high concentration of Cl salts and heavy metals. Thus, the washing process has the purpose to reduce the concentration of these unwanted compounds by using a liquid solution as leachate. Jiang et al. (2009) obtained that Ca, K, Na and Cl were removed with an efficiency of 72.8 % (minimum). Other applied method consisted in using CO_2 bubbling. This method performed by Ito et al. (2008) has revealed to enhance the insoluble Cl recovery from FA. Both acid and neutral water can be also applied. While the former method is neither economically nor environmentally suitable, the latter fosters the release of heavy metals (Kirby and Rimstidt, 1994), and the pH value is to be modulated adding chemical additives (Zhu et al., 2009). Eighmy et al. (1995) observed a drastic decrease of phases on a sample washed with water with respect to the untreated sample, meaning that most of the mineralogical phases characterizing MSWIFA are salts such as halite and sylvite. Besides, Wang et al. (2001) observed that after washing, new phases of calcium-containing aluminosilicates are formed, and these may contribute to the heavy-metals stability.

1.9.2 LEACHING PROCESS

The recovery of heavy metals using different chelating agents has been assessed on the basis of the literature review. Using chelating agents has the advantage that is not a pH dependent method (Youcai et al., 2002). EDTA showed good recovery capacity for Cu and Pb.

1.9.3 STABILISATION/SOLIDIFICATION METHOD

Lam et al. (2010) reported that due to the high concentration of salts in the MSWIFA, S/S method is not suitable for treating such a material. Kikuchi (2001) stated that the addition of MSWIFA for clinker production provokes a shorten of the setting time as well as a workability worsening. Derie (1996) tested a 4-step S/S process consisting in the elimination of the alkali chlorides, phosphoric acid addition, calcination, and solidification with cement. Applying this process, the threshold limits for the heavy metals in the leachate, after having conducted a leaching test, were respected. Mangialardi (2003) observed that the pH reduction obtained by acid addiction promoted the precipitation of aluminium oxide permitting the adsorption of Cd, Pb, and Zinc on its structure.

Aubert et al. (2004) observed that if MSWIFA are treated, the S/S method can be effectively applied with the addition of up to 50 % of FA to the binder and maintain acceptable mechanical properties. Despite this, the long-term durability has not been determined yet. Indeed, given the high reactivity of the MSWIFA, unexpected heavy metal leaching may occur when the structure undergoes deterioration (Triano and Frantz, 1992).

1.9.4 VITRIFICATION

The MSWIFA are heated at a temperature of approximately 1400°C forming a melted slag as final product. The drawback of this method is surely the high cost associated to guarantee the heating process. Furthermore, Lam et al. (2010) reported that leaching phenomena from the matrix may occur during melting. Regardless, Izumikawa (1996) observed a 100 % heavy metals removal efficiency in vitrified FA. Sakai and Hiraoka (2000) reported that smelted slag may be reused as resource (e.g a non-ferrous smelting material).

1.10 INSTRUMENTAL ANALYSIS THEORY

A brief introduction of the instruments being used in this thesis is here reported.

1.10.1 X-RAY POWDER DIFFRACTION ANALYSIS (XRPD)

X-ray diffraction is a widely used technique based on constructive interference of monochromatic X-rays and a crystalline sample. X-rays are produced using an x-ray tube in which a filament is heated emitting electrons, that are then accelerated to the anticathode (usually made of Cu and Co). Here, if electrons have the right energy, they may dislodge the inner-shell electrons inducing the emission of a characteristic x-ray spectrum which is partially monochromatized and collimated onto the powder sample. If the geometry of the incident X-ray impinging the sample satisfies the Bragg Equation ($n\lambda = 2d \sin\theta$, where n is a integer number, λ is the X-ray wavelength, d is the distance parallel lattice plans, and θ the angle between incident beam and the lattice planes) the "reflected" x-ray produces a peak in the diffractogram. The powder sample (**Fig. 14**) is fixed between the sealed x-ray tube and the detector which both perform a movement of an angle θ with respect the sample (θ- θ mode). This technique permits to quantify the amounts of mineral phase by modelling the XRD pattern using the Rietveld analysis as well as to perform kinetic analysis.

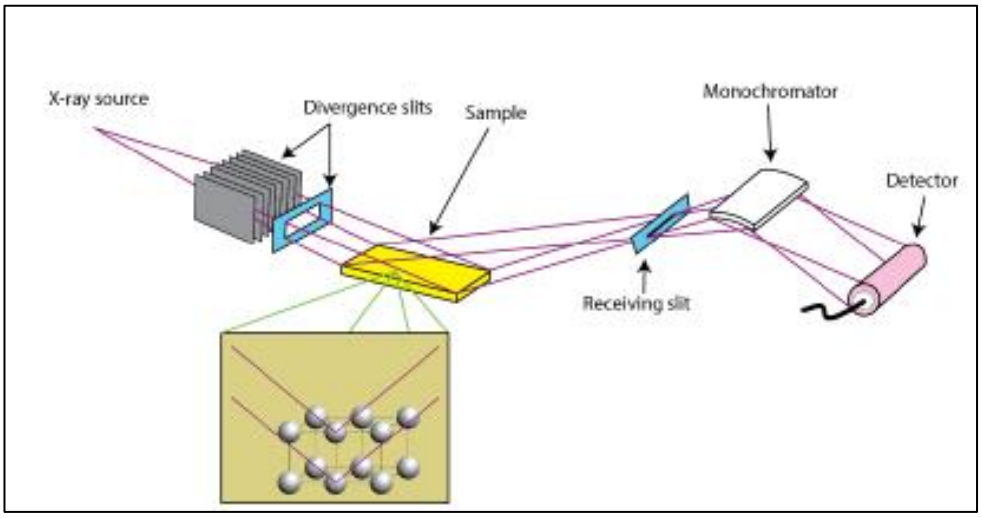

Fig. 14: *Classical XRD setup. The scheme illustrates the main components of the instrument.*

1.10.2 Scanning Electron Microscopy coupled with Energy Dispersed X-ray spectroscopy (SEM-EDX)

This technique is based on the use of a focused beam composed of high-energy electrons to obtain different information of the sample, such as texture, chemical composition, and crystal structure. By performing this analysis, 2-D images are obtained. Using SEM, it is also possible to get semi-quantitative chemical analysis using EDX. This latter is based on the interaction of the analysed sample with an electron beam to produce X-rays. The EDX detector contains a Si (Li) (or other materials) crystal that can convert individual X-rays

coming from the sample into electrical voltages. These electrical pulses correspond to the characteristic x-ray of the element that emitted the x-ray. The technique is particular useful to perform spot analysis in few seconds, as well as to carry out semi-quantitative analysis.
To enhance the peak resolution of elements as well as sensitivity of trace elements, Wavelength-dispersive spectroscopy (WDS) may be used in place of EDX. The measurement of an element abundance is a multi-step process in which 1) an atom on the sample produces x-rays 2) X-rays be diffracted by a crystal spectrometer to a detector 3) X-rays are converted to photoelectrons 4) these latter produce electrical signal with a magnitude proportional to the abundance of the element.

1.10.3 Inductively Coupled Plasma Mass Spectrometry (ICP-MS)

In the ICP-MS (**Fig. 15)** the ions generated in the plasma are directed into a quadrupole mass analyser with a resolution of mass from m-1 or m+1 (where m+1 refers to an ion with a mass one unit greater than that of the molecular ion, and m-1 a mass one unit lesser than that of the molecular ion). In order to extract the ions from the plasma into the vacuum environment of the mass analyser, the instrument is provided by two water-cooled nickel cones. The first one is positioned in the tail plume of the plasma allowing an expanding jet of material to pass through a 1.0 mm orifice into an intermediate vacuum region. A skimmer cone then permits to sub-sample this jet, carrying a small proportion of the ions into a higher vacuum region where they are accelerated into a quadrupole. The instrument can have two MS section, and the first, called “Quadrupole dynamic reaction cell” permits to remove isobaric interfering species having the same m/z as analyte ion. This is permitted because the dynamic reaction cell contains reactive gas such as O_2 and its electric field selects lower and upper masses of ions to pass through the cell, whereas interfering such as Ar^+ , ArH^+, ArC^+, ArN^+ etc. can be reduced reacting with the reacting-gas.

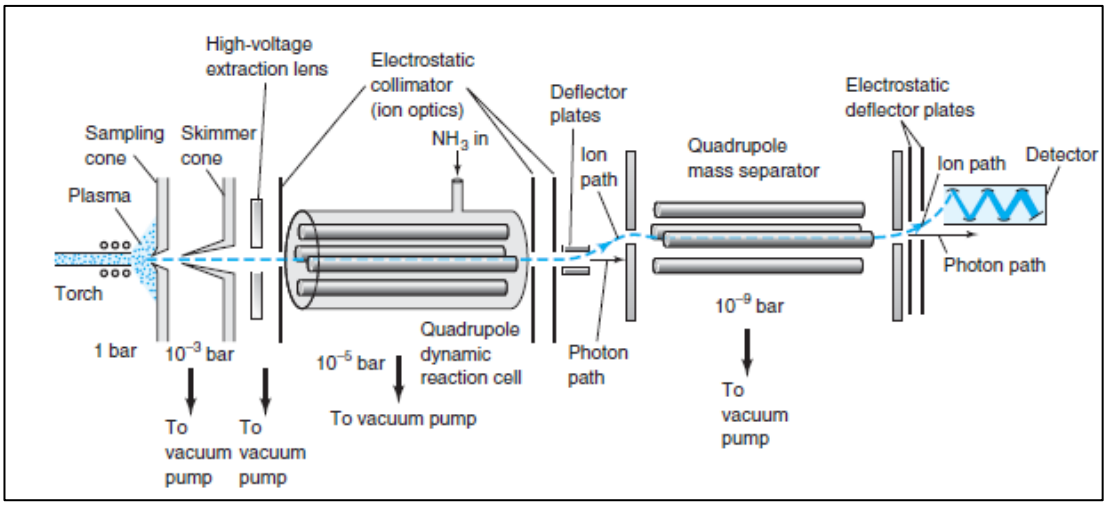

Fig. 15: *ICP-MS components set -up (source: Harris, 2016)*

This technique permits to achieve LOD values in the part per billion order or lower with the capacity to perform a multi-element and isotopic analysis.

2 PURPOSE OF THE STUDY

In the present study two different contaminated matrixes, a lead-contaminated soil coming from the brownfield of Bagnolo Mella, and a raw municipal solid waste fly ash (MSWIFA) were taken into account to study the effectiveness that the Solidification/Stabilisation method had using different binders.

With regards to the Bagnolo mella soil, a Calcium aluminate cement (CAC 70) was used. The issue of using this binder is given by the conversion process occurring at temperatures higher than 40°C. Aim of this part of the project is to understand whether the conversion reaction happen or not, and the effect that its occurrence could have on the material, when the contaminated soil is treated with CAC 70 at two different temperatures, that is 20 °C and 40 °C respectively, for a period of 28 days.

The purposes of the MSWIFA part are:

1) to study the raw MSWIFA under a mineralogical/chemical point of view.
2) to determine the chemical reactions occurring when the MSWIFA is respectively treated with an ordinary Portland cement, a calcium aluminate cement, and ground granulated blast-furnace slag.

3 MATERIALS AND METHODS

This section illustrates the experimental design adopted during the study as well as the used materials. In particular, the chapter is subdivided into two different sections, the first one concerning the soil of the former agrarian consortium of Bagnolo Mella, whereas the second one dealing with the municipal solid waste incinerator fly ash (MSWIFA).

3.1 BAGNOLO MELLA

The experimental design of this part of the thesis is conceived to obtain information on the effect that the curing temperature has on the CAC system, when this is present itself and combined with other matrixes. The investigation is made by using XRPD, SEM-EDX, and by performing compressive-strength analysis and leaching tests.

3.1.1 MATERIALS

A high-alumina cement (CAC 70) was used as binding material for all the considered samples. Its XRPD analysis is reported in **table 8**. CA (ICDD # 01-070-0134) was the main mineralogical phase along with CA_2 (ICDD # 23-1037) with a wt% equal to 50.6 and 38.9, respectively.

***Table 8**: Mineralogical composition of CAC 70.*

N	Phase	wt %	Error
1	Amorphous Content	10.36	0.35
2	CA	50.66	0.16
3	CA2 Grossite	38.98	0.12

The lead-bearing soil coming from the agrarian consortium of Bagnolo Mella was sampled and used for this experiment. The sample was collected from the surface to 1.5 meters depth, air-dried up to 10% weight/weight (w/w) moisture content and sieved at 2 mm prior to homogenization. A sample of soil collected outside of the contaminated area was considered as uncontaminated soil sample. This soil was collected at a depth between 15 and 35 cm, air-dried and sieved at 2 mm.

ICP-MS analysis was carried out for some selected elements (Pb, Se, Hg, Sn, As, Sb, Cu, Fe, Cd, Co, Zn, Ni, TI, Be, Cr, V, Mn and Al) in order to assess the chemical composition of the two considered soils.

The calculation of the enrichment factor (EF) (Qingjie et al., 2008) was carried out to ascertain the degree of contamination with respect to the background level, according to **Eq. 1**:

$$EF = \frac{\left(\frac{Cx}{Cref}\right)sample}{\left(\frac{Cx}{Cref}\right)Background} \quad \text{(Eq. 1)}$$

where C_x indicated the concentration of a certain element, C_{ref} the concentration of a reference element having no anthropogenic sources (i.e. Al), and Background is the geological background level. The limiting drawback of this method is that the enrichment factor for aluminium cannot be derived. Aluminium was considered as reference element as it is very improbable to have anthropogenic source of contamination, since it is almost insoluble under normal environmental conditions (pH 4.5-8.5) (Klöppel et al. 1997). Furthermore, ICP-MS analysis of the two samples of soil showed a similar aluminium concentration. As background level, the nearby soil was taken into account where no lead contamination was present. **Table 9** illustrates the classification method used to classify the type of pollution for the considered elements, according to Qingjie et al. (2008).

***Table 9**: Enrichment factor classification according to Qingjie et al., (2008)*

Class	Qualification of sediment	EF value (Qingjie et al., 2008)
0	Unpolluted	<1
1	Slightly polluted	1 < EF < 3
2	Moderately polluted	3 < EF < 5
3	From moderately polluted to strongly polluted	5 < EF < 10
4	Strongly polluted	10 < EF < 25
5	From strongly polluted to extremely polluted	25 < EF < 50
6	Extremely polluted	EF > 50

Using CAC 70 as binder, 4 different samples were prepared and named: sample 4, sample 3, sample 2 and sample 1 (**Table 10**). Two types of superplasticisers, named MAPEPLAST ECO-1 A and MAPEPLAST ECO-1 B, were added to decrease the amount of water needed. Mapeplast ECO 1-A is a hydrophobic additive that is used to decrease concrete water adsorption, whereas Mapeplast ECO 1-B is an acrylic-based superplasticizer that is used to better disperse cement particles. The water-to-solid ratio (w/c) was kept equal to 0.8 for the soil-containing samples (1 and 2), whereas a value of 0.4 was used for the samples without soil (3 and 4).

Total amount of 160 g for each sample were prepared mixing together the different components using a mechanical stirrer (Eurostar IK Labortechnik). Then, 140 g and 20 g were used to set up the monolithic samples and the cylinders (**Fig. 16**), respectively.

Table 10: *Mix proportion of designed samples.*

Used materials	Sample 1	Sample 2	Sample 3	Sample 4
% CAC 70	27	27	75	100
% Pb-contaminated soil	73	0	0	0
% uncontaminated soil	0	73	0	0
%gypsum	0	0	25	0
superplasticisers (g)	0.864	0.864	2.4	3.2
water/solid (w/c) ratio	0.8	0.8	0.4	0.4

The monoliths were used for carrying out the mechanical strength tests conducted after 28 days of curing, whereas the cylinders were used to perform SEM and XRPD analysis with a weekly periodicity. Four monoliths (15x15x60 mm) were casted for each sample, by pouring the obtained mixtures into Teflon moulds. Then, after the hardening process (approximately after 1 day), they were demoulded and two monoliths for each sample were treated at 20 °C and 40 °C for 28 days, respectively, in order to have a duplicate of each sample cured at different temperature.

Ten cylinders for each formulation were also prepared pouring the different mixes into cylindrical sample-holders. Five of them were cured at 20 °C and the others at 40 °C. Then, all the samples were analysed after 7, 14, 21, 28 and 35 days via SEM-EDX and XRPD.

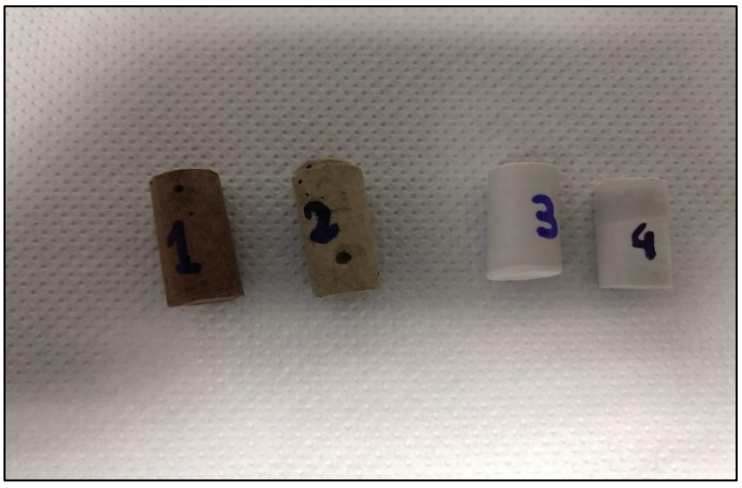

Fig. 16: *Demoulded cylindrical samples.*

3.1.2 INDUCTIVELY COUPLED PLASMA MASS SPECTROMETRY (ICP-MS)

ICP-MS analysis was conducted to determine heavy metal concentrations in eluates from leaching tests and on solid samples using a NexION 350D spectrometer (Perkin Elmer, Waltham, MA, USA), which was operated in standard mode, collision mode (Kinetic Energy Discrimination, KED) and reaction mode (Dynamic Reaction Cell, DRC). NIST-SRM 2711a (Montana II Soil) from NIST (National Institute of Standards and Technology, Gaithersburg, MD, USA) was used as a certified standard to validate the analytical methodology. All the analyses were performed in triplicate. All the instrumental settings are reported in **table 11**.

Table 11: *ICP-MS instrumental setting*

ICP-MS instrumental settings	
Component/Parameter	**Type/Value/Mode**
Nebulizer	Meinhard quartz microconcentric
Spry Chamber	Quartz cyclonic
Triple Cone Interface Material	Nickel/Aluminum
Plasma Gas Flow	18 L/min
Auxiliary Gas Flow	1.2 L/min
Nebulizer Gas Flow	0.96-1 L/min
Sample Uptake Rate	200-250 uL/min
Rf Power	1600 W
Collision Gas Flow (Helium)	4.3 ml/min
Reaction Gas Flow (Oxygen)	0.8 ml/min

3.1.2 SEM ANALYSIS

The microstructure of the specimens was studied by using a CamScan MX2500 with a LaB_6 source coupled with an energy dispersive X-ray analyser (SEM-EDX) in use at the Department of Geosciences (**Fig.17**). An accelerating voltage of 25 kV, high vacuum and spot size of 1 nm was used for obtaining backscattered electron (BSE) images. EDX spectra were acquired by means of the software EDAX SEMQuant Phizaf. The limitations of the EDX in distinguishing the Kα emission line of S (2.30 eV) and the Mα line of Pb (2.34 eV) were overcome with the use of a SEM coupled with a wavelength dispersive spectrometer (SEM-WDS). This was used on an ettringite particle of sample 1 as this method has significantly higher spectral resolution and enhanced quantitative potential with respect to EDX, because of the use of the following standards: FeS_2, $PbMoO_4$, $CaCO_3$, $CaMgSi_2O_6$ and $KAlSi_3O_8$. The prepared

cylinders cured at 20 °C and 40 °C were respectively demoulded after 7, 14, 21, 28 and 35 days and treated in an ethanol solution to stop the hydration reactions of the cement phases. Then, the sample was crushed by means of a hammer in order to obtain little fragments, thereafter, selected for conducting the SEM analysis. One or more fragments for each sample were impregnated with epoxy resin (**Fig. 18**) and dry polished using sandpapers with different granulometry. The polished specimens were coated with graphite to prevent surface charging for SEM analysis.

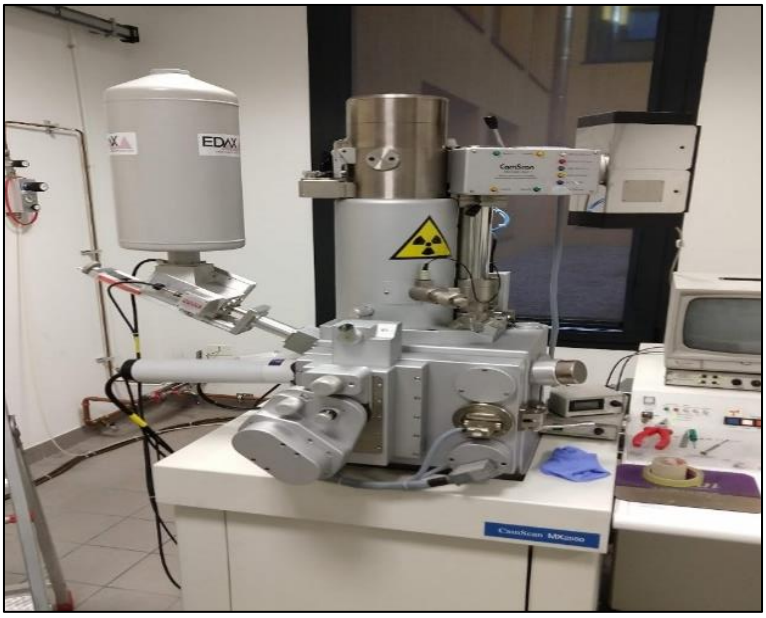

***Fig. 17**: SEM-EDS utilised for the analysis.*

***Fig.18:** Crashed cylinders samples numbered according the sample name impregned with epoxy resin before being analysed via SEM.*

Magnification of 20X, 50X, 200X, 500X and 1000X were adopted, to obtain both Backscattered electron (BSE) and secondary electron (SE) images. The particles were identified by comparing images acquired with BSE detector with the images of SE detector. A size distribution analysis of the grains of the Pb-bearing soil was carried out on a 20X BSE image using IMAGEJ. The "Analyze particles" tool was used assuming that the particles were circles, then the Waddel diameter was calculated according to **Eq. 2**. Waddel diameter corresponds to the diameter of a circle having the same area of the investigated particle.

$$Waddel\ diameter = \sqrt{\frac{4A}{\Pi}} \quad \text{(Eq.2)}$$

An EDX maps was also performed on sample 1 to obtain information about the association between particle sizes and element distribution as well as to observe the elemental distribution in the sample surface.

3.1.3 XRPD ANALYSIS

The demoulded cylinders respectively cured at 20 °C and 40°C were analysed via XRPD after 7, 14, 21, 28 and 35 days. Samples were powdered and then micronized in a micronizing mill, with ethanol to prevent hydration of cement phases and to yield the proper drying process (**Fig. 19**). Thereafter, 0.8 g of micronized sample was mixed with a 0.2 g of zincite (ACS Reagent, Thermo Fisher Scientific Inc., Waltham, MA, USA), used as internal standard, and homogenised by gentle grinding in a mortar. The sample was then transferred into a XRPD sample-holder (**Fig. 20**) and analysed. The instrument was an X'Pert PRO diffractometer coupled with a X'Celerator detector (anode: Co Kα, λ=1.79 Å) working in Bragg-Brentano geometry with a 2θ range 3°-85°. The X-ray source was operated at 40 kV and 40 mA. All the instrumental settings are reported in **table 12**.

Determination of mineralogical phases present in the different samples was carried out by means of the software High Score Plus v 3.0.5 (PANalytical B.V) using as databases both PDF-2 (Powder diffraction file, 2002) and COD-Oct 2014 (Crystallography Open Database, 2014). Quantitative Rietveld analysis were instead performed with Topas v. 2.1.

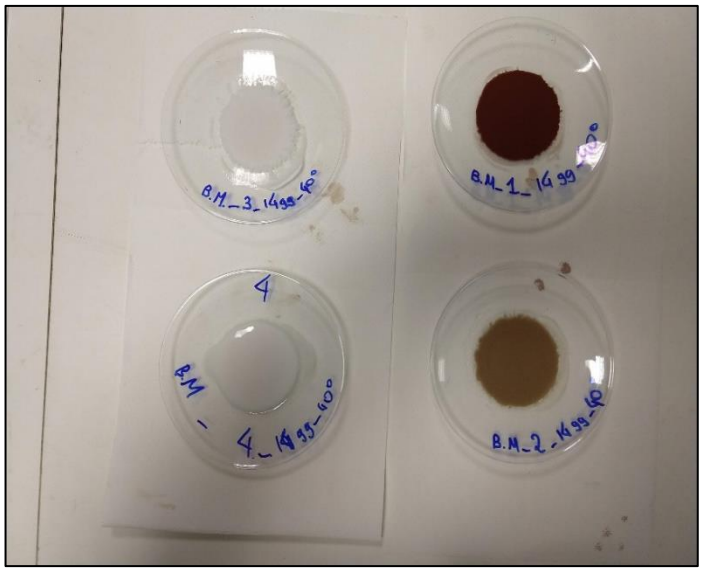

Fig. 19: *Micronized samples left to dry in glass watches.*

Fig. 20: *XRPD samples*

XRD instrumental settings	
Radiation source	Cobalt
Detector	X'Celerator detector
Geometry	Bragg-Brentano geometry
Optics	Soller slits 0.04 rad.; Bragg-Brentano^{HD}
2θ range	3-84°
Step size	0.017°
Time per step	100 s

***Table 12**: XRPD instrumental settings.*

A kinetic analysis on sample 4 was also carried out in order to determine the hydration evolution during the first 24 hours. The sample was prepared hydrating 3 grams of cement with 1.5 g of water, thus using a w/c ratio of 0.5. The sample was then transferred into a XRPD sample-holder and covered with a kapton layer (**Fig. 21**). Kapton was used because of its high mechanical and thermal stability, as well as high transmittance to X-rays. It is also relatively insensitive to radiation damage. The used instrument was an X'Pert PRO diffractometer with a PixCel detector (**Fig.22**) (Anode material: Cu Kα, λ=1.54 Å) working in Bragg-Brentano geometry with a 2θ range 6°-65°. The X-ray source was operated at 40 kV and 40 mA. The hydrating cement paste was monitored continuously during the first 24 hours after mixing with water, acquiring diffraction data with a total time per pattern of 20 minutes. Pattern acquisitions were continuously repeated to cover the 24 hours of hydration time. The acquired spectra were then processed with High Score Plus V. 3.0.5 using as databases both PDF-2 (Powder diffraction file, 2002) and COD-Oct 2014 (Crystallography Open Database, 2014).

Fig. 21: *Sample holder used for kinetic analysis performed on hydrated sample 4. The sample was covered by a Kapton layer.*

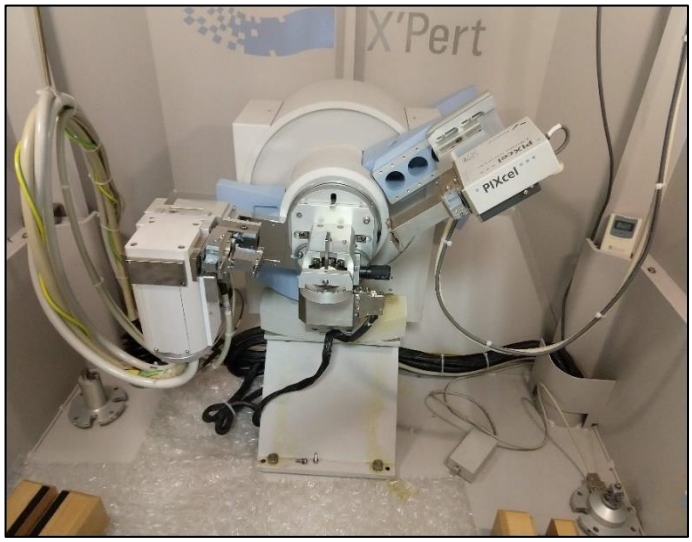

Fig. 22: *Diffractometer used to perform the kinetic analysis on hydrated sample 4.*

3.1.4 COMPRESSIVE STRENGTH TEST

Compressive strength test was performed on the samples after 28 days of curing.

Before starting the test, all the specimens were smoothed by means of sandpaper. Then, in accordance to UNI EN 12390-3 European standard, length (l), base (b) and high (h) of each parallelepiped were measured by using a digital calliper, and the samples were also weighted. Density (ρ) was thus calculated according to **Eq. 4.**

$$\rho = \frac{m}{V} = \frac{m}{l*b*h}$$ (**Eq. 4**)

The test was performed by applying the perpendicular force on the surface of each sample. 3 tests on each monolith were carried out, thus breaking it in 3 parts. Duplicated tests for each specimen were performed as 2 specimens for each sample were available. Six data for each sample were thus obtained. The material testing machine Galdabini Sun 2500 (**Fig. 23**), based on a hydraulic press, was used in this experiment. Unconfined Compressive Strength Data Acquisition Software was used for acquiring data. The material testing machine apply a compression loads in monotonic and cyclic mode. The load cell applied is 2500 N, and the instrumental precision of the machine is 0,5%. The final compression force ($F\perp$) was achieved upon the sample failed. Dividing this value by the superficial area (S) of the specimen, the compressive strength (σ) value was calculated (**Eq. 5**).

$$\sigma(MPa) = \frac{F\perp}{S}$$ (Eq.5)

The average of the three measurements were considered.

***Fig. 23**: Material testing machine used during the compressive strength test.*

3.1.5 LEACHING TESTS

Sample 1 has been exposed to three different pH values in order to determine to what extent the stabilised contaminated soil was able to resist once exposed to acid solutions. The considered pH values were: 7, 5.5 and 4.5. These pH values were taken into account as easily findable in the environment and, thus, to simulate what the behaviour would be, once the tested material is placed in the studied conditions. In fact, pH 7 is a neutral water pH, whereas 5.5 is the rainfall pH and pH 4.5 simulates the pH of an acid soil.

The buffer solutions were prepared using acetic acid at different concentrations to achieve the wanted pH values. Crushed monoliths of sample 1 resulting after the compressive strength test were used for this experiment. The fragments were furtherly grounded using a mortar and the particles having a diameter comprised between 1 mm and 2 mm were considered for the tests. Leaching tests were conducted in six different beakers (three for the samples cured at 20°C and three for the samples cured at 40 °C). The initial pH of each solution was tested using the HI 9829 multiparameter probe (HANNA Instrument). The water/solid ratio of the samples was kept equal to 20:1. The six solutions were thereafter stirred for 24 hours and the final pH was measured again. Eluates were filtered at 0.45 µm and acidified with HNO_3. The solutions were then analysed by ICP-MS. The following elements were thus analysed: Al, As, Ba, Be, Cd, Co, Cr, Cu, Fe, Hg, Mn, Ni, Pb, Sb, Se, Sn, Tl, V, Zn, Mo.

3.2 MUNICIPAL WASTE INCINERATOR FLY ASH (MWIFA)

The experimental design of this part of the thesis foresaw to determine the mineralogy of the MSWIFA as well as understand how it reacts when treated with different binders under a chemical point of view.

3.2.1 MATERIALS

MSWIFA was collected and stabilized with three different binders, namely Barbetti Portland cement CEM I 52.5 R, CAC 70 and ultrafine (3 µm) ground granulated blast furnace slag (GGBS). **Table 13** reports the different mixes used to prepare the three different samples. The formulations for FA-OPC and FA-CAC70 were established based on a study on a pilot plant process, whereas the last recipe was previously tested with coal FA by our research group.

Chemical characterization of the untreated MSWIFA was assessed via ICP-MS (NexION 350D spectrometer (Perkin Elmer, Waltham, MA, USA)) analysis. Untreated fly ash was analysed via XRPD in different days to test how the system reacted once exposed to ambient conditions and, in particular, to ascertain the mineralogical stability of the sample. The sample was grounded in a mortar (**Fig. 24**) and placed in a XRPD sample-holder and analysed. A quantitative investigation was also conducted on the untreated MSWIFA three months after the other analyses, using zincite as internal standard. The used instrument was an X'Pert PRO diffractometer coupled with a X'Celerator detector (anode: Co Kα, λ=1.79 Å) working in Bragg-Brentano geometry with a 2θ range 3°-85°. The X-ray source was operated at 40 kV and 40 mA. Determination of mineralogical phases present in the different samples was carried out by using the software High Score Plus v 3.0.5 produced by PANalytical B.V using as databases both PDF-2 (Powder diffraction file, 2002) and COD-Oct 2014 (Crystallography Open Database, 2014). Topas v. 2.1 was used to quantify the amounts of mineral phases by performing the Rietveld analysis. A kinetic analysis was also performed for all the considered samples using the X'Pert PRO diffractometer with a PixCel detector. A further XRPD analysis was also conducted after two months after hydration. The kinetic analysis was conducted in the same way as reported in par. 3.1.3 for sample 4 case.

Table 13: *Mix proportion of designed matrixes*

Used materials	FA-OPC	FA-CAC70	FA-GGBS
% OPC	20	0	0
% CAC 70	0	20	0
% GGBS	0	0	46
%MSWIFA	80	80	50
% $Na(CO_3)$	0	0	2.36
$Ca(OH)_2$	0.000	0.000	1.64
water/solid (w/c) ratio	1	1	0.8

Fig. 24*: fly ash mixed with zincite in the mortar*

4. RESULTS & DISCUSSION

The results concerning both the project of the lead contaminated soil of former agrarian consortium of Bagnolo Mella and the project of MSWIFA (Municipal solid waste incinerator fly ash) are presented in section 4.1 and 4.2, respectively. Experimental data obtained by ICP-MS, XRPD and SEM-EDX are described and discussed. Results of compressive strength are reported for the Bagnolo Mella case. Calcium Aluminate Cement (CAC 70) was the only binder investigated for stabilising the Bagnolo Mella soil. The focus of this study was to verify the effectiveness of CAC 70 binder in stabilising the contaminants in a long-term period.

For the MSWIFA case study, different binders were investigated, specifically CAC 70, OPC and GGBS. The aim of this part of the thesis was to verify the chemical interaction between MSWIFA and the binders previously cited.

4.1 BAGNOLO MELLA

The results regarding the Bagnolo Mella soil are here presented. The following section will firstly deal with the untreated soil characterization and, thereafter, with the stabilised samples. In particular, SEM, XRPD, leaching tests, and Compressive strength results will be presented and discussed

4.1.1 THE CONTAMINATED SOIL OF BAGNOLO MELLA

The analysis of the contaminated soil carried out via ICP-MS is reported in Appendix A together with the results for the uncontaminated soil (**Table A.1 and A.2**). The chemical composition of the contaminated soil was compared with the maximum concentrations allowed by Italian legislation (Ministerial Decree n. 152/06). The soil resulted highly contaminated by many metals and metalloids, and in particular lead resulted to be 400 folds higher than the limit reported in guidelines. In order to demonstrate that the contamination was caused by an anthropogenic source, the Enrichment Factor (Qingjie et al., 2008) was calculated.

Thus, according to the classification given by Qingjie et al. (2008), every element was classified, and the outcomes are reported in **Table 14**. By the calculation of the enrichment

factor, the soil resulted heavily contaminated by lead, selenium, mercury, tin, arsenic, antimony, copper and iron.

In **Fig. c1** in appendix C, the XRPD diffractograms of both contaminated and not contaminated soils are reported. The variances in terms of mineral composition between the two samples are remarkable. Such differences are related to the presence of anglesite, gypsum and jarosite, which are not present in the uncontaminated soil, as well as a 10 % more hematite in the contaminated one.

***Table 14**: Calculation of the Enrichment factor applied to the analysed elements into the soil*

Element	EF	Qualification of sediment
Pb	219.8	Extremely polluted
Se	551.3	Extremely polluted
Hg	32.8	From Strongly polluted to extremely polluted
Sn	26.0	From Strongly polluted to extremely polluted
As	14.9	Strongly polluted
Sb	14.0	Strongly polluted
Cu	5.5	From Moderaltely polluted to strongly polluted
Fe	5.4	From Moderaltely polluted to strongly polluted
Cd	5.0	Moderately polluted
Co	4.2	Moderately polluted
Zn	3.9	Moderately polluted
Ni	1.9	Slightly polluted
Tl	3.0	Slightly polluted
Be	0.6	Unpolluted
Cr	0.7	Unpolluted
V	0.8	Unpolluted
Mn	0.3	Unpolluted
Al	1.0	

These minerals are in fact the result of the past manufacturing activity, which provoked the contamination of the area. Other mineral phases typically encountered in soils as: quartz, dolomite, albite, calcite, clinochlore and muscovite, were detected in both soils.

In order to investigate the microstructure and the chemistry of the contaminated-soil particles, a scanning electron microscopy coupled with an energy dispersive X-ray spectroscopy (SEM-EDX) was performed on the contaminated-soil samples. The shape of the particles resulted to be irregular, as well as the size. Furthermore, by performing the particles analysis with ImageJ on the BSE image reported in Appendix B (**Fig. B.1**), it was possible to obtain the size distribution of the soil particles (**Fig 25**). Most of the particles presented a diameter of ~ 0.05 mm. It is to be taken into account that the soil underwent a sieving excluding the particle size under 2 mm. **Fig. 26** reports the distribution map of lead (in red)

and sulfur (in blue) obtained with the EDX analysis. The purple areas, reporting the combination between the above-mentioned elements, indicated the presence of either anglesite ($PbSO_4$) or galena (PbS), with the first mineral as most probable on the basis of the results obtained by XRPD analysis. A correlation between particle size and lead distribution was not significant as the purple areas were randomly distributed and not associated to a specific particle size. This observation permitted to determine that the smaller particles, having a higher surface area, were not the preferential sites for lead adsorption.

The BSE-SEM image reported in Appendix B (**Fig. B.2**) shows the presence of different phases, as indicated by the different grey levels. EDX analysis (**Fig. B.4**, appendix B) carried out on the white phase on the BSE-SEM image (**Fig. B.3**, Appendix B) indicated a high concentration of lead and sulfur, which could be interpreted as anglesite, whereas the hematite presence explains the iron peak. The presence of potassium, silicon and aluminium was likely related to feldspar minerals surrounding the white particle.

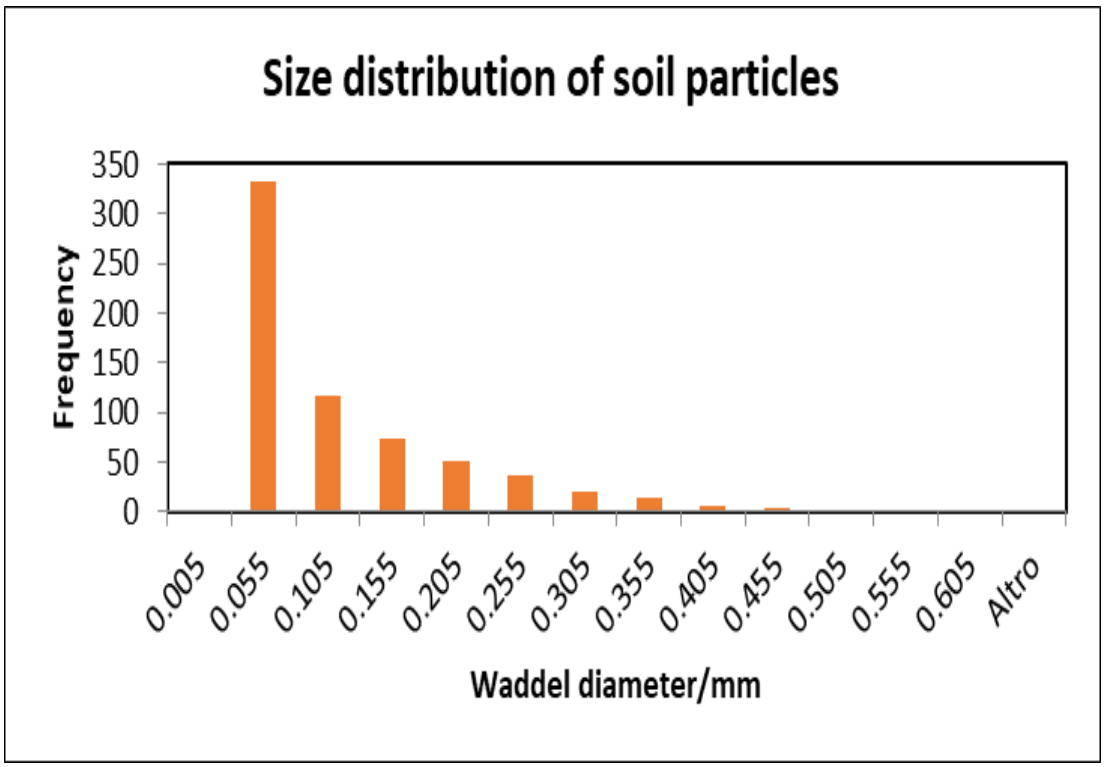

***Fig. 25**: Size distribution of the soil particles assuming particles as spheres.*

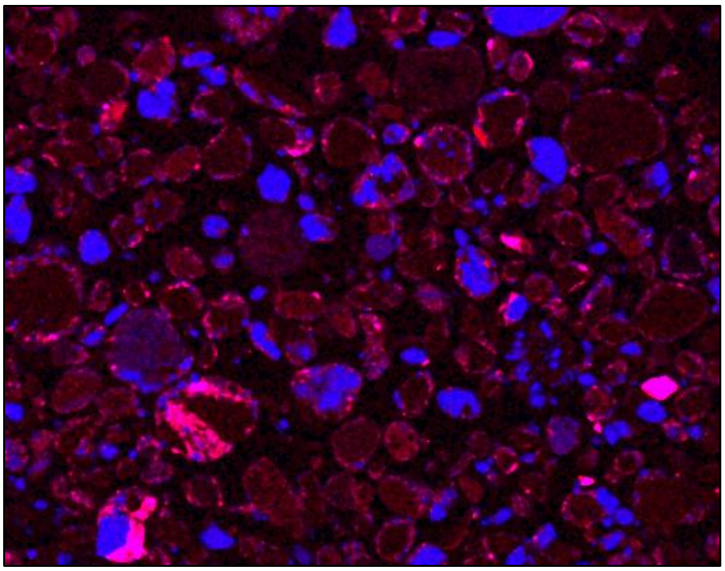

Fig. 26: *Elemental X-ray compositional map showing the overlapping area between sulfur (represented in blue) and lead (represented in red). The overlapping spots are those related to the presence of anglesite.*

4.1.2 SOLIDIFICATION/STABILISATION OF LEAD CONTAMINATED SOIL USING CAC 70

The next paragraph illustrates the results obtained for the four samples cured at two different temperatures (20 and 40° C) for 35 days. The results are grouped according to the curing temperature.

4.1.2.1 SAMPLES CURED AT 20 °C FOR 35 DAYS

In this section both the XRPD and SEM results of the samples cured at 20 °C are presented and discussed.

4.1.2.1.1 SAMPLE *4 (CAC 70)*

Figure 27 reports the results of the kinetic analysis performed at ambient temperature, showing the temporal evolution of the hydration process occurring in the CAC 70 during the first 24 hours of hydration. Even though the analysis consisted of 70 diffractograms, just 3 of

them were selected as representative of the changes occurring in the studied system. At the beginning, defined as T0 (black diffractogram in **Fig. 27**), just the anhydrous phases were detected in the system. These were: CA (ICDD # 23-1036) and CA_2 (ICDD # 96-350-0015).

According to our results, approximately after 9 hours, the hydration process accelerated, and the diffraction peaks localized at d-spacing values of 10.6, 5.40 and 2.88 Å appeared. These peaks were related to the formation of the AFm hexagonal phases: C_2AH_8 (ICDD # 45-564) and C_4AH_{19} (ICDD # 42-487) that reached the maximum after 12 hours (green diffractogram in **Fig.27**). Simultaneously, the peaks of the anhydrous phases CA and CA_2 lowered. This latter observation is consistent with the mechanism of formation of the two hexagonal phases C_2AH_8 and C_4AH_{19}. (Antonovič et al., 2013). Finally, in the last XRPD pattern (purple diffractogram in **Fig.27**) a further lowering of C_2AH_8 and C_4AH_{19} peaks was observed. The above-mentioned phases disappeared, and 4 new peaks were observed at d-spacing = 10.15, 7.40, 5.16 and 3.46 Å. These latter were probably given by unidentified metastable phases originated by C_2AH_8 and C_4AH_{19}.

Jensen et. al (2005) reported the formation of intermediate phases not identifiable due to the lack of crystallographic data. The most probable mineral phases explaining the pattern are related to the calcium aluminium oxide chromium hydrate (ICDD #52-654) and the calcium aluminium chromium oxide sulphate hydrate (ICDD # 43-47). Even though the SEM-EDX analysis of the CAC cement hydrated after 7 days reported the presence of some sporadic Cr-bearing particles, such particles could not be invoked for the interpretation of the before mentioned phases, since they are present as impurities and not abundant at all. Furthermore, using Al NMR, Cong and Kirkpatrick (1993) reported the formation of one or more intermediate hydration products attributed to a 4-coordinated aluminium unreported phase. This means that before the stabilisation of the system toward the cubic phases, other intermediate hexagonal phases are formed.

Likewise, CAH_{10} (ICDD # 12-408) having a hexagonal structure was also detected at 23 hours after hydration. This latter phase being formed may also explain the observed substantial lowering of the peaks of CA in the diffractogram.

Regarding the mineral phases contained in sample 4, an overview of the different amounts obtained via XRPD analysis carried out between the 7^{th} and the 35^{th} day of curing is reported in **table c.3** in appendix c. The temporal trend of the mineral phases after hydration occurred, is reported in **Fig. 28** along with the XRPD profiles obtained between the 7^{th} and the 35^{th} day (**Fig. 29**). Rietveld refinement quantified the amorphous amount as approximately equal to

40% (**table c.3**). Nonetheless, it is to be taken into account that into the amorphous part there is also the contribution given by the peaks of C_2AH_8, which could not be quantified due to the lack of a reliable structural model. The main phases after 35 days present in the sample were: CA_2 (ICDD # 96-350-0015), AH_3 (ICDD # 96-101-1082), CA (ICDD card # 23-1036), CAH_{10} (ICDD card # 12-408) and C_2AH_8 (ICDD # 11-205). Additionally, unknown phases were present, as indicated by the diffraction peaks at d-spacing of 10.4 and 5.22 Å, thus different from the unknown phase observed in the kinetic analysis. These peaks were probably associated to the presence of C_2AH_8 since a similar experiment conducted by Gosselin (2009) reported the presence thereof between 15 and 27 °C characterized by the same d-spacing values we have found. However, the C_2AH_8 phases in our available databases (ICDD # 11-205 and 45-564) presented values of 10.7 and 5.36 Å (**Fig. 30**). Thus, a Rietveld quantification of C_2AH_8 was not carried out given the lack of the structural model. A general temporal trend (**Fig.31**) that all phases may follow is not observed, instead an increment of the gibbsite concentration between the 21^{th} and 28^{th} day associated with a reduction of both CAH_{10} and CA_2 was observed. As regards the gibbsite behaviour, it must be taken into account that the peak is broad as the phase occurs in a gel form, thus indicating a low crystallinity of the structure. For this reason, a low crystal size value was used to describe the mentioned phase during the Rietveld refinement. Concerning CA, it did not undergo significative variations of its amount during the investigated time. Its concentration decreased from 60 wt% (value in the unhydrated cement) to 11 % after 7 days. This agree with what reported by Taylor (1997) who reported that Ca is the principal phase being hydrated. Thus, it may be supposed that in the first seven days of reaction, CA was the main phase being hydrated. Then, also CA_2 started to participate to the whole hydration process. Indeed, after 7 days its concentration was higher than that of CA and it showed a decreasing trend over the subsequent studied period as well. The increase of the gibbsite amount and the consequent diminishing of the CAH_{10} is likely imputable to the formation of C_2AH_8 according to reaction 6) reported in section 1.5.

In fact, we observed the rising of the C_2AH_8 peaks in the diffractogram particularly between the 28^{th} and 35^{th} day of curing. Even though similar studies (Antonovič et al., 2013; Taylor, 1997) reported that the major phases occurring at 20°C should be C_2AH_8 and gibbsite, our results slightly disagree with them. Indeed, we observe a higher formation of CAH_{10} than that of C_2AH_8. However, these considerations are made by analysing the peaks high that does not permit a reliable quantification.

Moreover, given that new phases did not appear in the sample cured up to 35 days, it is deducted that after 7 days all the hydrated phases were formed. Comparing these results

with the kinetic observations, we conclude that although an initial shift toward other metastable phases was observed, after 7 days the C_2AH_8 was again generated and maintained until the 35th day, which is a symptom of the huge variability of the metastable AFm phases.

SEM analysis performed on the sample 4 after the curing at 20 °C for 7 days (**Fig. 32**), revealed the presence of light grey particles surrounded by a matrix of hydration products, yielding a low-porosity microstructure. The EDX analysis of the light grey particles reported high amounts of Ca e Al, indicating the presence of unreacted CA and CA_2.

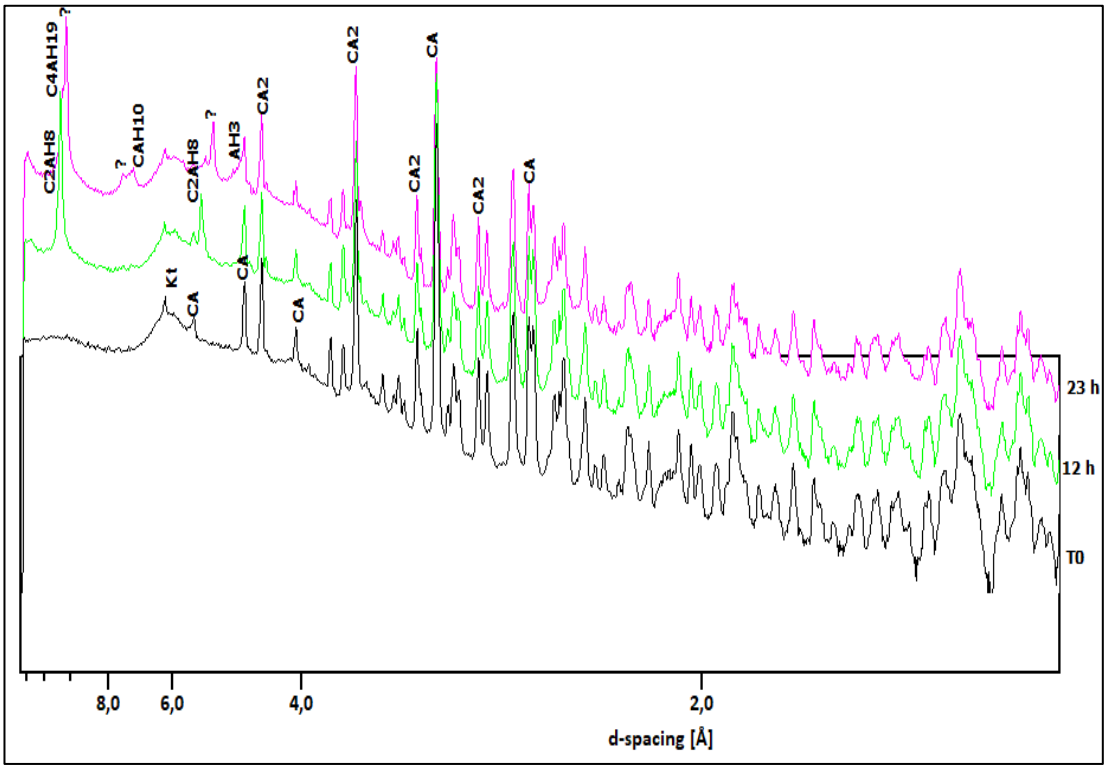

Fig. 27: *Selected diffraction patterns of CAC 70 recorded during the early 24 hours of hydration. At T0 just the anhydrous clinker phases were detected. After 12 hours the formation of the AFm metastable hydrates (C_2AH_8 and C_4AH_{19}) were observed. Thereafter in the last pattern, these AFm phases underwent a further transformation into an unidentified phase with peaks at d = 10.15, 7.40, 5.16 and 3.46 Å. Kt: Kapton*

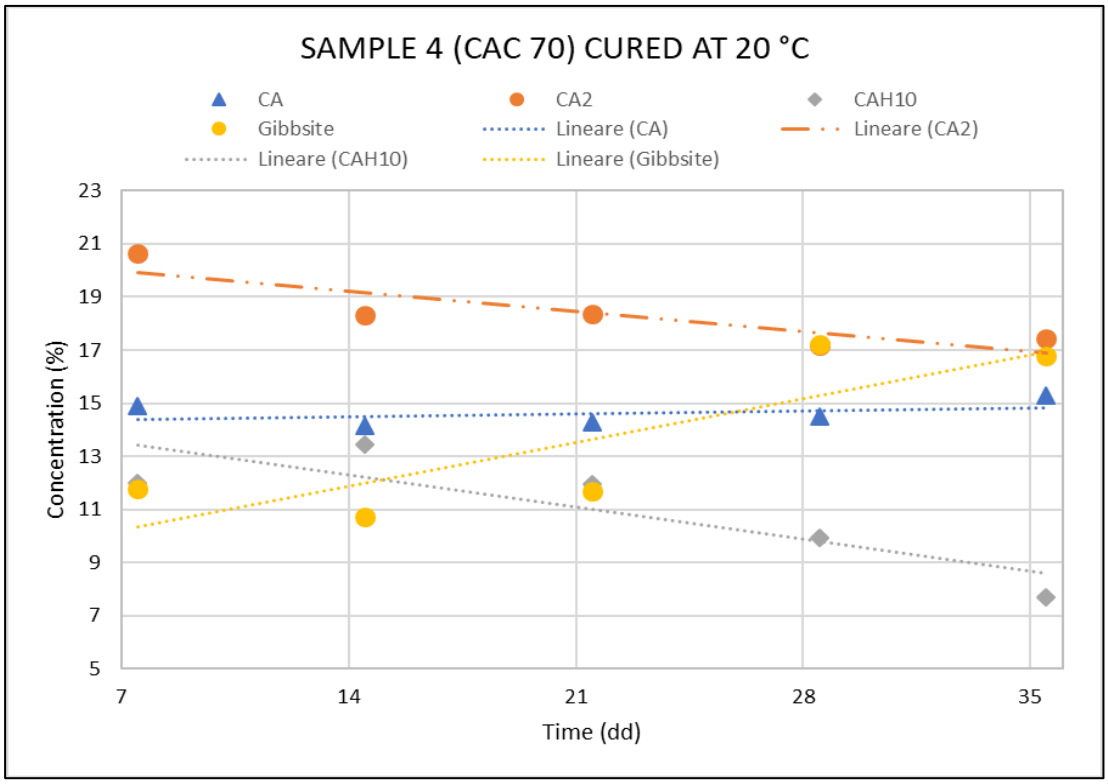

***Fig. 28**: Temporal trend of both anhydrous and hydrated mineralogical phases related to the CAC 70 in sample 4 cured at 20 °C.*

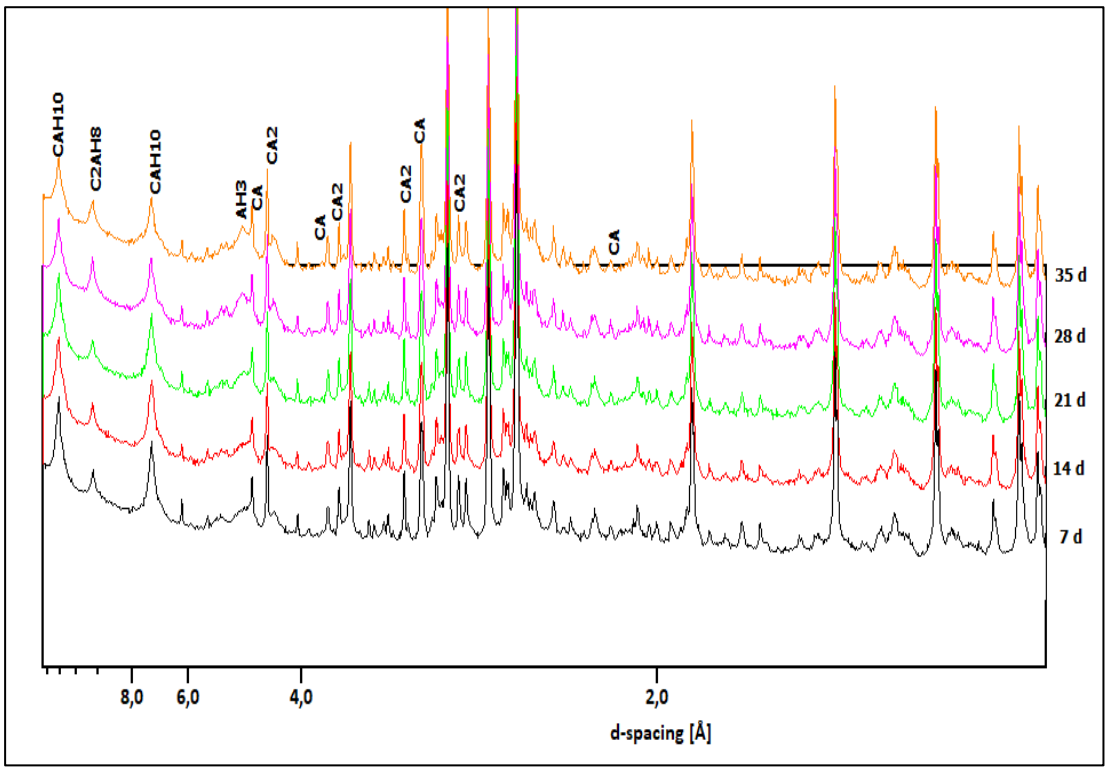

***Fig. 29**: XRPD patterns for sample 4 attained as a function of the curing time. An increase of AH_3 is noticed, as well as a lowering of CAH_{10}. However, the system is rather stable over time.*

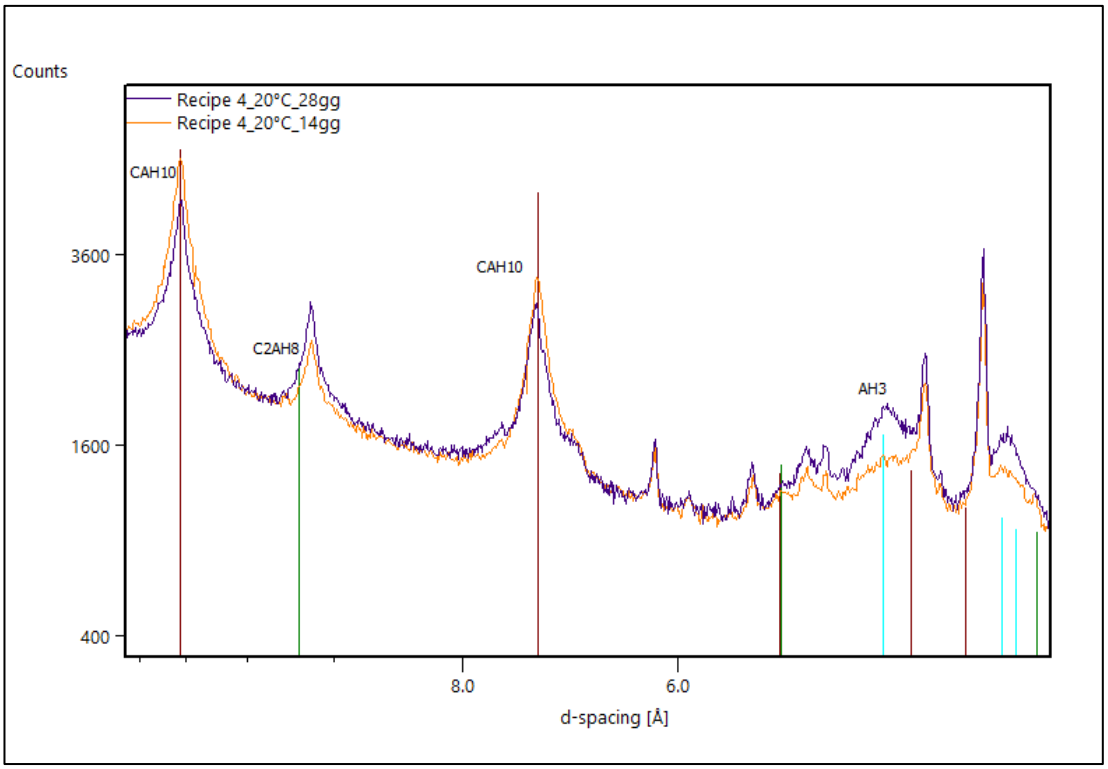

Fig. 30: *Comparison between the portion of the diffractograms at high d-spacing values obtained after 14 and 28 days of curing at 20 °C for sample 4. The C_2AH_8 candidates contained in the available databases were slightly shifted with respect to the observed peaks.*

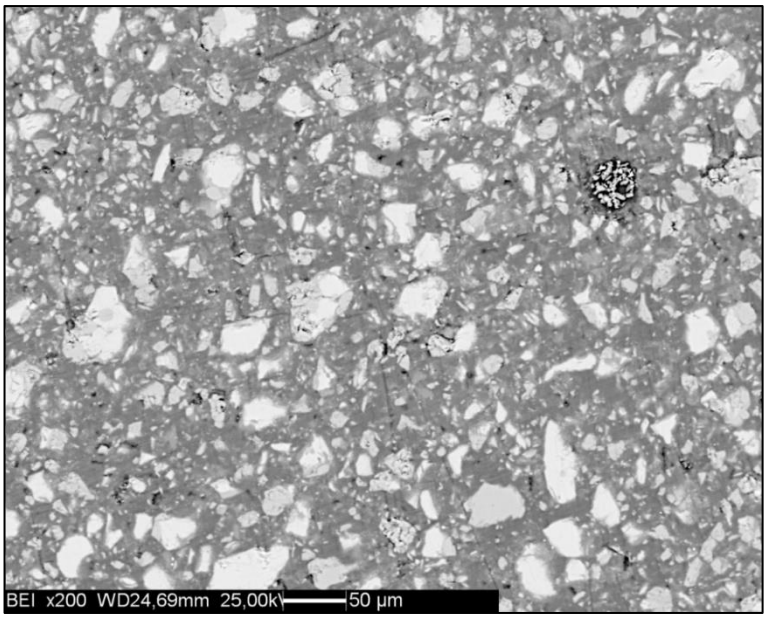

Fig. 31: *SEM image of CAC 70 cement cured at 20 °C for 7 days. The formation of metastable hydrates completely filled the available spaces between the unreacted anhydrous phases, lowering significantly the porosity of the system.*

4.1.2.1.2 SAMPLE 3 (GYPSUM + CAC 70)

Sample 3 was characterized by the presence of the following mineralogical phases: AH_3(ICDD # 96-101-1082), ettringite (ICDD # 98-000-5655),CA_2 (ICDD # 96-350-0015), CA (ICDD # 23-1036), AFm-14 [$CA_4Al_2O_6(SO_4) \cdot 14H_2O$] (ICDD # 42-62) and gypsum (ICDD # 01-074-1904) (**Table c.4**, appendix c). After 35 days of curing the concentrations of the above reported phases were: 23 wt%, 17 wt%, 14 wt%, 12 wt%, 6 wt% and 4 wt%, respectively. The evolution of these phases with time is reported in **Fig. 32**, whereas in **Fig. 33** the diffractograms obtained over the 35 days period are presented. Even in this case, a high background level was observed, however the amorphous content (**Table c.4**) was ~20 wt%. Gibbsite was the major phase observed and its trend was rather variable within the considered period. Indeed, it had a rising trend in the first 21 days, followed by a decrease. Ettringite and CA_2, on the other hand, were both characterized by a slight lowering trend. No significant variations were detected for CA and AFm-14, with refined weight fractions oscillating within the expected real errors of the Rietveld quantitative phase analysis. Gypsum was also stable over the time after the initial decreasing from 25 % to 4%. It might be supposed that in the first stages of hydration the CA reacted with gypsum to form ettringite, thereafter, when the concentration of gypsum dropped, CA reacted with Ettringite to form AFm-14. After the initial consumption of CA, it is likely that also CA_2 reacted with water, as indicated by its slight lowering during time. These observations were in good agreement with the results of Xu et al. (2012), who demonstrated that in an OPC/CAC/$CaSO_4$ ternary system CA_2 may participate in a parallel reaction in place of CA. SEM images (**Fig. 34**) of the sample indicate the presence of cracks occurring on the rim of the anhydrous cement particles. These cracks were caused by the dehydration of Ettringite under the high-vacuum conditions of SEM.

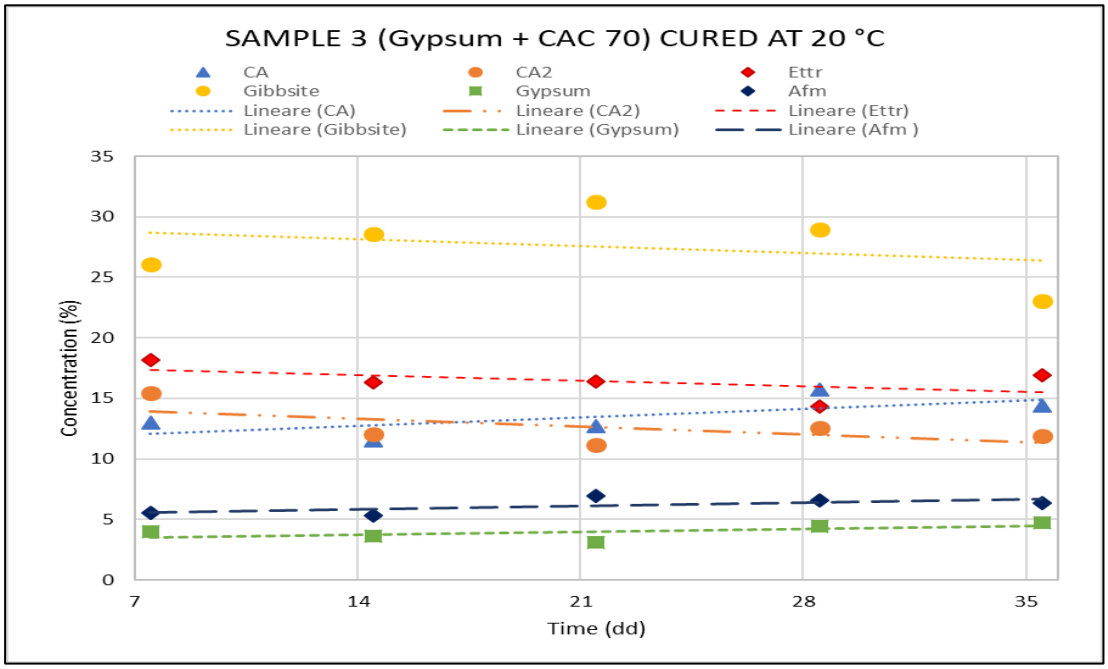

***Fig. 32**: Temporal trend of both anhydrous and hydrated phases related to the CAC 70 in sample 3 cured at 20 °C.*

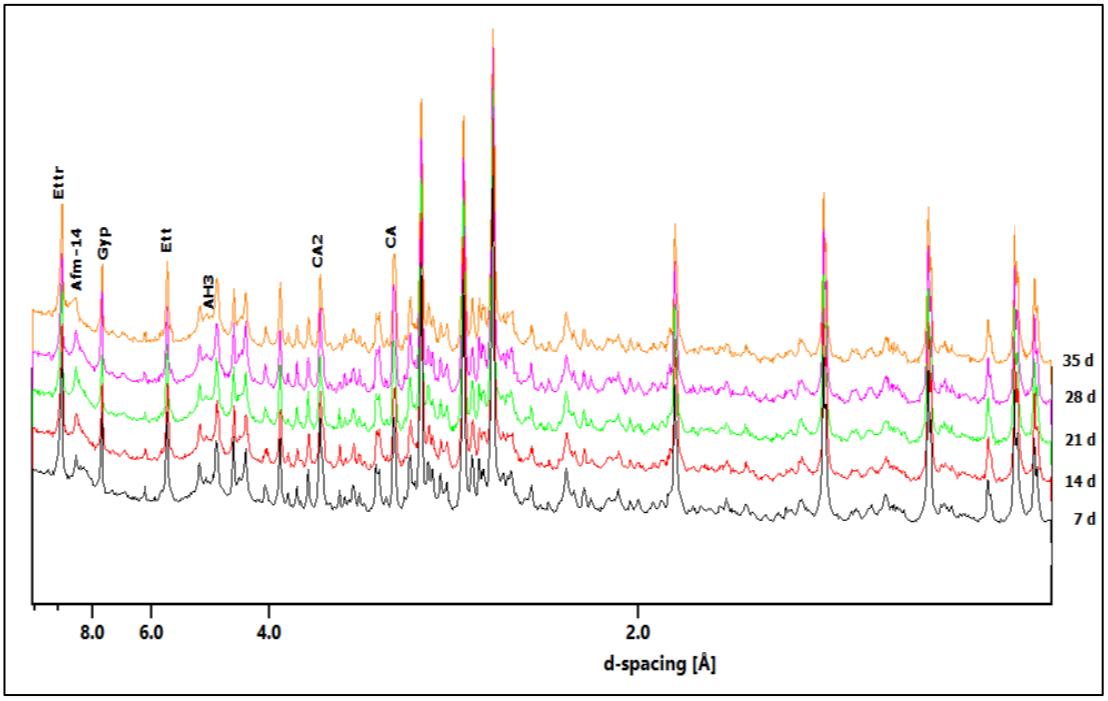

***Fig. 33**: XRPD patterns for sample 3 attained as a function of the curing time. Formation of new phases during the curing period was not observed.*

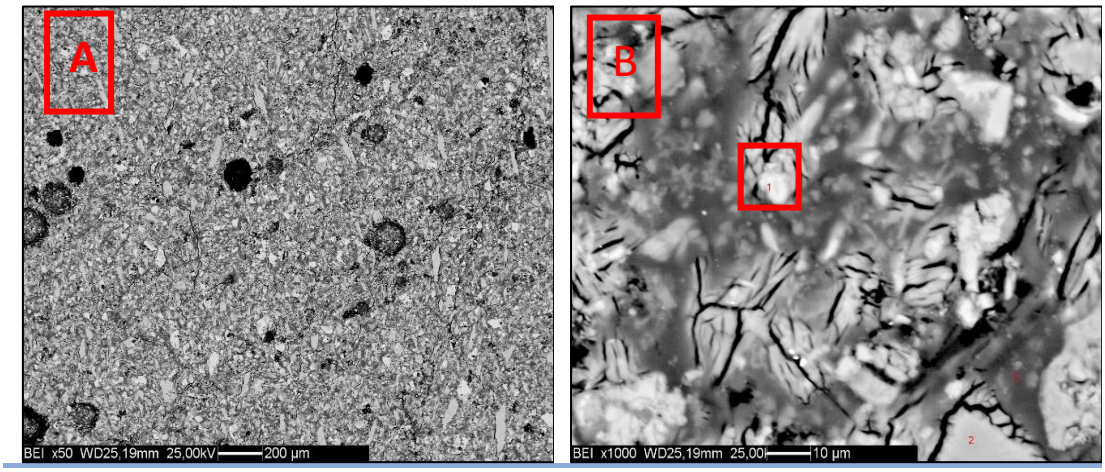

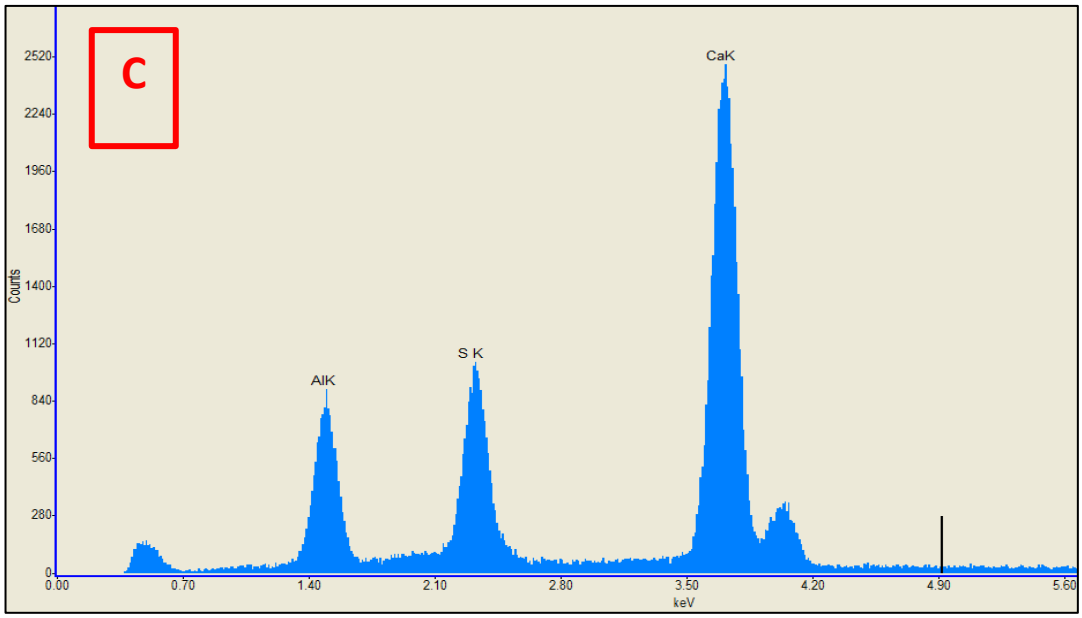

***Fig. 34**: SEM images of a section of sample 3 at low magnification (A) and, in detail (B) to appreciate the cracks imputable to dehydration of ettringite under vacuum. EDX analysis (C) carried out in red rectangle in figure B confirms the presence of ettringite suggested by the presence of Al,S and Ca.*

4.1.2.1.3 SAMPLE 2 (UNCONTAMINATED SOIL + CAC 70)

The results of the XRPD analysis are reported in **table c.5** in appendix c. In addition to the phases naturally occurring in the starting soil, the newly formed ones were detected: gibbsite (ICDD # 96-101-1082), monocarboaluminate [$3CaO \cdot Al_2O_3 \cdot CaCO_3 \cdot 11H_2O$](ICDD # 41-219), CA_2 (ICDD # 96-350-0015), CAH_{10} (ICDD # 12-408), CA (ICDD # 23-1036) and hydrotalcite (ICDD # 98-004-0993). The quantities of these phases after 35 days of curing were respectively: 12.6 wt%, 6.9 wt%, 3.6 wt%, 2.3 wt%, 1.6 wt% and 1.2 wt%.

The temporal trend of these phases during the studied period is reported in **Fig. 35**. The presence of soil dramatically complicated the interpretation of the obtained diffractograms, which were characterized by several overlapping peaks such as those related to CAH_{10} and clinochlore both present at d-spacing values of 14.1 and 7.0 Å as well as the peaks of monocarboaluminate and hydrotalcite at d-spacing value of 7.60.

As observed for the control sample (sample 4), a significant lowering of both anhydrous phases (i.e. CA_2 and CA) associated with a significant rising of AH_3 and CAH_{10} were appreciated. As mentioned before, this was imputable to the reaction forming the two hydrated phases (CAH_{10} C_2AH_8). In the diffractogram reported in **Fig. 36**, the peaks associated with C_2AH_8 or other related unknown phases were not observed though. Concerning this outcome, our results agree with those reported by Bensted and Barnes (2001) and Fentiman

(1985), which observed that at 25 °C and lower temperatures, CAH_{10} was the main hydration product when calcite is present in association with CAC.

The presence of calcite in the soil facilitated the formation of monocarboaluminate. Despite that an increasing of 4 wt% of calcite was observed in the sample 2 with respect to the uncontaminated soil. According to reaction 10 and 11, reported in section 1.5.2, calcite should be consumed forming monocarboaluminate, thus decreasing its concentration in the sample. We may hypothesise that some unreacted free alumina combines with CO_2 forming calcite. However, this must be verified.

Monocarboaluminate seems to be formed at the expense of C_2AH_8 at 25-60 °C (Fentiman, 1985). Reactions 10) and 11), reported in section 1.5.2, illustrates the mechanism of formation of monocarboaluminate from CA and CA_2, respectilvely. In reaction 10 2 moles of gibbsite are formed, whereas in reaction 11), 5 moles are formed. This may justify why gibbsite is the main mineral phase in the sample. Anyhow, comparing the concentrations of gibbsite resulted in sample 4, a lowering of it is observed. This is maybe due to the soil presence that reduce the cement hydration by adsorbing water otherwise consumed during the hydration process.

The formation of hydrotalcite, which showed a rather stable trend within the studied time, was probably related to the reaction between CAC and dolomite. Indeed, the concentration of dolomite in the uncontaminated soil of 28.8 wt %, decreases to 20 wt.% in the samples cured at 20 °C. A similar reaction has been reported by Machner et al. (2018) although Portland cement and metakaolin were used in the study.

SEM images of sections of sample 2 are reported in **Fig 37**. Compared to the control sample (**Fig. 31**), a remarkable increase of porosity was observed. Indeed, more black areas and cracks were found in the sample, given by the fact that the soil particles were not always surrounded by the cement paste. This could be either due to a limited homogenization of the sample or, more probably, to the fact that soil particles adsorbed part of the water otherwise available for CAC hydration. A similar result has been reported by Contessi (2019), who observed an increase of porosity in soil-cement systems regardless of the type of binder or the curing method. **Fig. 38** reports a fractured dolomite particle not completed surrounded by a matrix. This has resulted to be a CAC hydration product by performing an EDX analysis (**Fig. 38 B**).

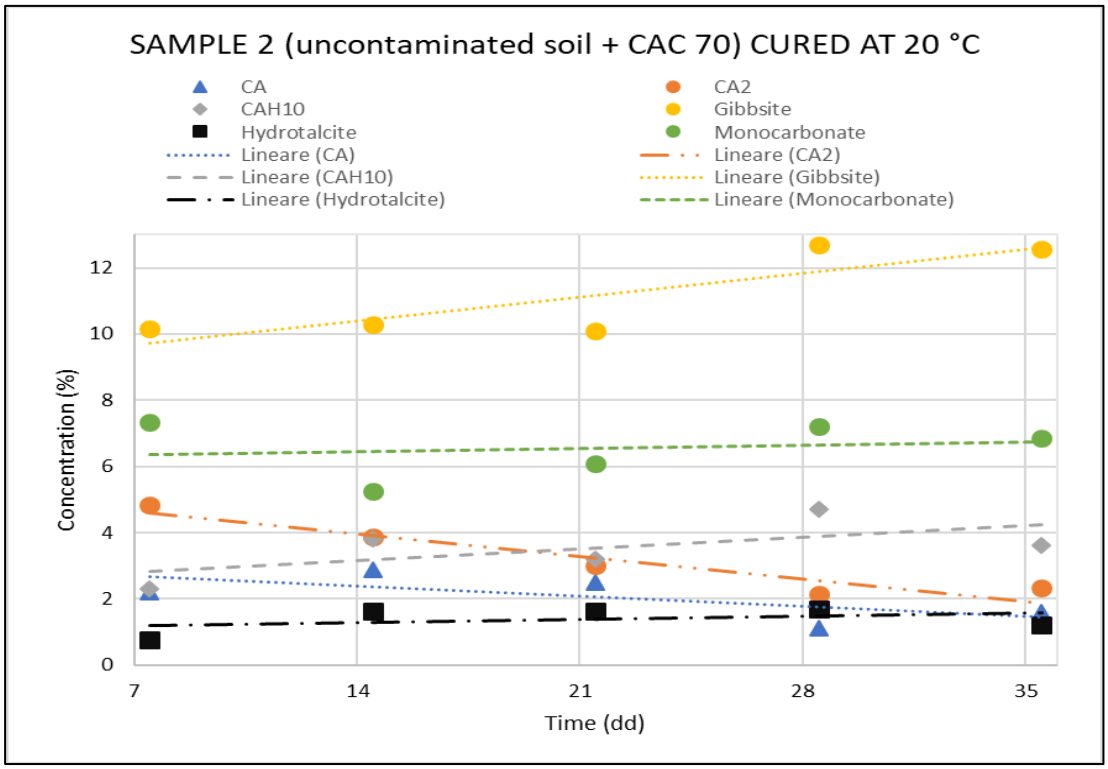

***Fig. 35**: Temporal trend of both anhydrous and hydrated phases related to the CAC 70 in sample 3 cured at 20 °C.*

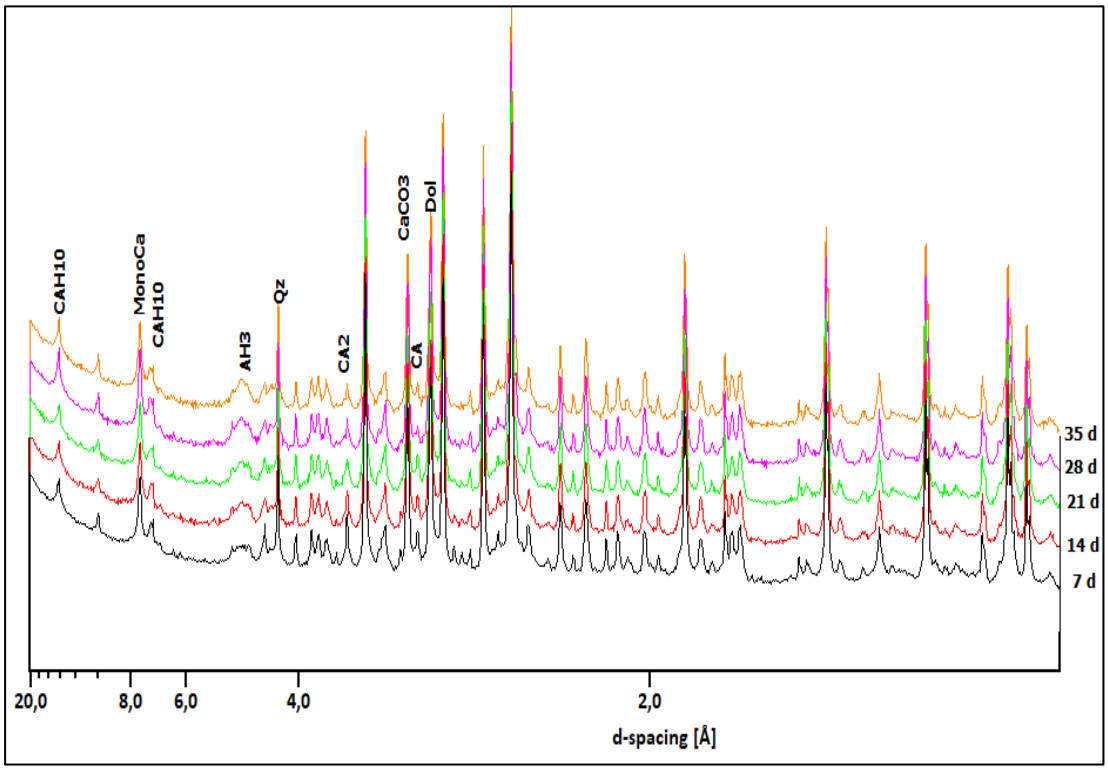

***Fig. 36**: XRPD profiles for sample 2 attained as a function of the curing time. MonoCa: Monocarboaluminate, Qz: Quartz, $CaCO_3$: calcite, Dol: Dolomite*

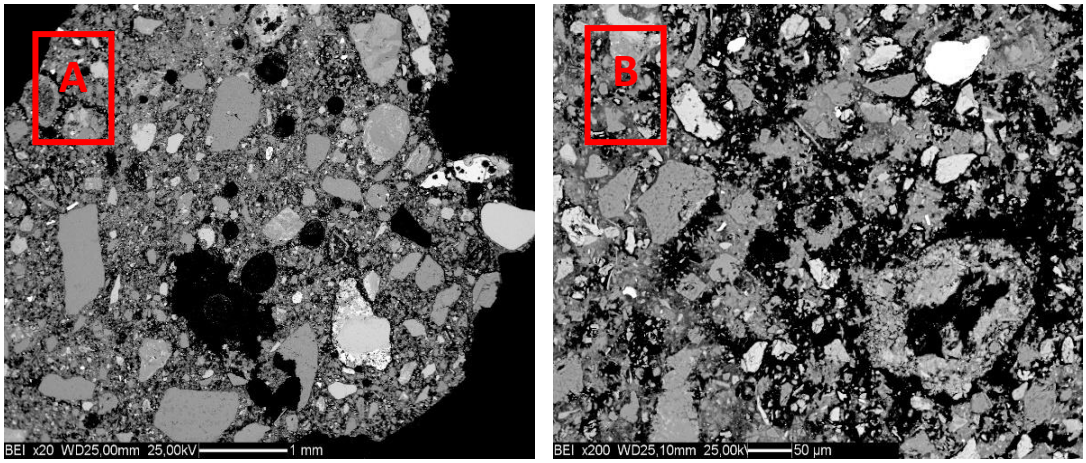

Fig. 37: *SEM image of a section of sample 2 at low (A) and high (B) magnification. In (B) unfilled voids around the particles are observed.*

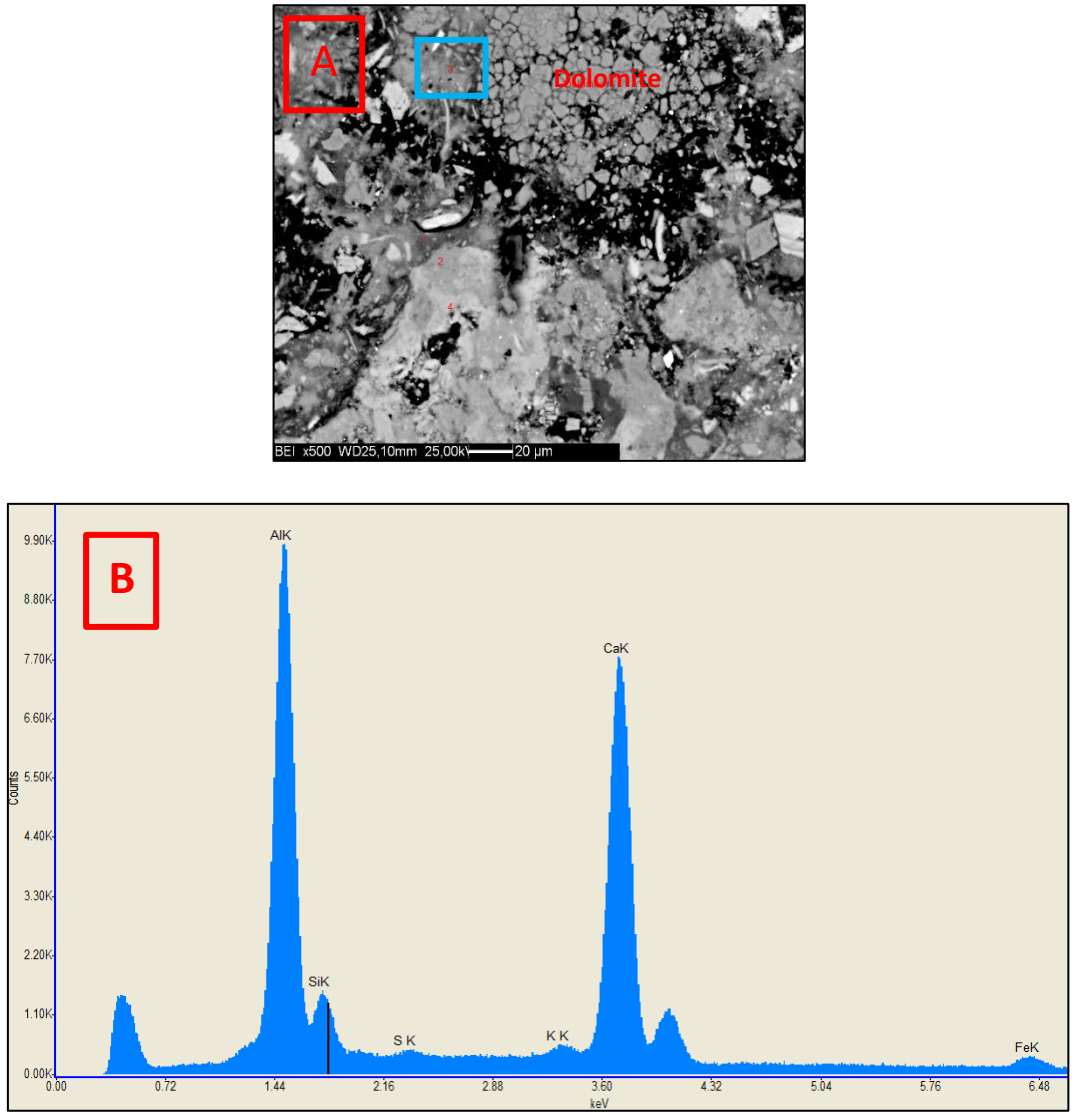

Fig 38*: SEM image (A) of a section of sample 2 at 500 X magnification. A cracked dolomite particle is partially surrounded by CAC ascertained by EDX analysis (B) performed in the pale blue square*

4.1.2.1.4 SAMPLE 1 (LEAD-BEARING SOIL + CAC 70)

Results of XRPD analysis performed on sample 1 at different curing times are reported in **table c.6**, Appendix c. In addition to soil phases, the anhydrous and newly formed hydrated phases are: CA (ICDD # 23-1036), CA_2 (ICDD # 96-350-0015), ettringite (ICDD # 98-000-5655) and gibbsite (ICDD # 96-101-1082). After 35 days of curing the concentrations of the mentioned phases were: 4.9 wt%, 7. 0 wt%, 9.4 wt% and 11.5 wt%. The evolution of these phases over time is reported in **Fig. 39**. Also, gypsum is reported as it participated in the ettringite's reactions (reaction 8 and 9 section 1.5.1). In the diffractograms reported in **Fig. 40** anglesite was not detected, which is indicative of dissolution of this phase at early stages. This has been reported also by Contessi (2019).

Contrary to Peng et. al (2006) and Navarro et al. (2013) results, who observed a 7-days delay in the ettringite formation caused by the presence of lead species in solution, we observed that ettringite formation occurred. After 1 week of curing time, the amount of ettringite detected in the sample was 10.3 wt%, which is a quantity significantly lower than that observed in sample 3 though. This is reasonably due to the lower amount of gypsum present in the sample (9%). Except for gibbsite, which experienced a rising trend, the other phases were rather stable within the considered period. Additionally, gibbsite concentration is comparable to that obtained in sample 2, that is significantly lower than that observed in the two control samples (sample 3 and 4). As previously stated, this may be due to the soil presence which adsorb water, reducing the hydration of the anhydrous phases to form gibbsite. Comparing these results with those obtained in samples 2 and 3, we did not observe neither monocarboalluminate, AFm-14 nor CAH_{10}. Regarding monocarboaluminate, despite the presence of calcite should have promoted his formation, Taylor (1997) stated that in case of ternary system containing CAC, gypsum and calcite, the preferential reaction is the one engaging gypsum and CAC.

On the other hand, Le Saoût et al. (201) reported that in a ternary system containing CAC, $CaSO_4$ and limestone, the exceed of CA tends to react with calcium carbonate to form monocaroboaluminate-hemicaroboalumuniate, which is of higher thermodynamic stability than monosulfoaluminate. In addition to this, Bizzolero and Scrivener (2015) reported that by increasing the ratio between sulphate and aluminate, the extent of limestone reaction decreases. The dearth of CAH_{10} may be explained by the presence of calcite. Indeed, Luz and Pandolfelli (2012) stated that the conversion of CAC hydrates is inhibited by adding $CaCO_3$. Moreover, given that the preferential reaction was between CAC and gypsum, the system

followed the reaction mechanism observed in sample 3. Concerning the lack of AFm-14, its formation depends upon the quantity of reactive gypsum available (Christensen et al., 2004). Additionally, Kakali et al. (2000) reported that in pastes containing $CaCO_3$, the conversion of ettringite into monosulphate is delayed. In particular, they observed that calcium carbonate suppresses the conversion of ettringite to monosulfate and favours the replacement of monosulfate by monocarbonate. Hence, we may assume that its lack in our sample might be associated with the calcite presence.

Hydrotalcite formation was not observed, in spite of the overlapping of its peaks with those of gypsum further complicated the elucidation of the mineralogical composition. **Fig. 41** illustrates a SEM image of a section of sample 1 whereby it is visible the formation of hydrates amid a dolomite particle and ettringite. EDX analysis (**Fig. 41 B**) performed in the hydrated area (encircled within the yellow line) indicated that it contained Al, Ca, Si, Pb and Fe. Additionally, a little amount of Mg (maybe coming from dolomite) is also present. Another EDX analysis **(Fig. 42 C)** performed in an ettringite particle in **Fig. 42,** revealed the presence of Pb and Fe in a remarkable concentration in association with ettringite.

Additionally, via SEM-WDS analysis, the lead-ettringite close relation was ascertained: **table 16** reports the quantitative analysis performed on a cracked area (spectrum 2 in **Fig. 43**) which confirmed the presence of both Pb and of the constitutional elements of ettringite (Ca, Al, S).

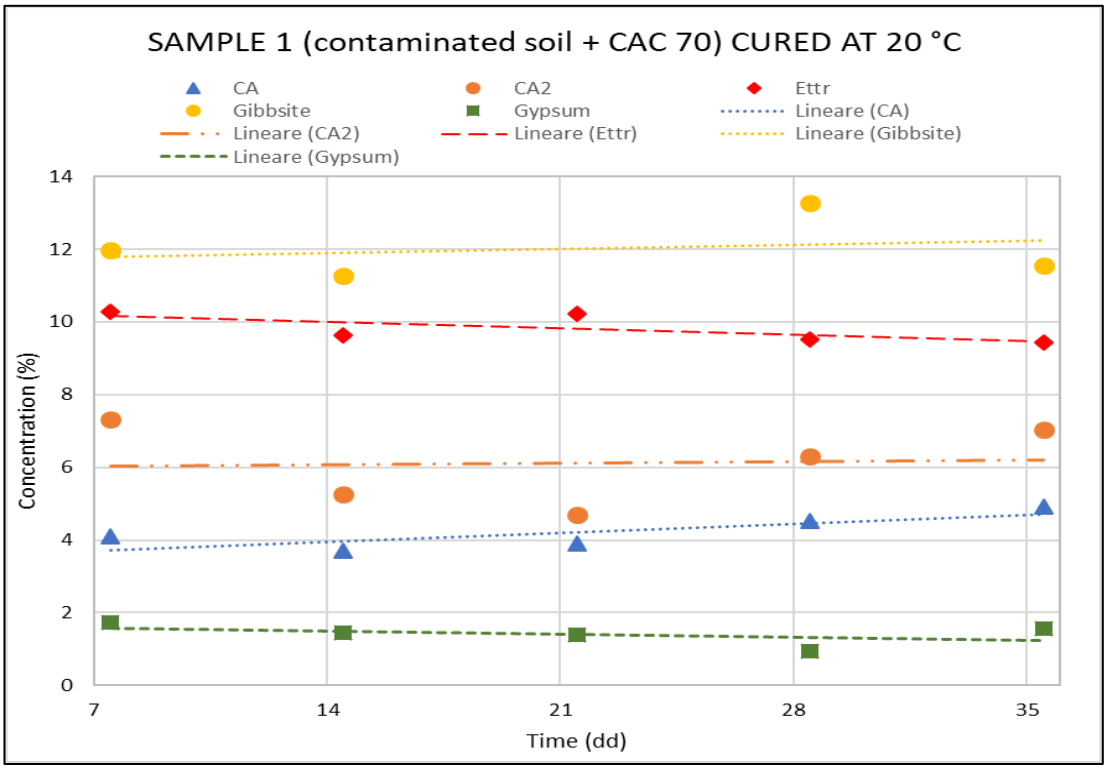

Fig. 39: *Temporal trend of both anhydrous and hydrated phases related to the CAC 70 in sample 1 cured at 20 °C. Point concentration of gibbsite at 21 days was excluded as presenting a different concentration with reference to the other analyses.*

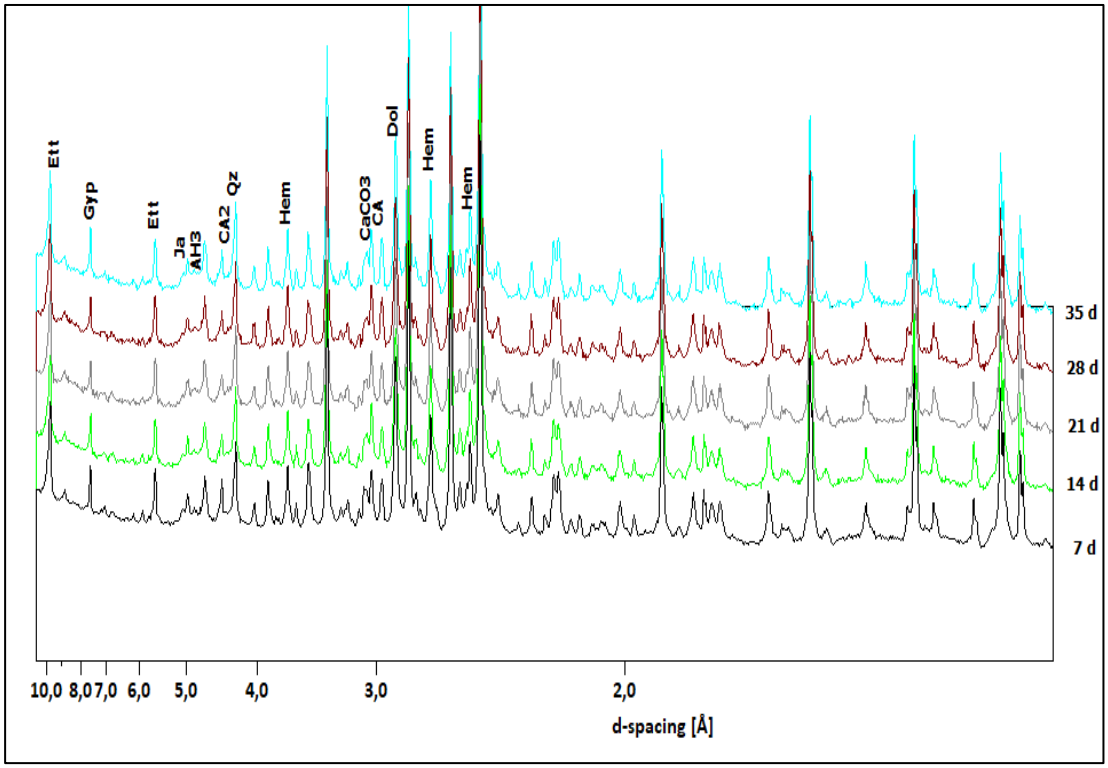

Fig. 40*: XRPD profiles for sample 1 samples attained as a function of the curing time. Ett: Ettringite, Gyp: Gypsum, Qz: Quartz, $CaCO_3$: calcite, Hem: Hematite, Dol: Dolomite, Ja:Jarosite.*

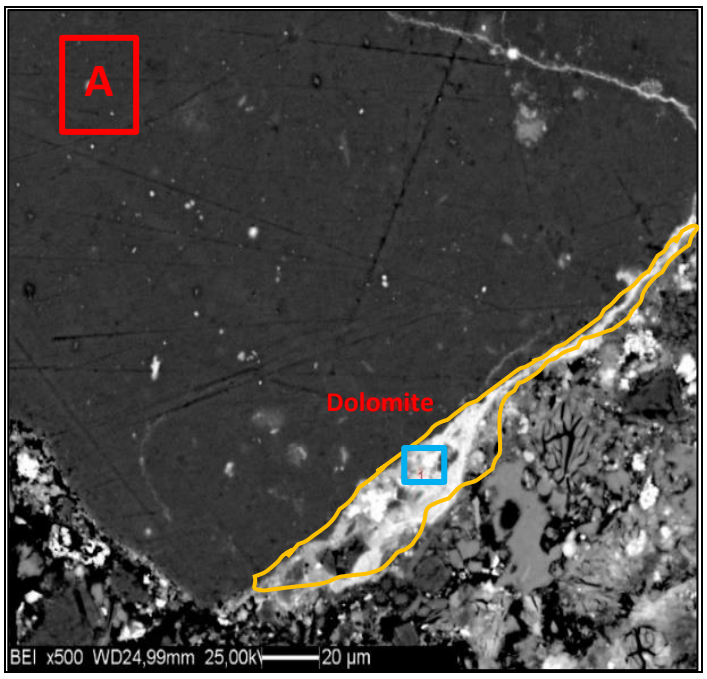

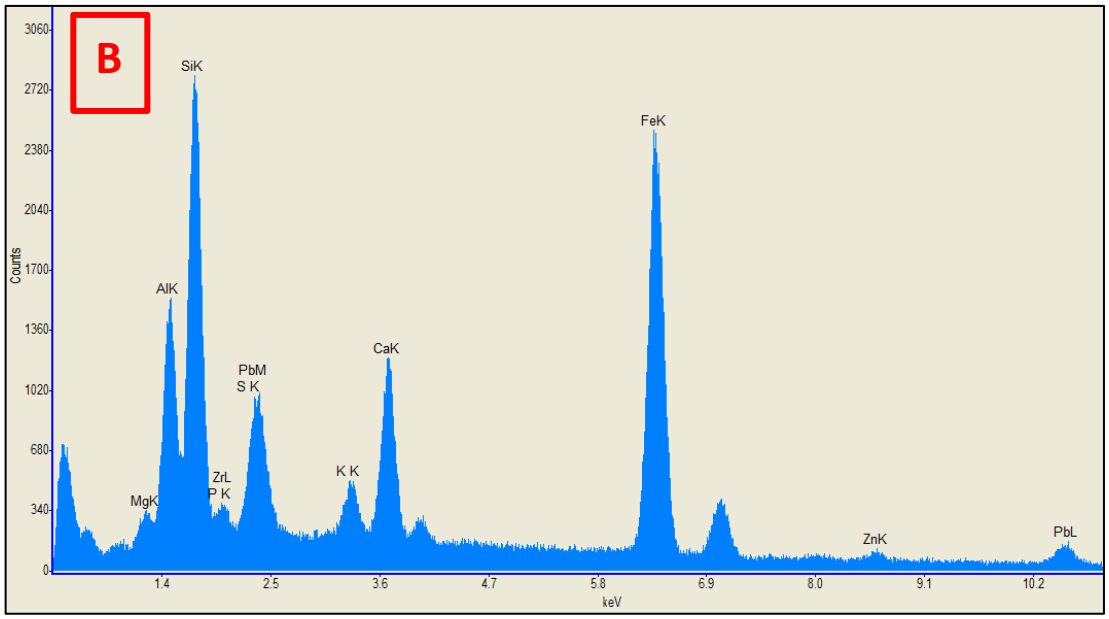

Fig. 41: *SEM image of a dolomite particle rimmed with a reacting hydrate bearing metals (A). EDX analysis (B) performed on the pale blue square in Fig. A, reveals presence of Al and Ca in addition to Mg, Si, Pb, S, K, Fe and Zn.*

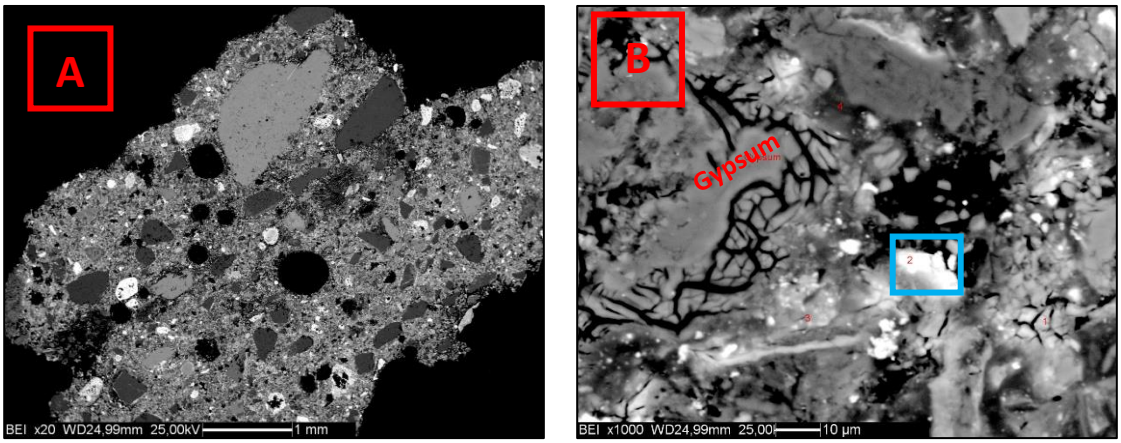

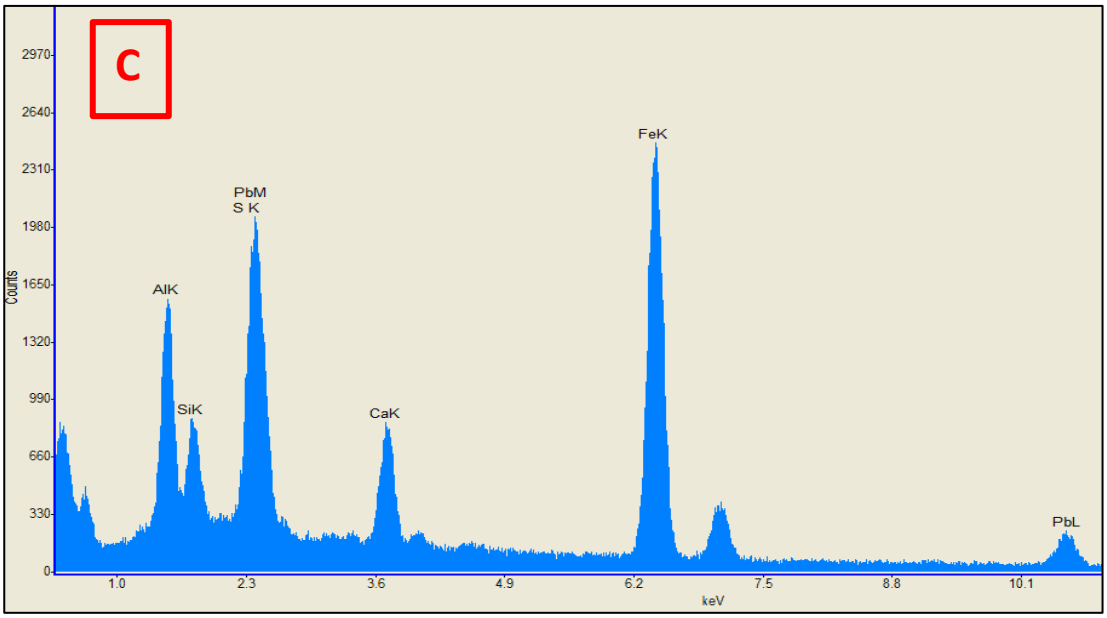

***Fig. 42**: SEM images at lower magnification (A) and higher magnification (B) of sample 1 sample. EDX pattern (C) carried out on the light blue rectangular in Fig. B, reveals the presence of both lead and iron probably associated with ettringite. The presence of silicon is imputable to the soil occurrence in the sample.*

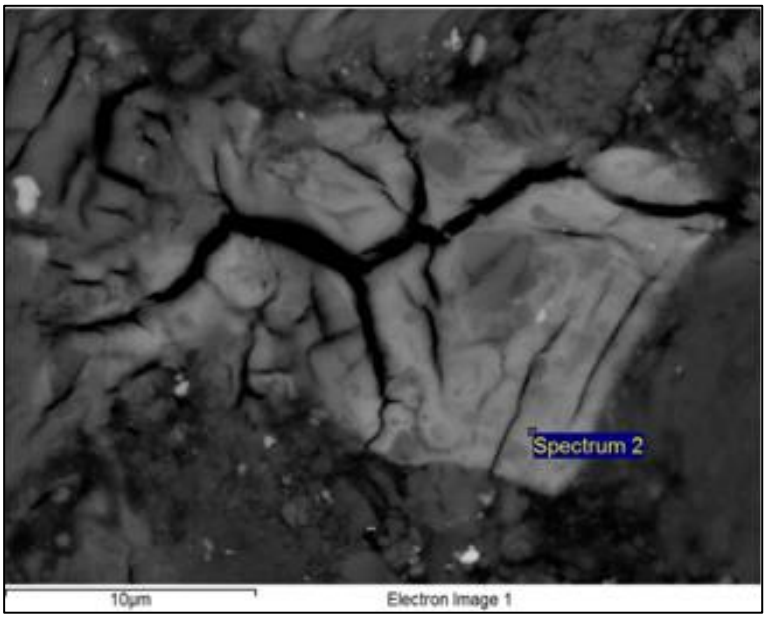

***Fig. 43:** SEM image of an ettringite particle in which a WDS analysis was carried out in the point labelled Spectrum 2.*

Element	Data Type	Line	Weight%	Atomic%
S	WD	Ka	8.631	9.654
Pb	WD	Ma	12.519	2.167
C	ED	K	1.166	3.481
O	ED	K	26.577	59.581
Mg	ED	K	0.255	0.377
Al	ED	K	6.855	9.112
Si	ED	K	0.418	0.534
Ca	ED	K	16.699	14.944
Fe	ED	K	0.233	0.150
Totals			73.354	

***Table 16**: SEM-WDS results demonstrated the presence of ettringite together with lead as indication of the close association between the metal and the hydration product.*

4.1.2.2 SAMPLES CURED AT 40°C FOR 35 DAYS

SEM and XRPD results obtained after curing the four samples at 40 degrees are presented below. A focus on the comparison with the results obtained at 20 degrees is also given.

4.1.2.2.1 SAMPLE 4 (CAC 70)

Concerning the XRPD analysis carried out on sample 4, all the samples analyzed at different curing time (**Fig.44**) were characterized by a relatively high content of amorphous-unknown component ranging between 38% and 47% (**Table c.7**, Appendix c). It is to note that poorly crystalline phases, which are not described by a structural model in the Rietveld refinement, are encompassed into the amorphous-unknown quantity. This is the case of C_2AH_8 phase, for which a reliable structural model was not available.

A rather stable trend for all the phases was observed (**Fig. 45)**. By comparing these results with those obtained at 20 °C for the sample 4, we detected the new phase C_3AH_6. The quantity of gibbsite was slightly increased with reference to the sample cured at 20 °C. Taylor (1997) reported that when conversion occurs, much water is released, so that even if the pores contains no water, more CA and CA_2 can hydrate. Speaking of which, both CA and CA_2 was lower in sample 4 cured at higher temperature after 35 days and, gibbsite was slightly higher. This demonstrates that more cement anhydrous phases have been hydrated forming more gibbsite. In addition, the crystallinity of the gibbsite was higher given that a crystal size of 15 nm was used in the Rietveld analysis, whereas a value of about 10 nm was used for the sample cured at 20°C. This agree with Taylor (1997). The relatively constant values of phase quantities between 14 and 35 days of curing time indicated that the reaction rate was very low in this time interval. The large part of the hydration process occurred at earlier ages. This agree with what reported by Taylor (1997), Lea (2004) and Antonovič et al. (2013). However, the literature data also indicate a predominance of C_3AH_6 in the system that we did not observe. In relation to this, Midgley and Pettifer (1971) suggest that a transformation time of about 3 months at 40 °C is required to convert CAH_{10} and C_2AH_8 into C_3AH_6 (reaction **5, 6 ,7** in section **1.5**), whereas the transformation time is reduced to one week at 50 °C. The evolution of the C_2AH_8 phase was monitored by examining its diffraction peak at d-spacing of 10.4 Å. Lacking a structural model for this phase, it was not possible to directly quantify it by using the Rietveld method.

The diffraction peaks of C_2AH_8 showed a decreasing trend over time, which is a symptom of the occurrence of the conversion reaction. In **fig. 46** a SEM image of a section of the hydrated CAC at 40 °C is presented. No significant differences were reveled with respect to the sample cured at 20°C. Fractures in the sample were probably due to the mechanical stress applied to the sample during the hammering of the sample. Furthermore, the higher porosity observable on the outer part of the sample may be imputable to the same process.

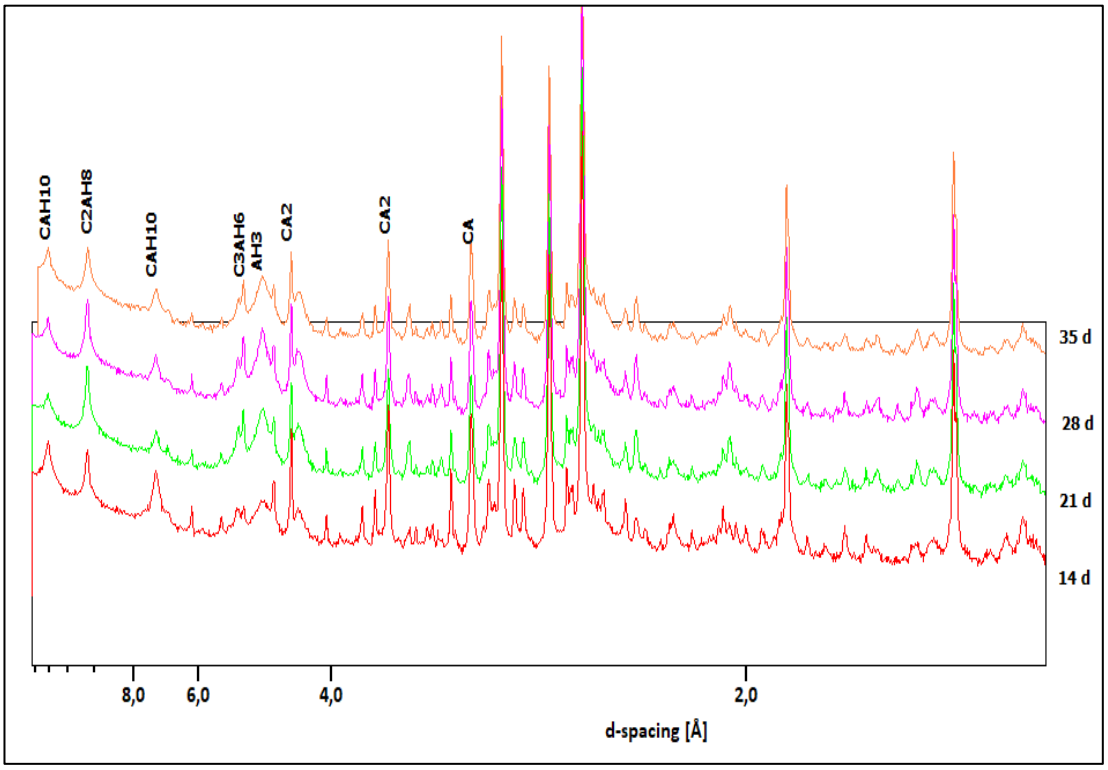

Fig. 44: *Diffractograms of the sample 4 cured at 40 °C analysed from 14 to 35 days. Phase' names are indicated above the principal peaks for each phase.*

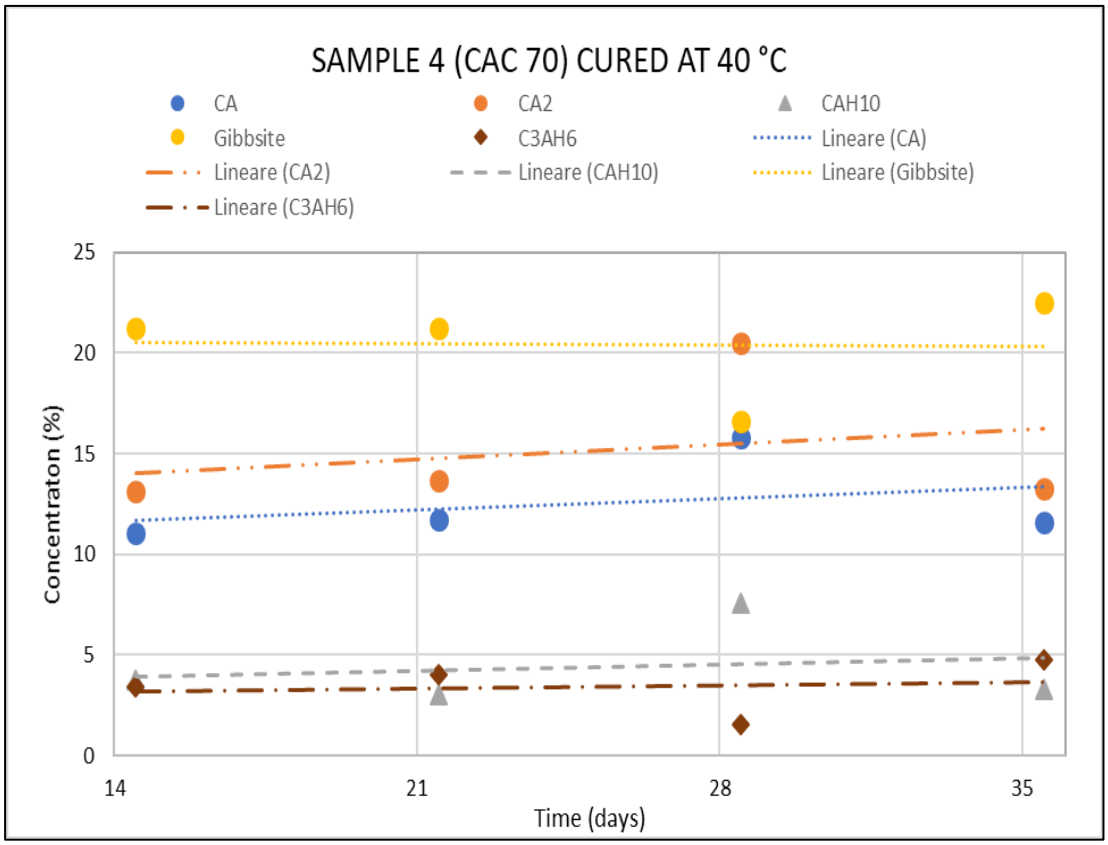

Fig. 45: *Temporal trend of the CAC anhydrous and hydrated phases within the 35 days of curing at 40 °C. The phases revealed to be rather stable over time.*

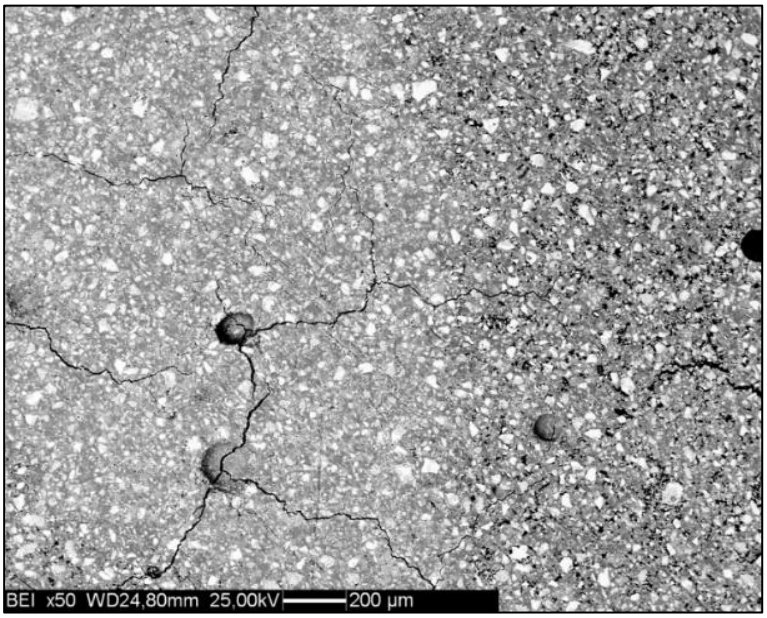

Fig. 46: *SEM image carried out on sample 4. Cracks on the surface was visible, and probably caused by the lapping/hammering process the sample underwent. An increasing porosity on the outer part is observable. This was also probably given by the mechanical activities the sample underwent.*

4.1.2.2.2 SAMPLE 3 (CAC 70 + GYPSUM)

Sample 3 cured at 40 °C for 35 days did not present relevant differences than that cured at 20°C. Temporal trend and diffractograms obtained weekly between 7 and 35 days are reported in **Fig. 47** and **Fig. 48**, respectively. The only observable variance concerned the monosulphate (Afm-14), which presents a decreasing trend in this case. This may be due to the quicker dissolution of both aluminate and sulphate phase that occurred by increasing the temperature (Xu et al., 2012). The decreasing trend affecting AFm-14 might be symptomatic of a reaction between it and CA/CA_2 in place of both gypsum and ettringite which, on the contrary, presented a rather stable trend over time. Damidot and Glasser (1992) reported that ettringite was always stable with respect to the monosulphate at 25 °C, while sulfate remained in solution at low concentrations. The consumption of the reactive gypsum before and ettringite thereafter may be assumed in this case. As regards to the lack of C_3AH_6, which is the thermodynamically stable hydration product of calcium aluminate cement, it was firstly due to the fact that small amounts of sulphate destabilised C_3AH_6, thereby combining much of the available alumina as ettringite rather than as hydrogarnet (Damidot and Glasser, 1993). As regards to the SEM analysis performed on sample 3, no differences were reported neither with the sample cured at 20 °C nor within the time.

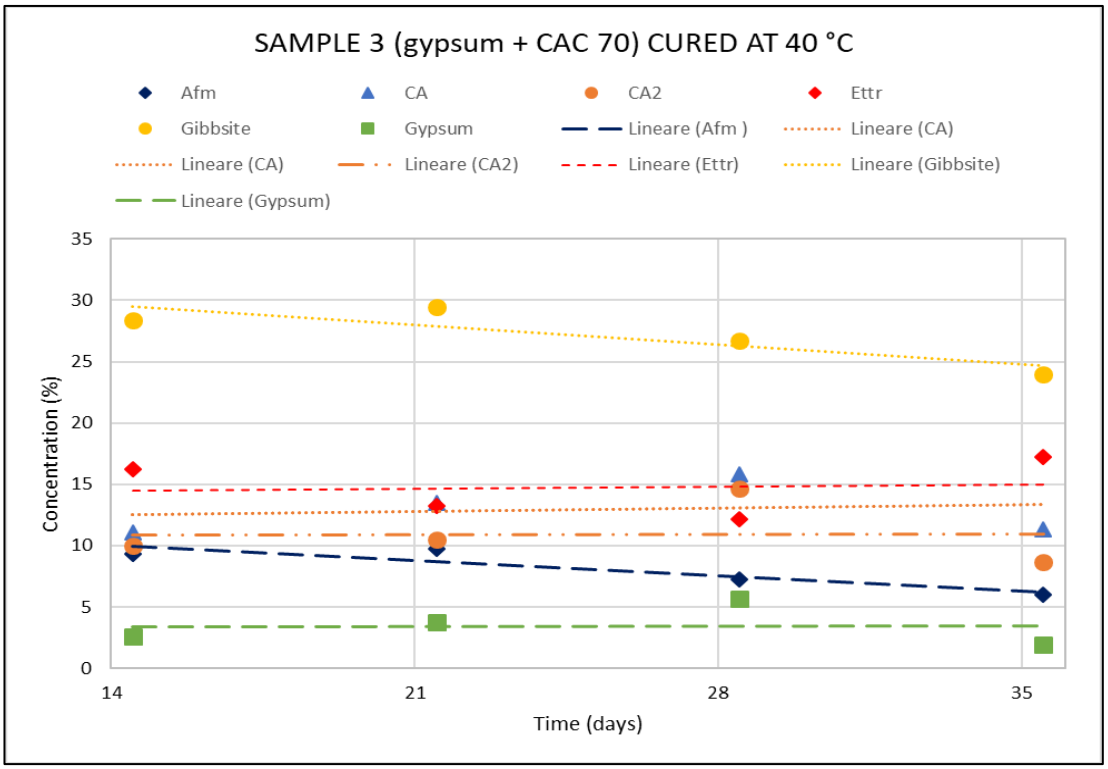

Fig. 47: *Temporal trend of the anhydrous and hydrated phases detected in sample 3 treated at 40 °C for 35 days.*

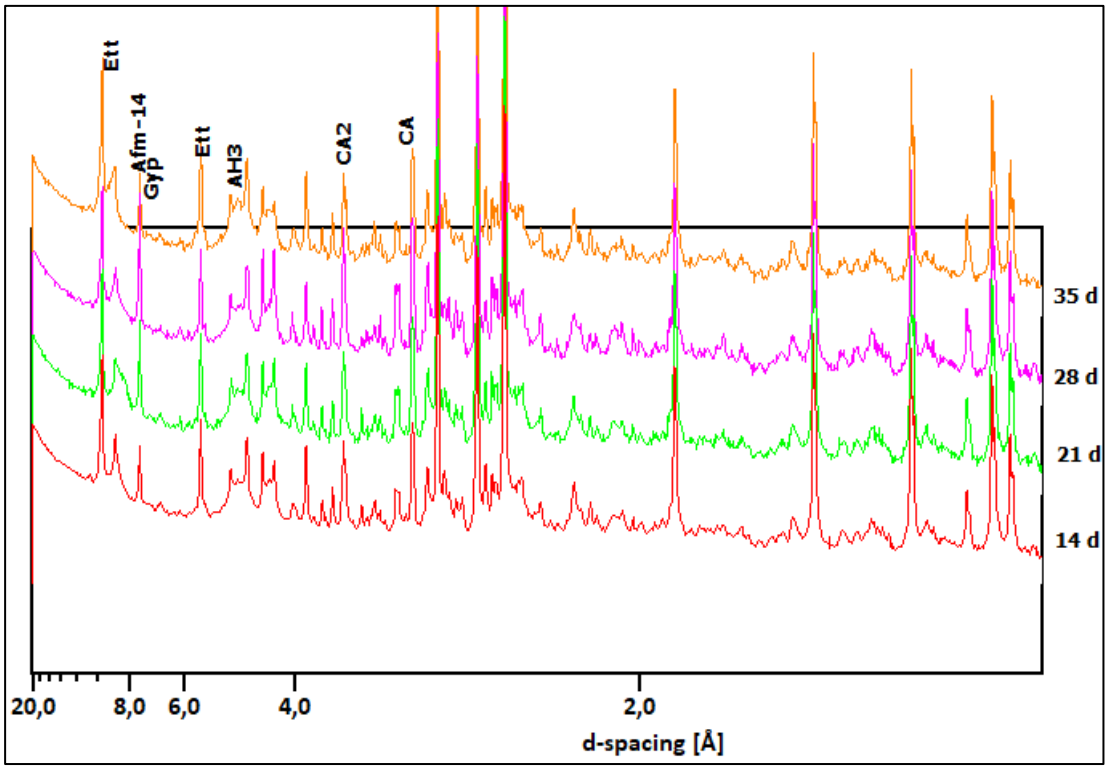

***Fig. 48**: XRPD patterns of sample 1 cured at 40 °C. Ett= Ettringite, AFm-14= monosulfoaluminate, Gyp= Gypsum.*

4.1.2.2.3 SAMPLE 2 (UNCONTAMINATED SOIL +CAC 70)

After 35 days of curing at 40 °C, in addition to the phases coming from the starting soil, sample 2 presented the following ones: gibbsite (13.4 %), monocarboaluminate (8.8 %), CAH_{10} (2.4 %), CA_2 (1.6 %), CA (1.0 %) and hydrotalcite (0.8 %). **Fig. 49** reports the time trend of these phases. The diffractograms (**Fig. 50**) were characterized by an amorphous content resulted to be approximately 20 wt%, overall (**Table c.7**, appendix c). Even in this case an increase of the crystal size of the gibbsite was observed, symptomatic that temperature promotes the crystallization of the gibbsite.

Concerning the trend that the abovementioned phases followed, a slightly different behaviour was observed by comparing these phases to those treated at 20 °C. Indeed, in this case a stabilisation of the trend pattern of CAH_{10}, and CA_2 was observed, as well as a decrement of both hydrotalcite and CA. Instead, a slight rising trend related to both monocarboluminate and gibbsite was reported. These two phases followed the same trend during the considered period. In addition, the conversion of the hydrated hexagonal phases was prevented by the presence of calcite. However, in disagreement with the results of Luz and Pandonfelli (2012), which observed a suppression of the CAH_{10} and C_2AH_8 formation, in

our experiment the CAH_{10} was observed even though at low concentration (2.4%). As in the sample treated at 20 °C, we observed a calcite increment of 4 wt%. According to reaction of the monocarboaluminate formation from calcite (reaction 10 and 11, section 1.5.1), a calcite reduction was expected though. Regardless, given that the calcite trend was stable around 11 wt%, it may be assumed that the monocarboaluminate formation was given by the calcite already dissolved in the matrix and this dissolution occurred before the 14th day. The increased temperature (40°C) enhanced the monocarboalluminate production as well as reduced the CAH_{10}. Furthermore, many studies (Kuzel and Baier, 1996; Wojciech, 1990) reported a partial dissolution of the monocarboaluminate at 40 °C with a subsequent calcite increasing, however we did not observe that after 14 days.

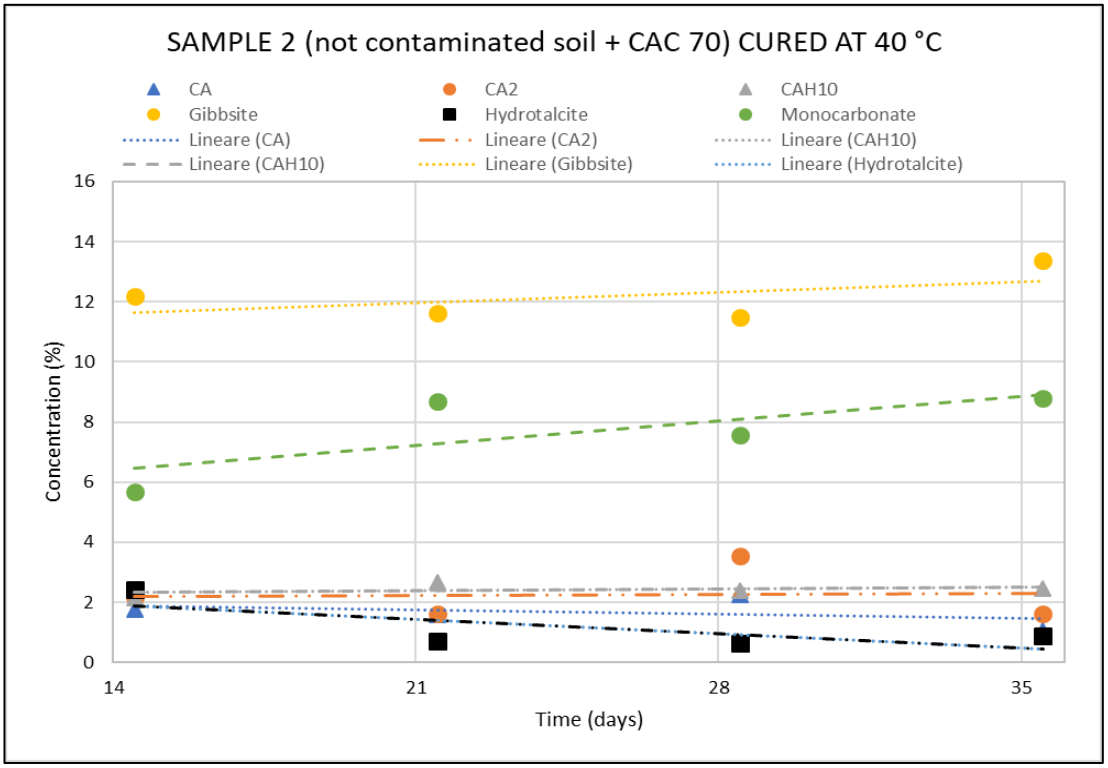

Fig. 49: *Temporal trend of the sample 2 cured at 40 °C for 35 days. CAH_{10} was still present in the sample but the moncarboaluminate presence staved the conversion off.*

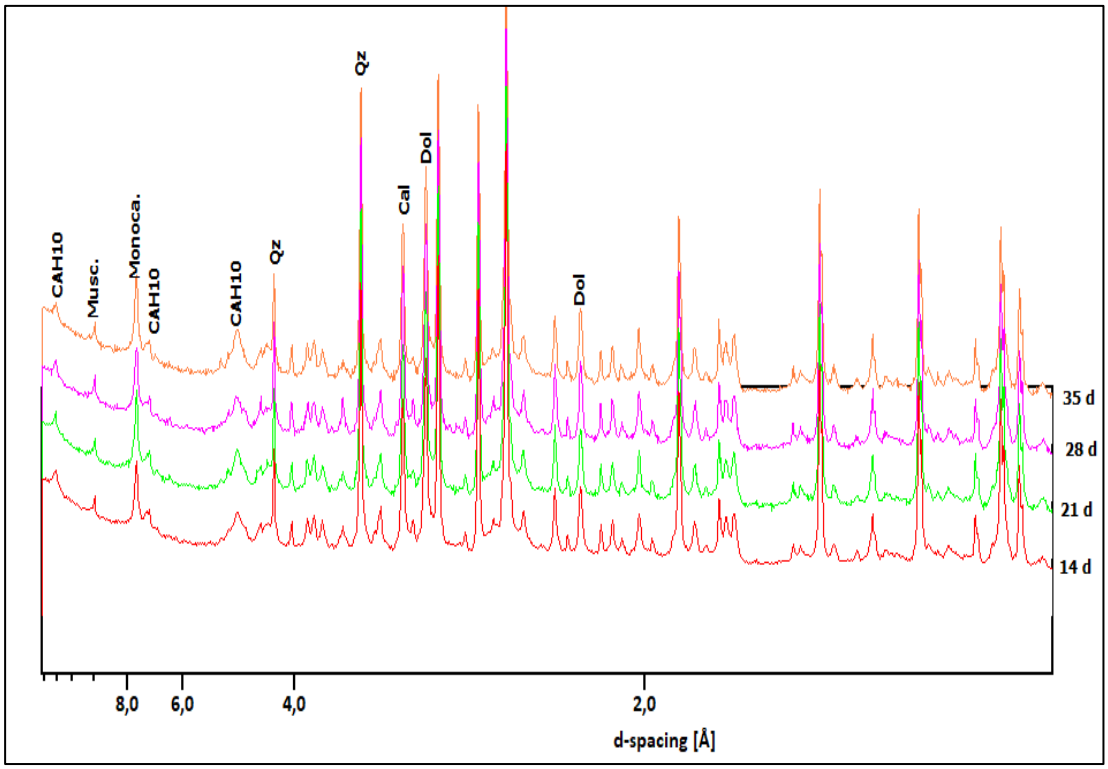

Fig. 50: *XRPD patterns of sample 2 cured at 40°C from 14 to 35 days.*

4.1.2.2.4 SAMPLE 1 (LEAD-CONTAMINATED SOIL +CAC 70)

XRPD analysis outcomes are reported in **table c.8**, appendix c, shows the same phases detected on the sample cured at 20°. In **fig. 51** the XRPD patterns obtained overt the considered time are reported. After 35 days these were: gibbsite, CA (4.8 wt%), CA_2 (6 wt%), ettringite (10.6 wt%), gypsum (1.4 wt%) and calcite (4 wt%). In this regard, the different curing method did not provoke a significant change in terms of different hydration products being formed (**Fig. 52**).

As observed in the control sample (sample 4 and 2), hydrogarnet was not formed in sample 1. As previously stated in paragraph 4.1.2.2.1 and 4.1.2.2.3, both calcite and gypsum hindered the formation of C_3AH_6. As regards to the scarcity of both AFm-14 and monocarboaluminate formed in samples 3 and 2, different reasons intervened. Bizzolero and Scriviner (2015) reported that in high sulphate environments, calcite acts purely as filler not reacting with CA to form monocarboaluminate. In particular, calcite provides more sites to accommodate hydrates and to work as nucleation site (Kocaba, 2009). Regarding AFm-14, Bizzolero and Scrivener (2015) demonstrated its lack in the ternary system containing CAC-

gypsum and calcite, having an excess of calcium sulfate. This is because the principal reaction occurring in the system is the formation of ettringite.

The examination of SEM images (**Fig. 53**) obtained at 20X magnification evidenced a higher porosity on the boundary of the sample. This feature might be associated with the hammering and lapping treatments the sample has been subjected. Therein, a crumbled effect on the outer part of the sample may be assumed, and the inner parts may be less subjected to this phenomenon. Nonetheless, a porosity worsening of the sample may be observed due to the soil presence. Hence, there was not an observable effect related to the curing temperature related to a porosity amelioration/worsening, at least at the magnification we used in our analyses. In **Fig. 54**, we observed again the association between ettringite, and lead given by the presence of Al-S-Ca and the peak due to Pb-L energy channel to confirm the lead presence. A hematite particle is also observed.

EDX analysis carried out on the area delimited by the pale blue square in **Fig. 55 A** determined the presence of lead bearing ettringite (**Fig. 55 B**) along with two unreacted gypsum particles in the surrounding area. This was another demonstration of the capacity of the ettringite to bind lead.

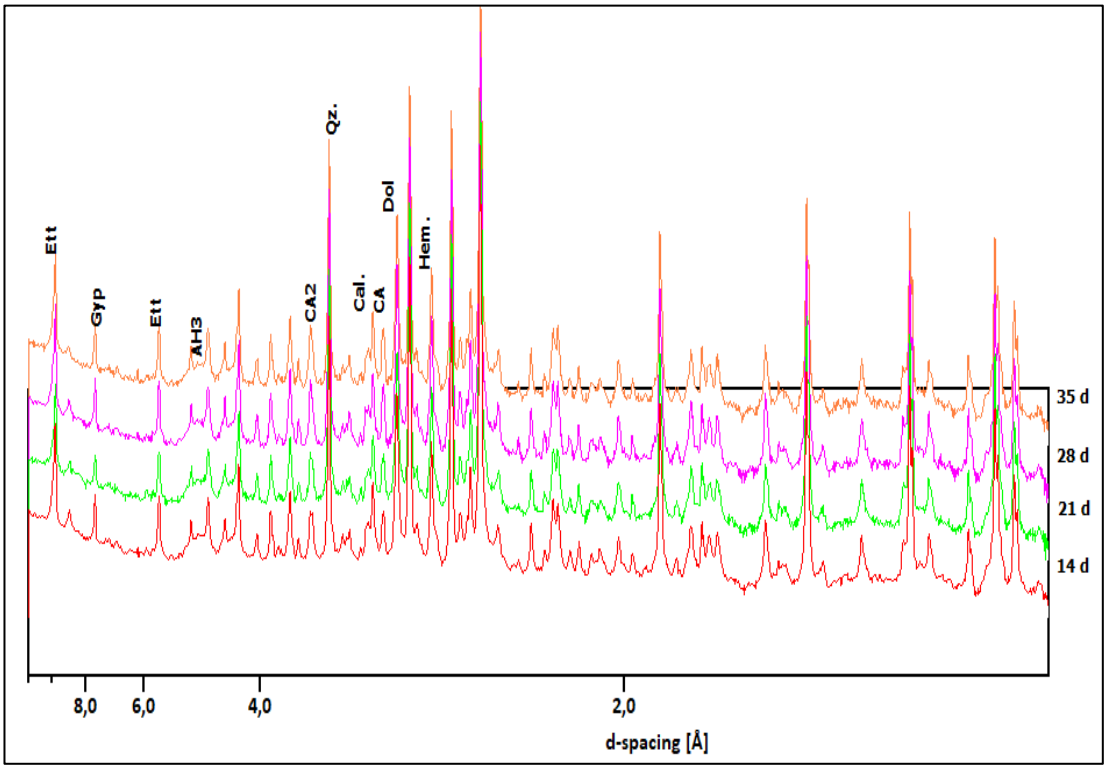

Fig. 51: *XRPD patterns obtained analysing sample 1 cured at 40 °C weekly for 35 days. The mineralogical phases do not differ over time, neither the hydrates phases nor the soil phases. Ett = ettringite, Gyp = gypsum, Qz = quartz, Cal = calcite*

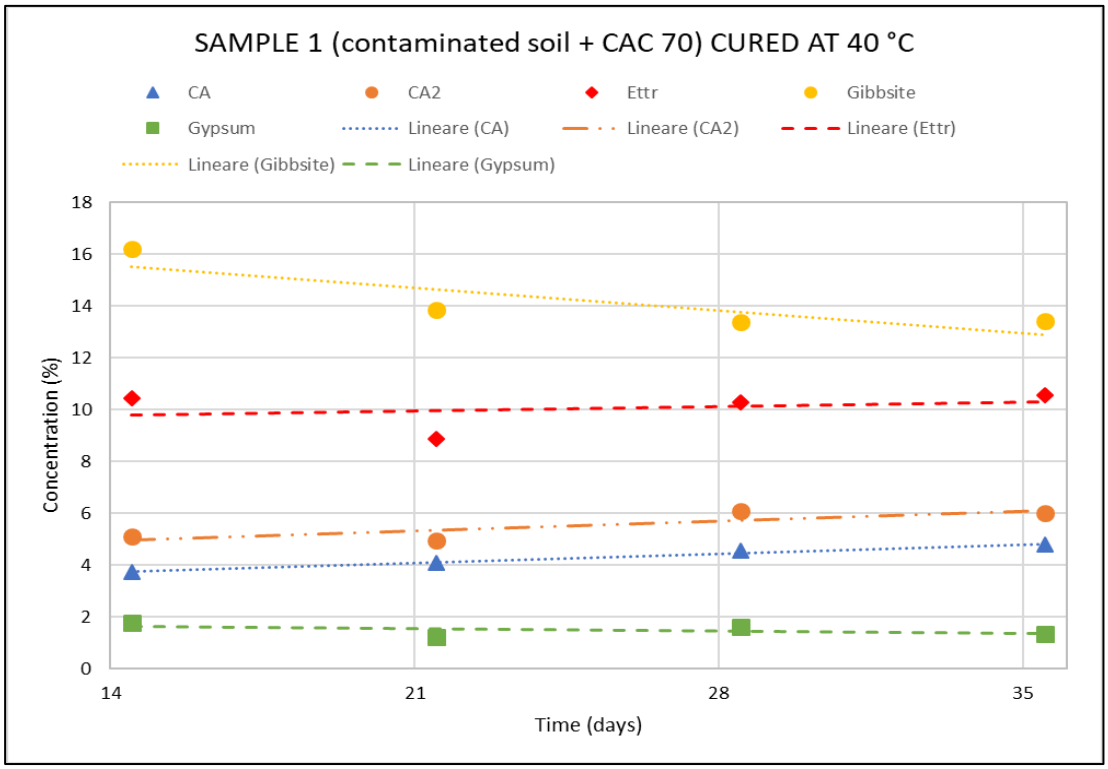

***Fig. 52**: XRPD trends of the observed phases in sample 1 treated at 40 °C for 35 days. There are not significant variations of the phases, and the system may be considered relatively stable. Nonetheless, a slight decrease of the gibbsite (yellow line) was observed.*

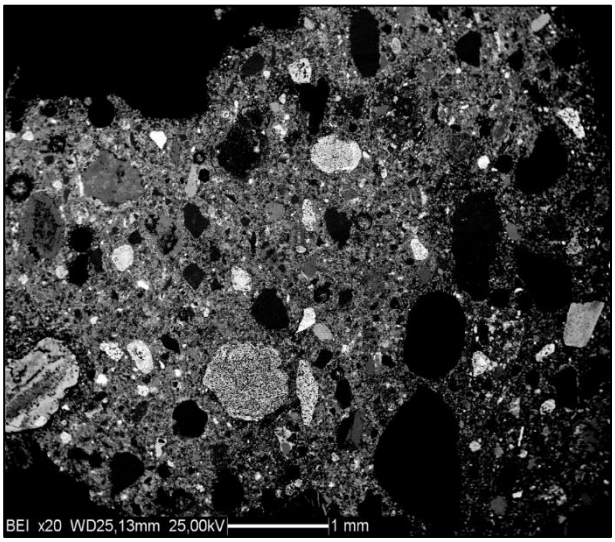

***Fig. 53**: SEM image obtained with 20X magnification. The presence of soil particles along with cement hydrates intercalated in the matrix were observed. White particles are those containing elements having high atomic number, that is, metals. The higher porosity observed on the boundary is probably due to the treatment at which the sample underwent. The phenomenon was not related to the temperature treatment as reported also in the 20°C cases.*

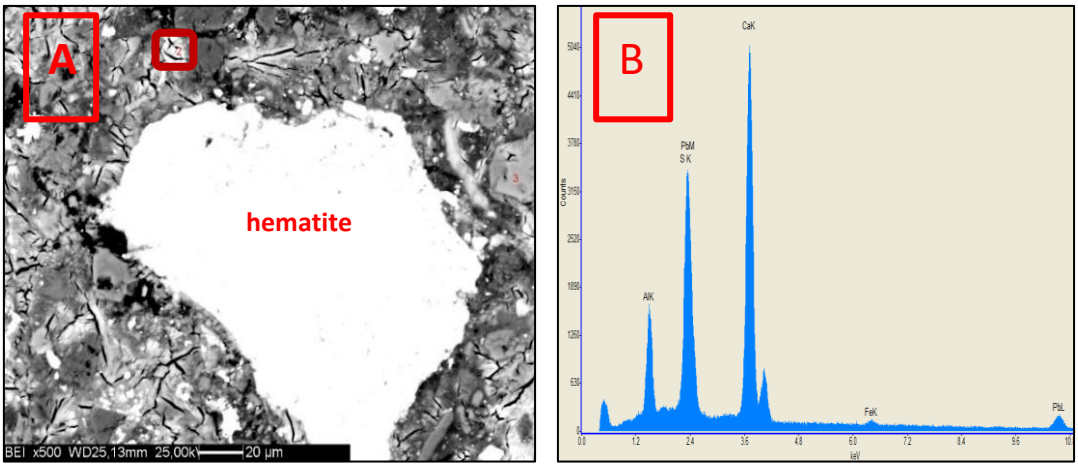

Fig. 54: *A) SEM-EDX analysis revealed that bigger white grain was hematite. EDX analysis (B) carried out in the red square revealed the presence of lead bearing ettringite.*

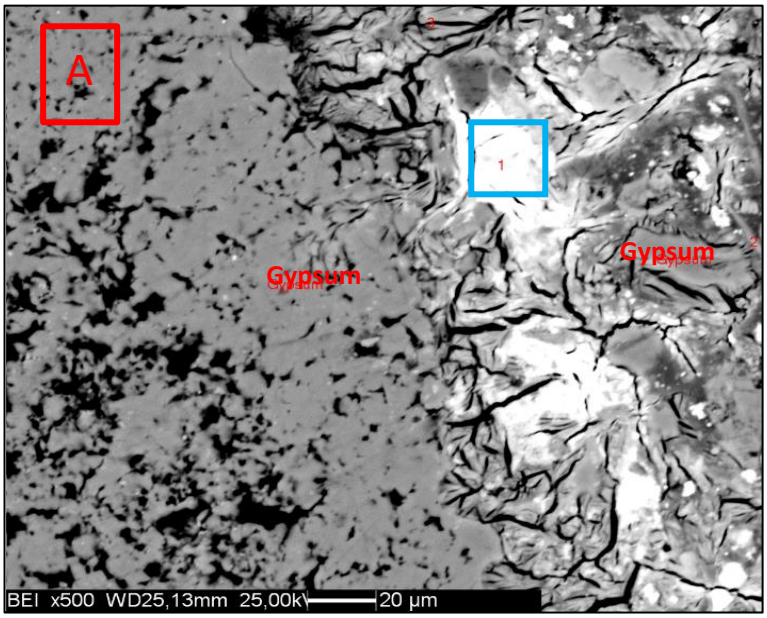

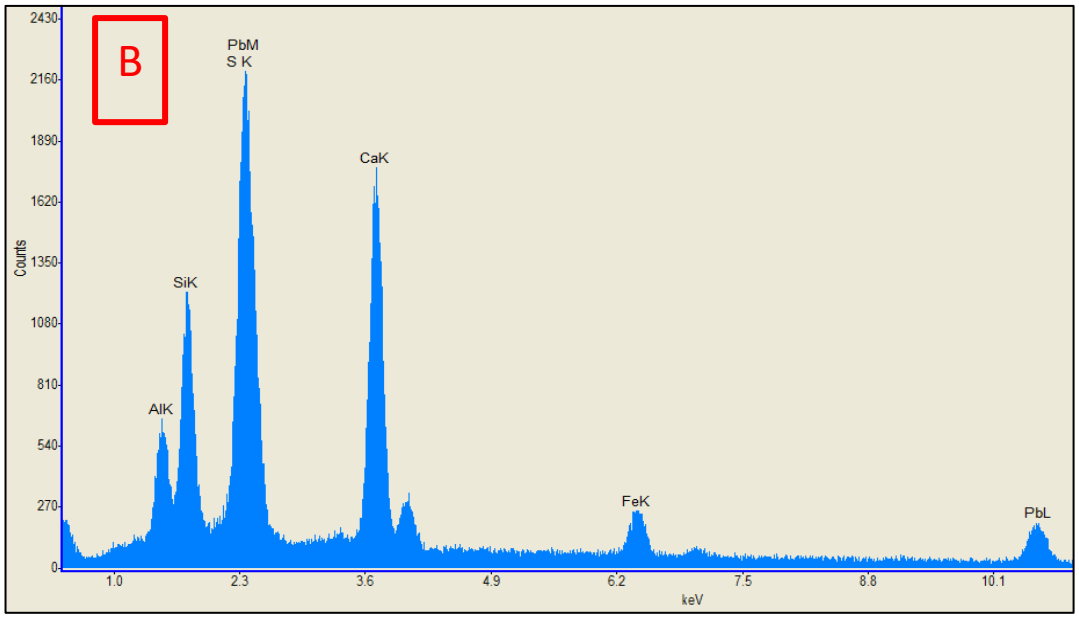

Fig. 55: *Ettringite formation amid two gypsum particles. The presence of lead was revealed via EDX analysis (B) carried out on pale blue rectangular in Fig. A.*

4.1.2 COMPRESSIVE STRENGTH ANALYSIS

The compressive strength results obtained after 28 days are reported in **Fig. 56**. Firstly, a significant difference of strength between the samples cured at 20°C and 40 °C was not observed for all the tests. The considerable variability obtained for the different specimens of sample 4 cured at 40° was given by the heterogeneity of the sample surface presenting different dips on it. For this reason, these compressive strengths outcomes presented larger variability in comparison to the other samples. Anyhow, a reduction of strength between the samples bearing soil and cement, and those containing either CAC and gypsum (sample 3) or just CAC 70 (sample 4) was observed. Particularly, by comparing the average values obtained for the soil bearing-samples and the samples having no soil, the strength was reduced by as much as 47 %, regardless the curing temperature. We may thus conclude that the soil presence, as expected, dramatically lowered the resistance.

In sample 4 (containing just CAC 70) a remarkable difference between the compressive strength associated to the two different curing type was expected. In particular, the sample cured at 20 °C was expected to show a higher resistance than that cured at 40 °C since the conversion between hexagonal to cubic phases in the latter case. Nonetheless, we observed

the opposite behaviour. The average values of compressive strength obtained for the samples cured at 40 °C and 20°C were equal to 58.91 ± 13.99 MPa and 52.61 ± 6.33 MPa, respectively. The higher standard deviation observed for the first sample was due to the presence of irregularities on the sample surface, as previously stated. The better performance characterizing the sample cured at 40 °C might be due to the formation of gibbsite during the conversion reaction. Indeed, according with the SEM observations of Antonovič et al. (2013), AH_3 gel completely or partially covers the irregular cubic C_3AH_6 crystals. However, Taylor (1997) reported that a higher crystallization of AH_3 could also reduce its pore-filling capacity and efficiency as binder. Given that in sample 4 cured at 40 °C, the AH_3 concentration is equal averagely to 20 % and that of C_3AH_6 to approximately 3.50 %, is plausible to state that the gibbsite concentration may counteract the negative impact given by the conversion despite its crystallization rise. Furthermore, Lea (2004) reported that if anhydrous cements remain after the initial formation of metastable hydrates, then it will be available to react with the water released by the conversion reaction, leading to an increase in strength. As reported in the XRPD analysis, CA and CA_2 were still detected after 35 days. Additionally the concentrations of the two anhydrous phases were minor in the sample cured at 40 °C as probably they hydrated forming hydrogarnet. Similarly, Taylor (1997) reported the importance of the W/C ratio upon the conversion effects. In particular, with low ratios, as in our experiment (i.e. W/C = 0.4), there is insufficient space for the hydrates' formation. When conversion occurs, much water is released, so that even though the pores contains no water, more CA can hydrate compensating the effect of conversion. For these reasons, the higher value obtained for the sample 4 cured at 40 °C was plausible.

On the other hand, sample 3 (CAC 70 + gypsum) presented a similar behaviour between the two samples cured at different temperatures. Indeed, the two average compressive strengths obtained were comparable, being them equal to 46.16 ± 4.01 and 42.97 ± 1.39 MPa for the sample cured at 20 °C and 40°C, respectively. The two compressive strength values are comparable to those obtained for the sample 4 and this means that both ettringite and monosulphate (AFm-14), that are the only hydrated compounds to be formed in this system, play an important role upon the compressive strength. Monosulfate formation resulted in the reduction of solid volume of hydrated phase, the increase of porosity, and the drop of mechanical properties (Mehta and Monteiro, 2006; Park et al., 2016). Regardless, the early strength given by the two compounds is directly comparable to that given by the formation of hydrated phases in the sample 4.

Concerning sample 2 (uncontaminated soil + CAC 70), a similar compressive strength between the two sample was observed given that the average values were equal to 25.25 ± 2.33 and 25.79 ± 2.30 MPa for the sample cured at 20 °C and 40°C, respectively. The strength was reduced by as much as 52 % and 56 % for the sample cured at 20 °C and for that cured at 40 °C, comparing them with the sample 4. A drastic strength reduction was thus produced by porosity increase given by the soil presence. These results agree with those reported by Rossler and Odler (1985). The compressive strength results were equally remarkable given that the values were 25 folds higher than that indicated by the Environmental Agency to place it in a landfill (1 MPa) (Environmental Agency, 2010) and also it was similar to the compressive strength developed by an OPC after 4 weeks of curing. Filling of the voids by the hydrate phases could ascribe for the good performance of the sample as the porosity reduction makes the paste less vulnerable to mechanism of deterioration (Akhter et al., 1990). Notwithstanding, sample 4 showed better performance at 40 °C, in this case, the differences were small and comparable, symptom that once again, the higher curing temperature did not worsen the mechanical properties of the material also because there was no formation of C_3AH_6, according to XRPD analysis. Indeed, the hypothetical loss of strength of the system has been avoided by the presence of monocarboaluminate preventing conversion (Cussino and Negro, 1980). Indeed, this latter is formed at the expenses of C_2AH_8 and C_3AH_6 at 25-60 °C (Taylor, 1997). Moreover, the little difference of mechanical strength found between the two samples cured at different temperatures might be ascribed at the similar concentration in terms of both gibbsite and monocarbonate presented in the sample.

Concerning sample 1, in our results we did not observe a detrimental effect given by the presence of Pb into the soil as the compressive strengths of samples 1 and 2 were comparable. This outcome does not agree with that reported by Navarro-Bisco et al. (2013) in which in 28-days aged Pb-bearing mortars the strength was reduced by 75 %. This may be because the mentioned study considered just a system containing $PbNO_3$ at high concentrations (1 wt% metal/cement), while in our study a soil containing sulphates, that thus form ettringite, was considered. Malviya and Chaudhary, (2006) and Bobrowsky et al., (1997) reported that a 3 % addition of metals like Zn, Ni, Pb cold result in strength reduction of 99%. We may thus conclude that ettringite formation drastically improve the compressive strength, in spite of the presence of retarders. The higher compressive strength observed for the sample cured at 40 °C, might be due to a greater amount of AH_3 found (13.43%) with respect to that cured at 20 °C (11.5%) even though the differences are not significant. Moreover, the samples containing soil developed a confrontable strength, symptom that the

presence of lead at high concentration does not affect the hardening properties of this cement. As for the sample 2 though, a lowering of the mechanical properties in comparison with the standard sample (sample 3) was observed. This is likewise ascribable to the soil presence that increase the porosity of the system. Anyhow, mixing CAC with soil permits to obtain a material exhibiting good performances under the mechanical point of view. Our results obtained for sample 1 were even better than those obtained by Zhang et al. (2018) in which a ternary CAC-$CaSO_4$-limestone system cured at 50 °C for 25 days resulted to develop approximately 26 MPa. Comparing these results with those obtained by Contessi (2015) in which a similar soil was treated with OPC and cured in water, an increment of 20% on the compressive strength was obtained for the sample cured at 20 °C.

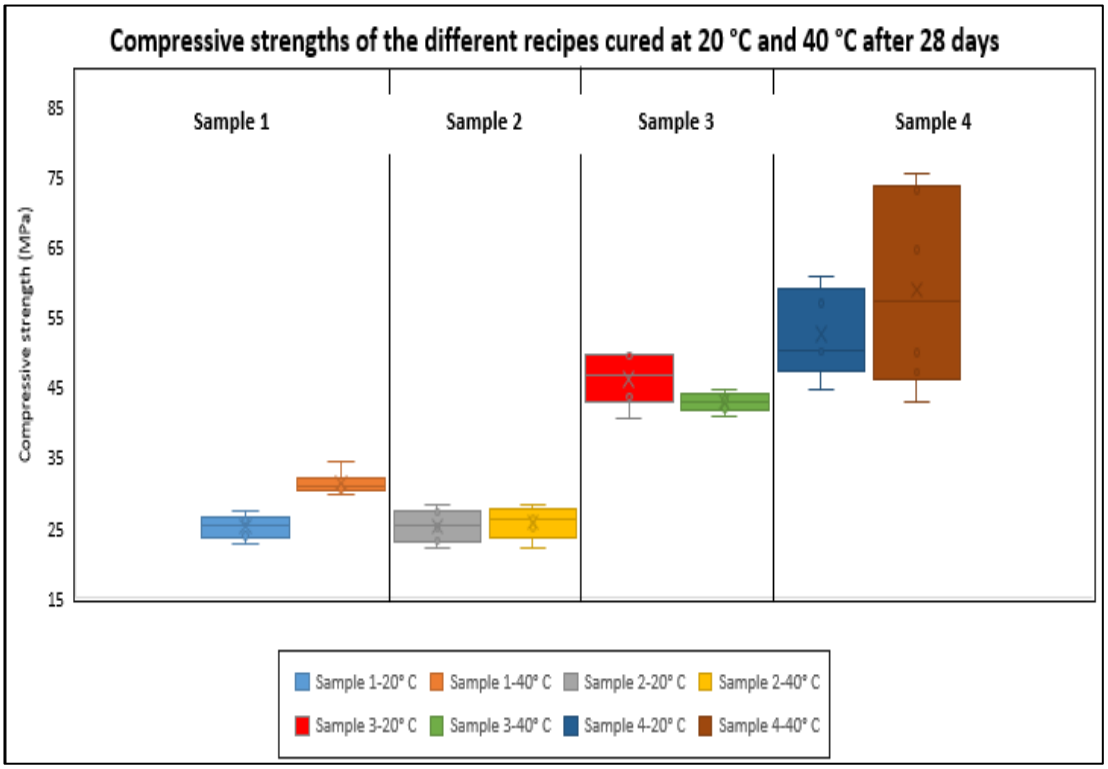

Fig. 56: *Box plot illustrating the compressive strengths obtained for each sample under the two different curing conditions.*

4.1.3 LEACHING TESTS

The variation of concentration of leaching elements with pH follow three different patterns including cationic, oxyanionic, and amphoteric patterns (Komonweeraket et al., 2015). In addition to pH, also newly formed phases observed in the samples could be good candidates for lead retention. Leaching processes causes the partitioning of chemical species between

the solid and the aqueous phase, and they can often be described by processes such as ion exchange/sorption, complexation, precipitation/dissolution and incorporation into a mineral phase (Dijkstra et al., 2004).Concerning the possibility that gibbsite has a role on binding heavy metals, Vithanage et al. (2007) reported that the adsorption thereof was low and thus we may assume that the only binder phase to be considered was ettringite formed in sample 1 at highest concentration, together with the organic matter present in the soil itself. Furthermore, Chrysochoou and Dermatas (2006) stated that gibbsite, hydrogarnet and portlandite cannot play a significant role in the immobilization of hazardous oxyanions. Thus, in our system ettringite may be considered as the only phase able to incorporate metals. WDS analysis ascertained the capacity of ettringite to bind Pb via either substitution of SO_4^{2-} or Ca^{2+} or Al^{3+} that are the most efficient sorption process for several oxyanions and cations, respectively (Perkins, 2000). Despite the EDX analysis are not reliable because of the misidentification between S K and Pb M family peaks, in our analysis we found the presence of Pb in the cracked particles associated with ettringite presence since the 7^{th} day after hydration. Hence, we may assume that Pb may be sorbed by ettringite in the early phases of hydration as also reported by Contessi et al. (2019).

Table 16 reports the variations of pH the sample underwent once exposed to the buffer solutions at pH 7, 5.5 and 4.5. As it may be seen, pH 7 does not affect the final pH, be resulted 11.6. Instead, when treated with acid pH, the buffer capacity of the cement failed as pH significantly decreases. Concerning this, Spence and Shy (2004) stated that above pH 11.6, C-S-H, ettringite, monosulfate, hydrogarnet, brucite, and hydrotalcite also may contribute to ANC (Acid Neutralization Capacity), but below a pH of 9, the solid matrix is generally degraded to the point that these solid phases do not exist. This agree with our results as we may assume that decreasing pH below 7, the dissolution of ettringite occurs, thus decreasing dissolving completely and losing its ANC. The leached concentration of the most critical elements as a function of pH are reported in **Fig. 57**. The legislation limit imposed by the ministerial decree 186/06 is also reported even though the threshold concentrations concern a different standard test (UNI EN 12457-2) not used in our experiment. For this reason, conclusions about whether the material may be considered as reusable cannot be posited. Regardless, the limit is reported as reference to determine the efficiency of retention of the stabilised matrix. Additionally, **Fig. 58** reports the solubility of hydroxide metals as a function of pH. As It may be observed, most of the metals present in our sample are characterized by an amphoteric behaviour, having a greater solubility at low and high pH, and forming the typical V-shape in the solubility-pH plot.

Initial pH	Final pH after 24 h
4.50	5.15
5.50	6.70
7.00	11.40

Table 16: *Initial and final pH of the soil sample in contact with the buffer solutions.*

The most problematic trace elements were those showing an amphoteric behaviour and having higher concentrations in the matrix such as lead and selenium. This was probably due to their release from ettringite which starts to dissolve at pH lower than 10.6 according with Gabrisolvii et al. (1991). For this reason, trace elements such as lead and selenium were well stabilized at the pH range at which ettringite was stable (10.6-12), thereafter showing a dramatic release lowering the pH. This shows also the important role of the hydrate phases. As the pH drops below the material pH, all hydrate phases are destabilised and the adsorbed or incorporated metals in these phases are mobilised (Engelsen et al., 2010). Stegemann and Shi (1997) reported the AFt-based waste form dissolved very quickly in acid environment. This agrees with our results in which As, Cd, Cu, Pb and Se showed higher leachate concentration at the lower pH. The effect of the pH in this system is thus dramatic, and it must be taken into account depending on the final use of the stabilized soil. In fact, the pH regime of the S/S solid is one of the most important parameters and concerns for the success of the treatment, both at the initial stage and over time (Chrysochoou and Dermatas, 2006).

The curing temperature at which the sample was treated slightly affected the leaching pattern for some elements. In particular, regarding the trace elements showing an amphoteric trend, the sample cured at 40 °C showed always minor released concentration, in particular at lower pH, whereas the trend was reversed at higher pH. This could be due to the slightly different amount of ettringite in the two different samples, with the sample cured at 40 °C showing a 1 % more ettringite after 35 days of curing. These differences might not be significative to explain the difference though. As regards to the Mo a linear correlation between pH and leached concentration was observed, in particular increasing its leachate concentration with pH. The low capacity of the system to uptake Mo is due to the large size of MoO_4^2. Kumarathasan et al. (1990) and Saika et al. (2006) reported that uptake of the mentioned ion by ettringite is low or non-existent. Indeed, these compounds were very mobile at basic pH possessed by the cement and lowering the pH at which the reducing conditions can exist, promotes the formation of no-soluble compounds.

Even for selenium case the retention at higher pH was excellent. These results disagree with Baur and Johnson (2003) who stated that selenate incorporation in ettringite is unlikely.

Under oxidizing conditions, the oxyanionic species selenite (SeO_3^{2-}) and selenate (SeO_4^{2-}) are the predominant forms of selenium (Baur and Johnson (2003)). Selenite is considered the less mobile species as may form inner-sphere complexes with surface functional groups under neutral to acid conditions (Su and Suarez, 2000). On the other hand, selenate has low affinity for oxide surfaces. Baur and Johnson (2003) reported a better adsorption of selenate operated by monosulphate by means of a substitution between selenate and sulphate ions. On the other hand, Kumarathasan et al. (1990) and Zhang and Reardon (1995) report that at basic pH, selenate should substitute sulfate in the ettringite structure. In our results we observed that a sorption effect by ettringite may be occurred as at basic pH, the leached concentration was reduced. In addition, the two different leaching patterns obtained at 20°C and 40°C, showed a different behaviour. The same result was obtained for the Sn. More investigations, possibly taking into account the whole pH range, are needed to understand whether this effect was due to an instrumental error or to a different phenomenon. However, we may assume that the first option is more probable as the two samples cured at different temperature contain similar ettringite concentrations.

We observed a worsening of the sorption performances of our system by lowering the pH, in particular for the amphoteric elements. By lowering the pH indeed ettringite is destabilized and releases the elements previously embedded. This means that ettringite is pH dependent species.

Comparing the results of Pb leaching obtained at a pH of 7 with those obtained by Contessi (2015) in which a sample containing 73.5 % of soil, 13.27% of FA, 13.27% OPC and 3.4 % Mapefast Ultra was demonstrated to be the best to stabilize the same soil, releasing 35 ppb, we may conclude that under the same conditions CAC shows better performance as the released concentration was 1.14 ppb for the sample treated at 20 °C. As stated by Navarro-Basco et al. (2013), Pb is fully retained in the CAC matrix by ettringite replacing Ca^{2+} as it forms less amphoteric, and so less soluble hydroxides that are totally encapsulated in the CAC mortars. As regards to the amphoteric trend, this agreed with the results of Du et al. (2018) in which an amphoteric V curve with a minimum at 8.4 in MSWIFA treated with OPC was obtained.

Calcium leaching might be examined to determine whether a degradation process by means of the aggressive solution has occurred during the leaching test.

As regards to the Cr^{6+} sorption our results demonstrated that the CAC was able to well adsorb it in a better way than that observed in an OPC system. This may be due to the absorption of CrO_4^{2-} by ettringite as reported by Perkins (2000).

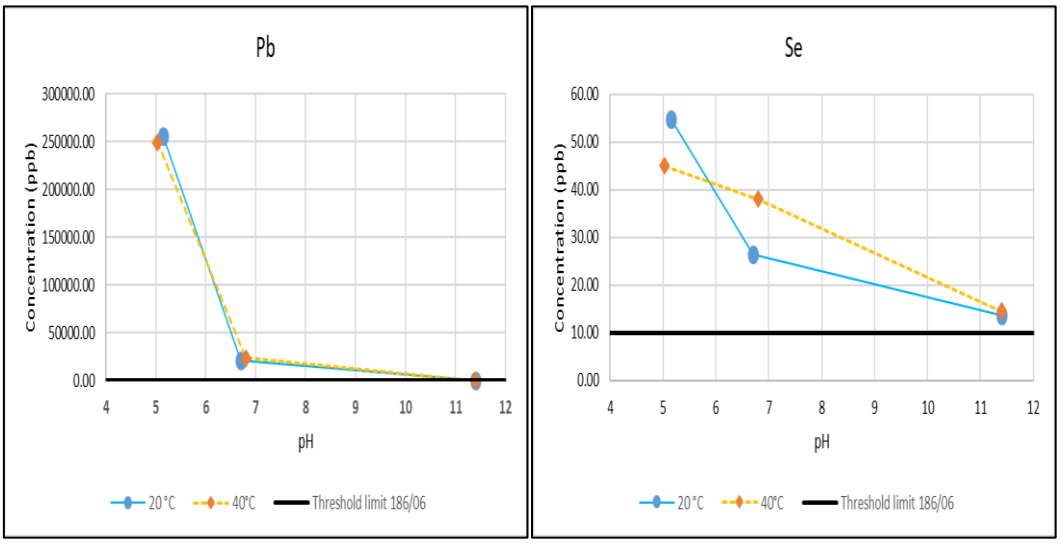

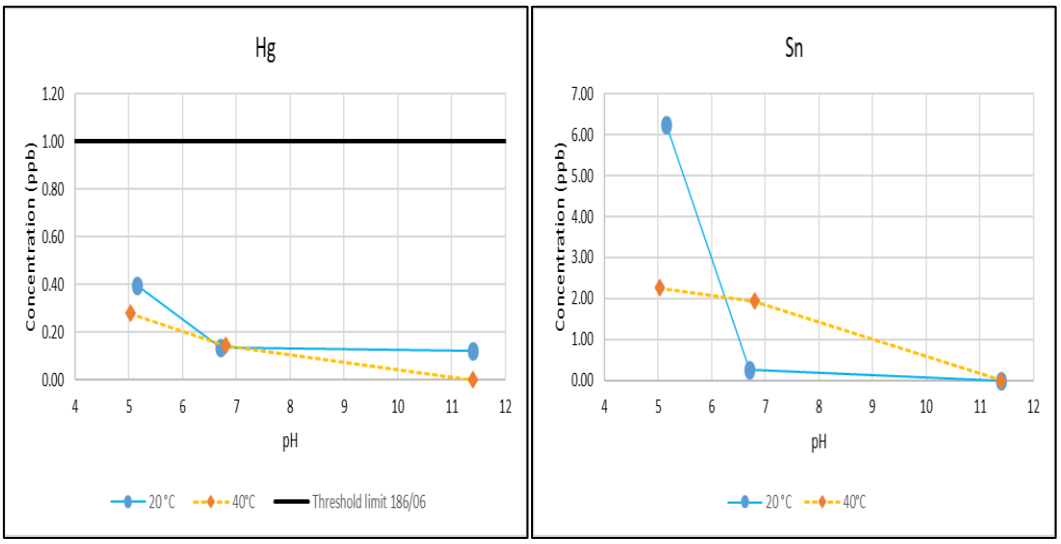

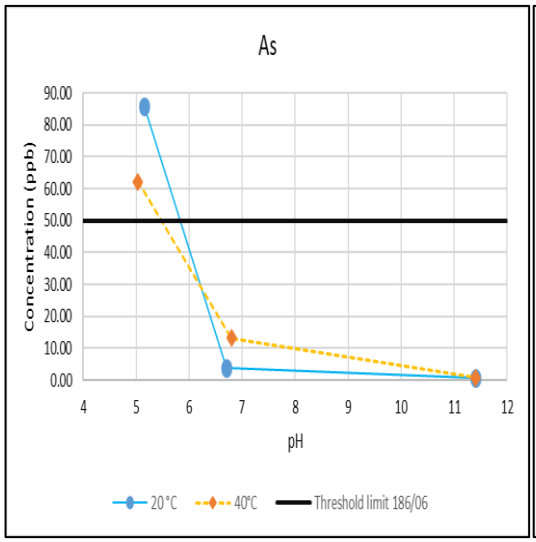
As
Concentration (ppb)
90.00
80.00
70.00
60.00
50.00
40.00
30.00
20.00
10.00
0.00
4 5 6 7 8 9 10 11 12
pH
20 °C
40°C
Threshold limit 186/06

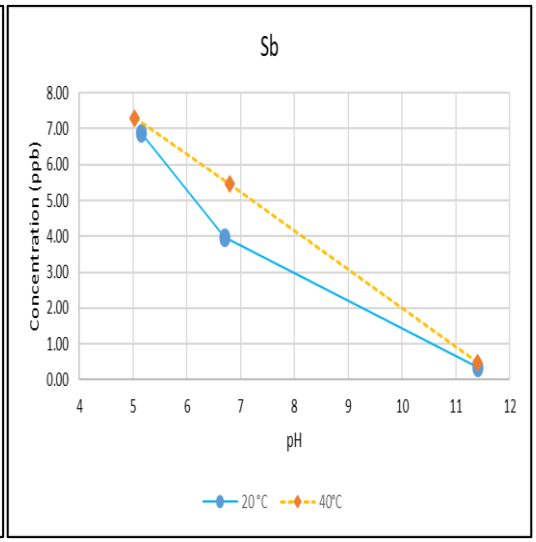
Sb
Concentration (ppb)
8.00
7.00
6.00
5.00
4.00
3.00
2.00
1.00
0.00
4 5 6 7 8 9 10 11 12
pH
20 °C
40°C

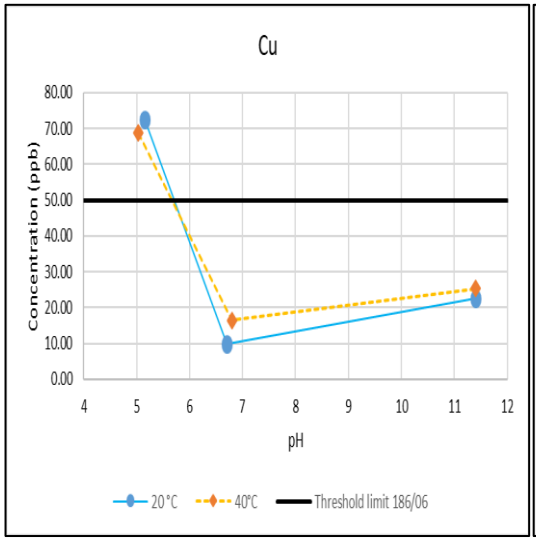
Cu
Concentration (ppb)
80.00
70.00
60.00
50.00
40.00
30.00
20.00
10.00
0.00
4 5 6 7 8 9 10 11 12
pH
20 °C
40°C
Threshold limit 186/06

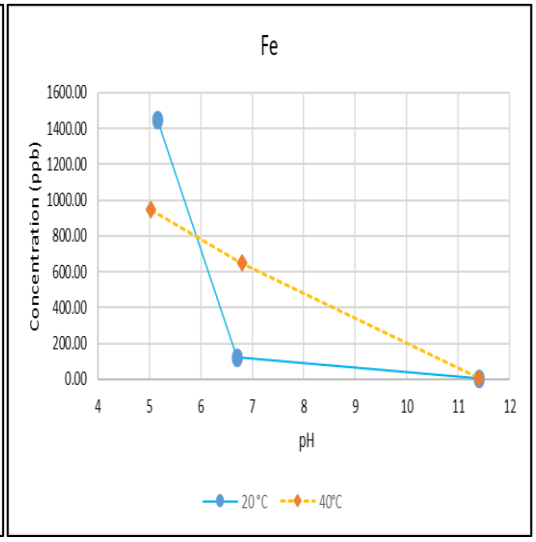
Fe
Concentration (ppb)
1600.00
1400.00
1200.00
1000.00
800.00
600.00
400.00
200.00
0.00
4 5 6 7 8 9 10 11 12
pH
20 °C
40°C

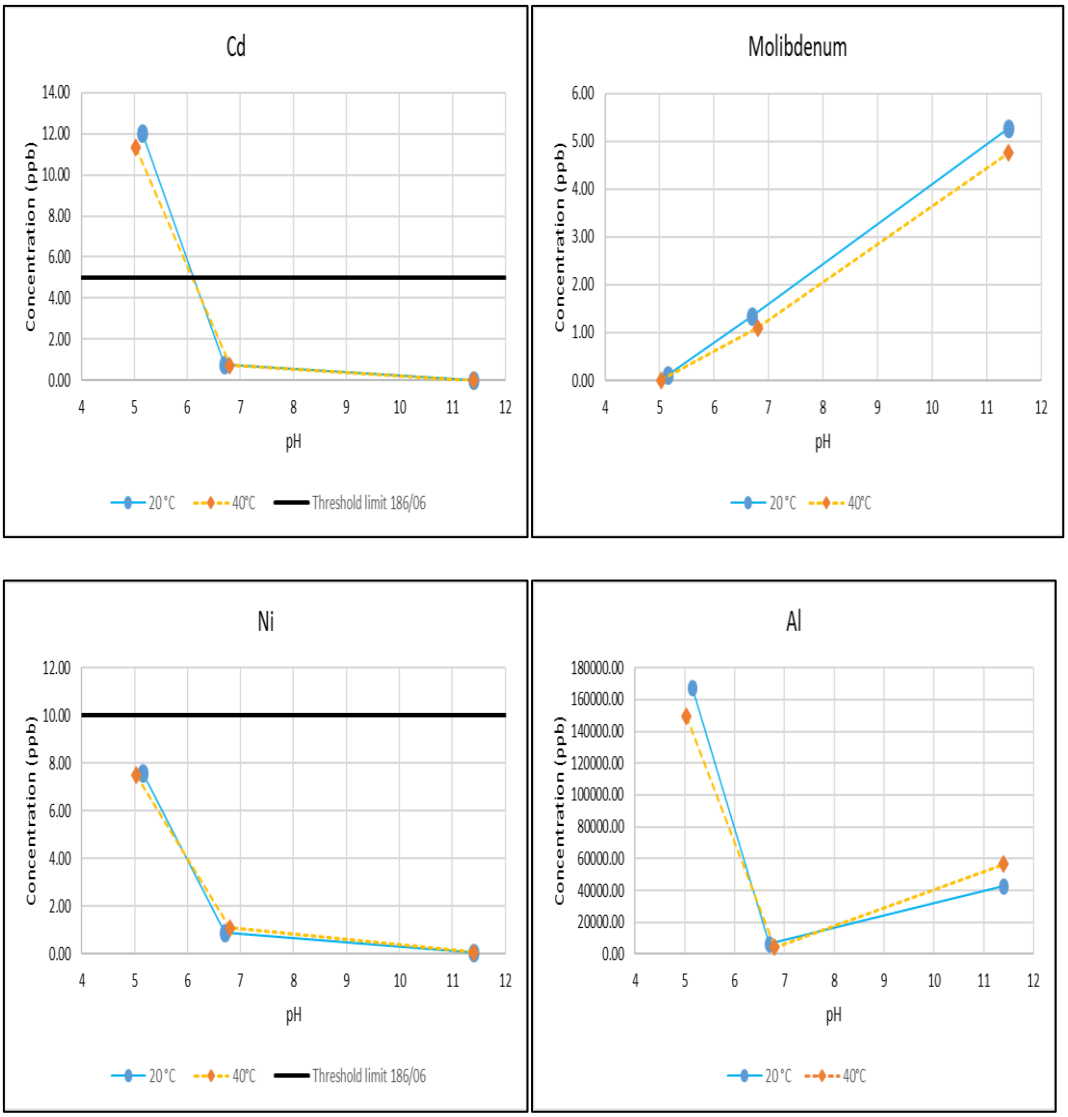

Fig. 57: *leaching (ppb) of the main elements having higher concentrations in the soil as a function of pH. The concentrations of each element were compared with the Italian threshold limit 186/06.*

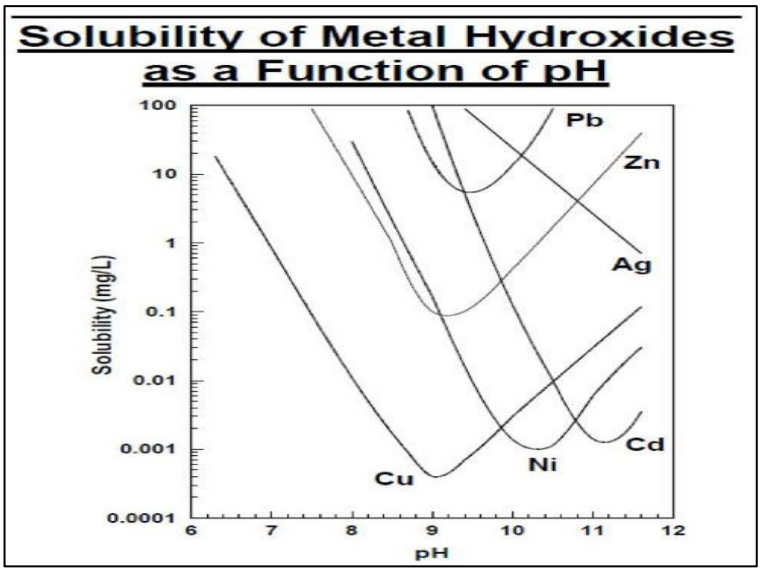

Fig. 58: *Solubility of hydroxide metals showing amphoteric behaviour (Source: EPA 625/8-80-003)*

4.2 MUNICIPAL SOLID WASTE INCINERATOR FLY ASH (MSWIFA)

4.2.1 UNTREATED MSWIFA

The results of ICP-MS analysis carried out on the sample of untreated MSWIFA are reported in **Table 17**. The samples collected at different times in the same MSWI are also reported. The concentrations of the heavy metal depend on the type of waste being incinerated, the binding environment of the metals and the operating conditions of the incinerator (Weibel et al., 2017). As it may be observed, the concentrations of the different elements vary considerably among the different samples. Similar studies reported concentrations that may vary of many orders of magnitude (Eighmy et al., 1995; Shi and Kan, 2009; Liu et al., 2015). However, an important observation is that heavy metals with high vapour pressure and a low boiling point such as Zn, Pb and Cd are highly enriched in the fly ash as shown in previous studies (Le Forestier and Libourel, 1998; Li et al. 2004; Bayuseno and Shmahl, 2011; Weibel et al., 2017). Our historical dataset agreed with this latter observation. Furthermore, the presence of chlorides and sulphides is remarkable. Therefore, it is clear that the studied material requires a stabilisation or inertisation process prior to be disposed into landfills or reutilised (Karamanov at al., 2003).

Element	U.m	July 2017	August 2017	September 2017	October 2017	Novemeber 2017	January 2018	SAMPLE
Al	mg/kg s.s.	7230.0	9531	35017	9674	29993	10818	
As	mg/kg s.s.	12.6	9.9	7.8	8.2	<1	4.0	19.31
B	mg/kg s.s.	56.6	55	126	73	121	78	
Ba	mg/kg s.s.	228.4	236	900	422	183	412	616
Be	mg/kg s.s.	0.1	<0,5	0.7	<0,5	0.9	<0,01	0.72
Cd	mg/kg s.s.	133.3	105.6	77	105	51	84	92.6
Co	mg/kg s.s.	6.2	7.1	20	16	17	10	12.5
Cr	mg/kg s.s.	57.2	47.5	154	99	143	77	156
Cu	mg/kg s.s.	528.9	490	941	592	720	591	643
Fe	mg/kg s.s.	2513.0	2988	10026	4489	12545	2996	
Hg	mg/kg s.s.	7.3	6.5	2.5	3.1	2.7	6.0	6.37
Mn	mg/kg s.s.	184.8	214	587	430	537	415	603
Mo	mg/kg s.s.	8.1	7.9	16	8	21	7	19.63
Ni	mg/kg s.s.	27.5	28	88	48	68	30	98.4
Pb	mg/kg s.s.	2326.0	1755.0	1146	1574	1151	1595	1750
Sb	mg/kg s.s.	571.1	481	344	418	346	360	471
Se	mg/kg s.s.	4.0	3.3	6.7	3.9	13	18.0	3.21
Sn	mg/kg s.s.	239.5	234	59	125	70	131	303
Tl	mg/kg s.s.	3.3	1.4	12	10	20	6	0.54
V	mg/kg s.s.	13.8	18.9	73	24	66	39	16.23
Zn	mg/kg s.s.	10988.0	9511	8200	9205	5939	6200	7094
Cloruri	g/kg s.s.			130	144	196	148	
Solfati	g/kg s.s.				1.4	5.2		

***Table 17**: Total content concentrations of different MSWIFA samples analysed in different months. Last column is concerned the sample used in this thesis.*

Although the calcium and the aluminium were not analysed in our sample, Weibel et al. (2017) reports average concentrations of 190,000 and 30,000 mg/Kg, respectively. Regarding Al, the samples collected during the different times agreed with those range of concentration.

Multiple XRPD analyses (**Fig. 59**) were conducted on the same sample, resulting in a very low reproducibility of data due to the great reactivity of the material. As observed by Bayuseno et al. (2009), fly ash is very highly reactive and subjective to mineralogical alteration when in contact with environmental conditions. Also, Izquierdo et al. (2011) reported that MSWIFA has the capacity of adsorbing a large amount of water. Indeed, except for some phases (like halite, sylvite, calcite and anhydrite) that were always observed in all the XRD patterns, new hydrated phases were observed, indicating that MSWIFA was subject to undergo hydration due to the hygroscopic behaviour of halite, sylvite and anhydrite. **Fig. 60** illustrates the sample-holder with the MSWIFA after 3 days. It is possible to see that the sample hydrated even inside the sample holder. These observations agree also with what reported by Polettini et al. (2001), Wan et al. (2018), and Baysuseno and Schmahl (2011).

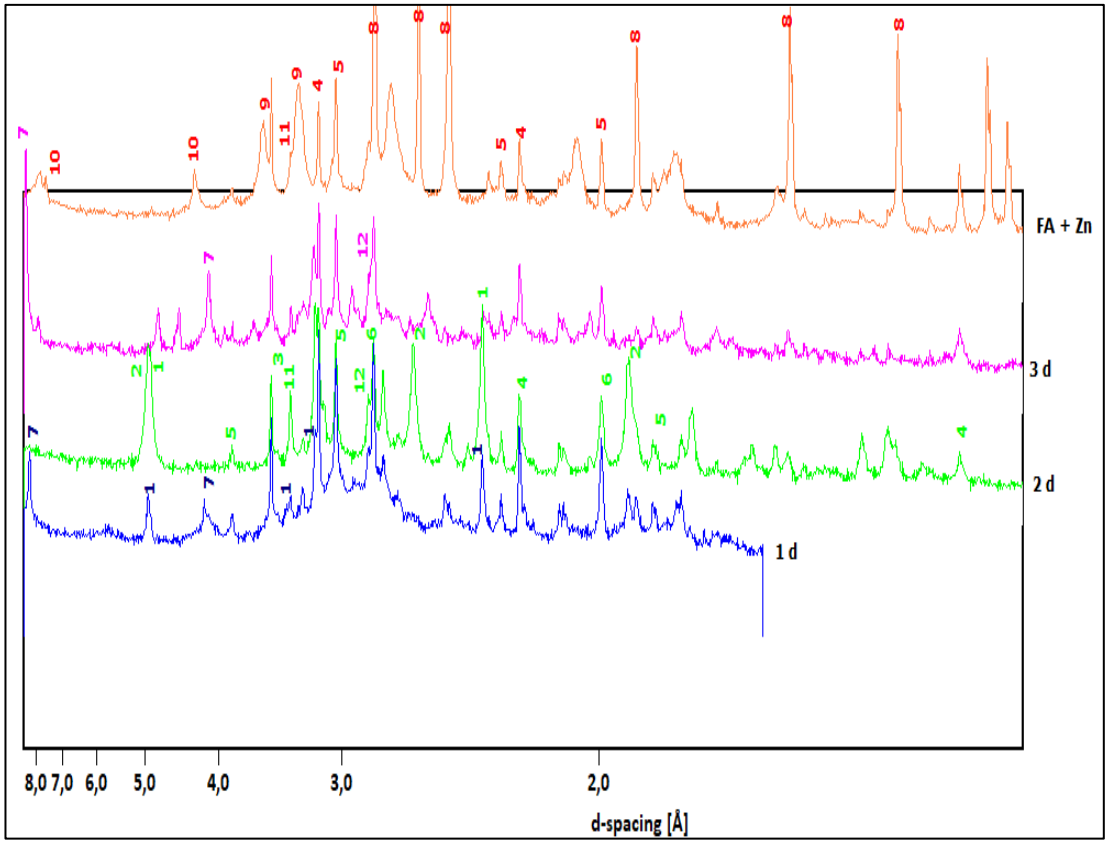

***Fig. 59**: XRPD diffractograms performed on the untreated MSWIFA sample, analysed for 3 consecutive days. A quantitative analysis was attempted using Zincite as internal standard (orange pattern). Many phases were unknown and an astonishing variability of the sample upon exposure to*

air was registered. This is observable through the rapid change of the phases over time. 1: ZnClOH, 2: portlandite 3: anhydrite 4: sylvite 5: calcite 6: halite 7: calcium chlorate hydroxide 8: zincite 9: vaterite 10: gypsum, 11: quartz, 12: gehelenite

In our study, Zinc chlorate hydroxide (ICDD # 41-715) was found in MSWIFA sample analysed in the first day and after 3 days (respectively, blue and purple patterns in **Fig. 59**). Bayuseno et al. (2009) reported the presence of significant amount of a similar phase, i.e. K_2ZnCl_4, reporting to be unusual but in well agreement after having performed a Rietveld refinement. However, we did not ever find this phase in our samples. The presence of gehlenite in MSWIFA is also reported by Liu et al., (2009), Ohbuchi et al. (2019).

An XRPD quantitative analysis (**Table 18**) of the MSWIFA, using Zincite as Internal standard, was performed 3 months before the other qualitative analysis. The phases quantification reported the 55.71% of the sample to be composed of Vaterite. In addition, calcite, halite, hydrocalumite, anhydrite, periclase, sylvite and quartz were present. The lack of vaterite in the other samples may be due to its transformation into the more stable calcite once exposed to the ambient conditions for 3 months. The presence of hydrocalumite was also found by Bayuseno and Schmahl (2011) in a 12-months aged MSWIFA. Since XRPD patterns did not show peaks related to heavy metals phases, these latter are most probably present either as impure, complex compounds or as amorphous species (Polettini et al., 2001).

SEM analysis carried out on the sample of MSWIFA (**Fig. 61**) revealed that the grains were characterized by a significant dimensional heterogeneity with particles characterized by different shapes: some were rounded, whereas others more elongated. Flat and fibrous grains were not detected though. Larger particles were surrounded by sub-micron grains randomly distributed to form a sort of matrix. It was not possible to consider these latter particles in the dimensional distribution analysis (**Fig. 62** and **63**), reported below, because of the difficulty to discern these particles singularly. The particles size frequency (**Fig. 63**) presented a bimodal distribution with two maximum values at the diameter of 20 and 100 µm. No particles showing a diameter greater than 1 mm were found, whereas dimensional uncertainty on the smaller particles is due to the limits of the used method, which did not consider particles diameters below 5 µm. Weibel et al. (2017) reported a bimodal particle distribution with two groups between 20-200 µm and 200-400 µm in diameter, in accordance to our results. A similar study conducted by Gilardoni et al. (2004) reported a different size distribution with most of the particles belonging to the submicron regions, at 0.5 µm. However, in the same study no correlation between particle size and chloride presence was found, with this latter evenly distributed over all the dimensional ranges.

To ascertain the chemical composition of the analysed particles, SEM-EDX was used (**Fig. 64** and **65**). These investigations reported that larger particles were generally characterized by a significant amount of Cr, Pb, Fe and Ni together with Cl, Ca, and Si. Since no metals-bearing phases were found in the XRPD analysis, except for Zn that presented higher concentrations, these metals are most probably just dispersed in the sample, not forming mineralogical phases, as concentrations are too low. Furthermore, SEM-EDX analysis confirmed the presence of some particles having a composition ascribable to that of gehlenite ($Ca_2Al[AlSiO_7]$) or wollastonite ($CaSiO_3$), the former reported in all the XRPD analysis, whereas the latter probably present as minor component. As previously reported, the XRPD analysis revealed the presence of Cl in remarkable amounts and no association with the particle size was pinpointed. However, it was detected a slight enrichment of Cl in the areas outside the larger particles and in the smaller dark-gray particles present among the larger ones (**Fig. 65**).

Fig. 60: *Sample of fly ash exposed to ambient conditions for 3 days. Swelling is observed.*

N	Mineral Phase	Concentration (%)	Error (%)
1	Vaterite	55.71	0.40
2	Amorphous content	17.97	0.76
3	Calcite	8.75	0.06
4	Halite	4.98	0.03
5	Hydrocaluminte	4.10	0.03
6	Anhydrite	3.12	0.02
7	Periclase	3.10	0.02
8	Sylvite	2.02	0.01
9	Quartz	<1	

Table18: *MSWFA XRPD quantitative analysis revealed that approximately half of the sample was composed of vaterite. However, qualitative analysis performed after 3 months on the same material reveals the presence of calcite.*

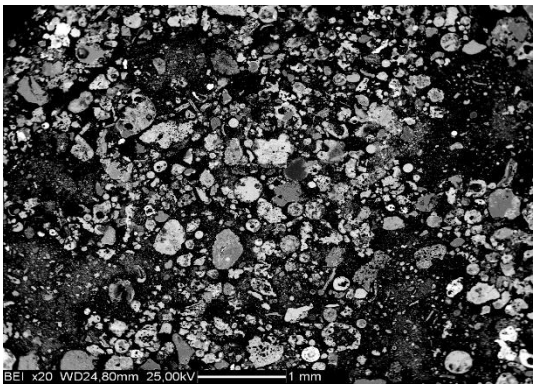

Fig. 61*: SEM image of the MSWIFA obtained at 20x magnification, used to analyse the particle size***.**

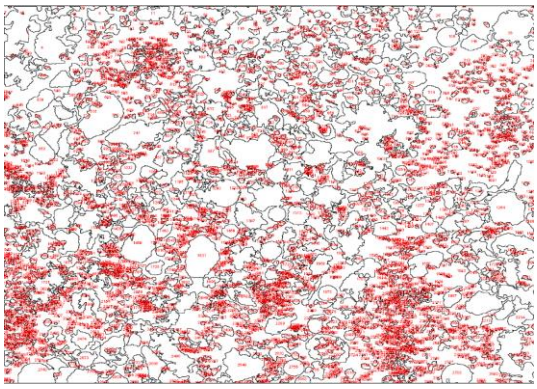

Fig. 62: *Boundaries of the analysed particles.*

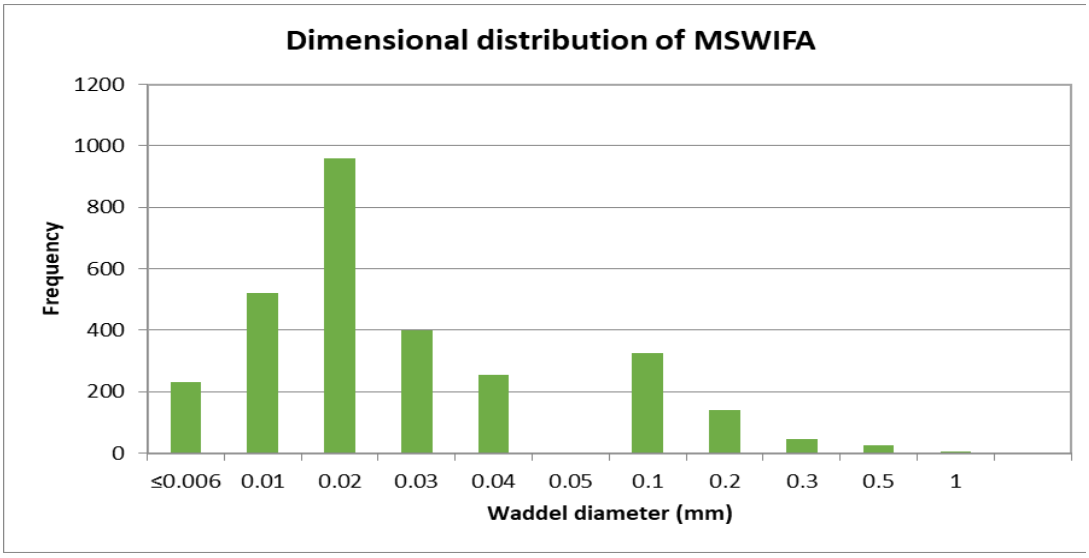

Fig 63*: Dimensional distribution analysis of MSWIFA. A bimodal distribution with two maximums at 0.02 and 0.1 mm, respectively were obtained. Regardless, the size of the particles did not exceed the mm as upper limit. Instead more uncertainty existed for the lower limit as the method was not capable to discern particle sizes with a dimension smaller than (5 µm).*

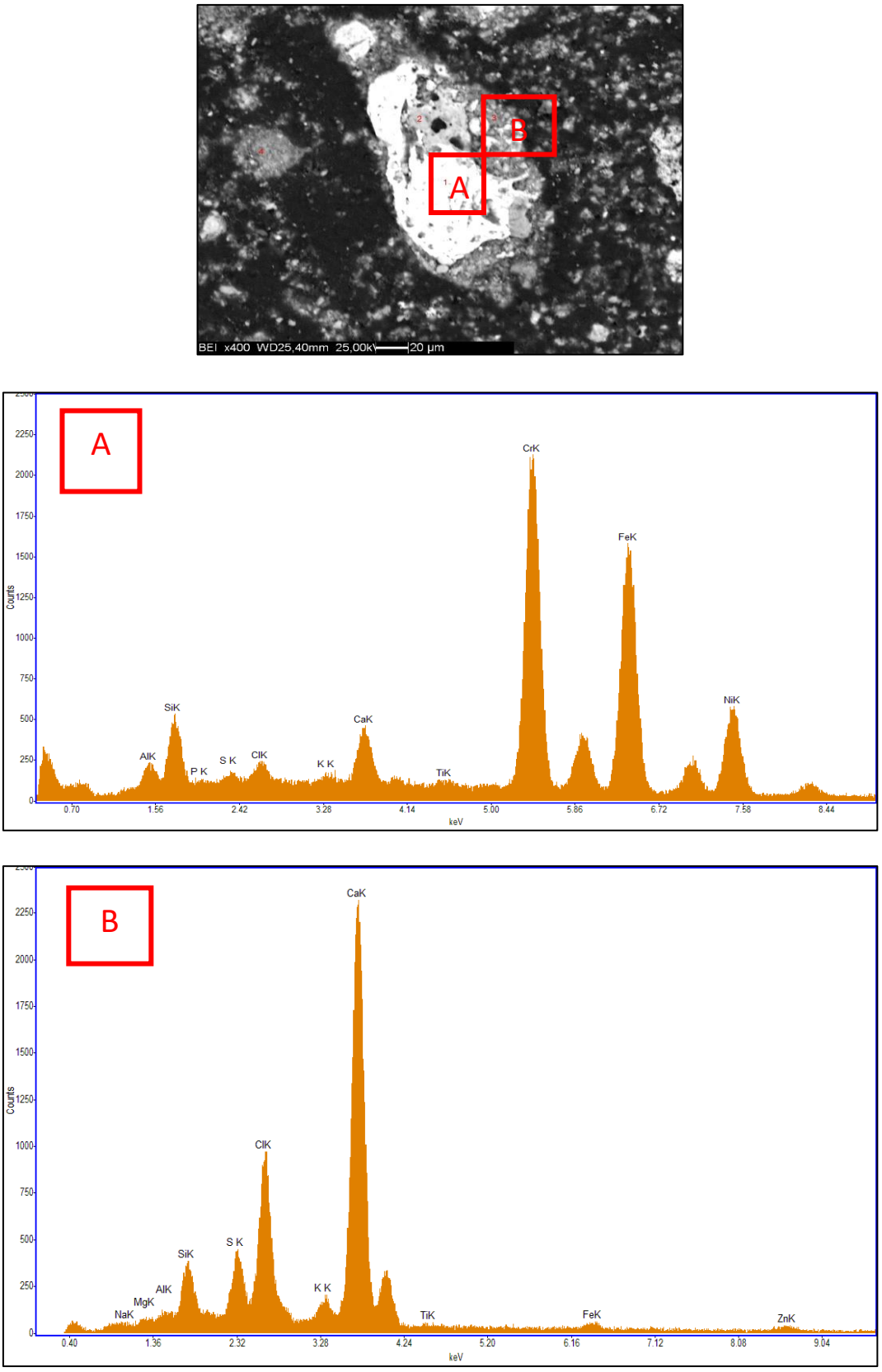

Fig 64: *SEM image of a particle of the MSWIFA sample. EDX analysis in point A detected the presence of Cr, Fe and Ni in high abundance. Point B revealed the presence of Calcium sulphate (probably anhydrite), Si and Cl.*

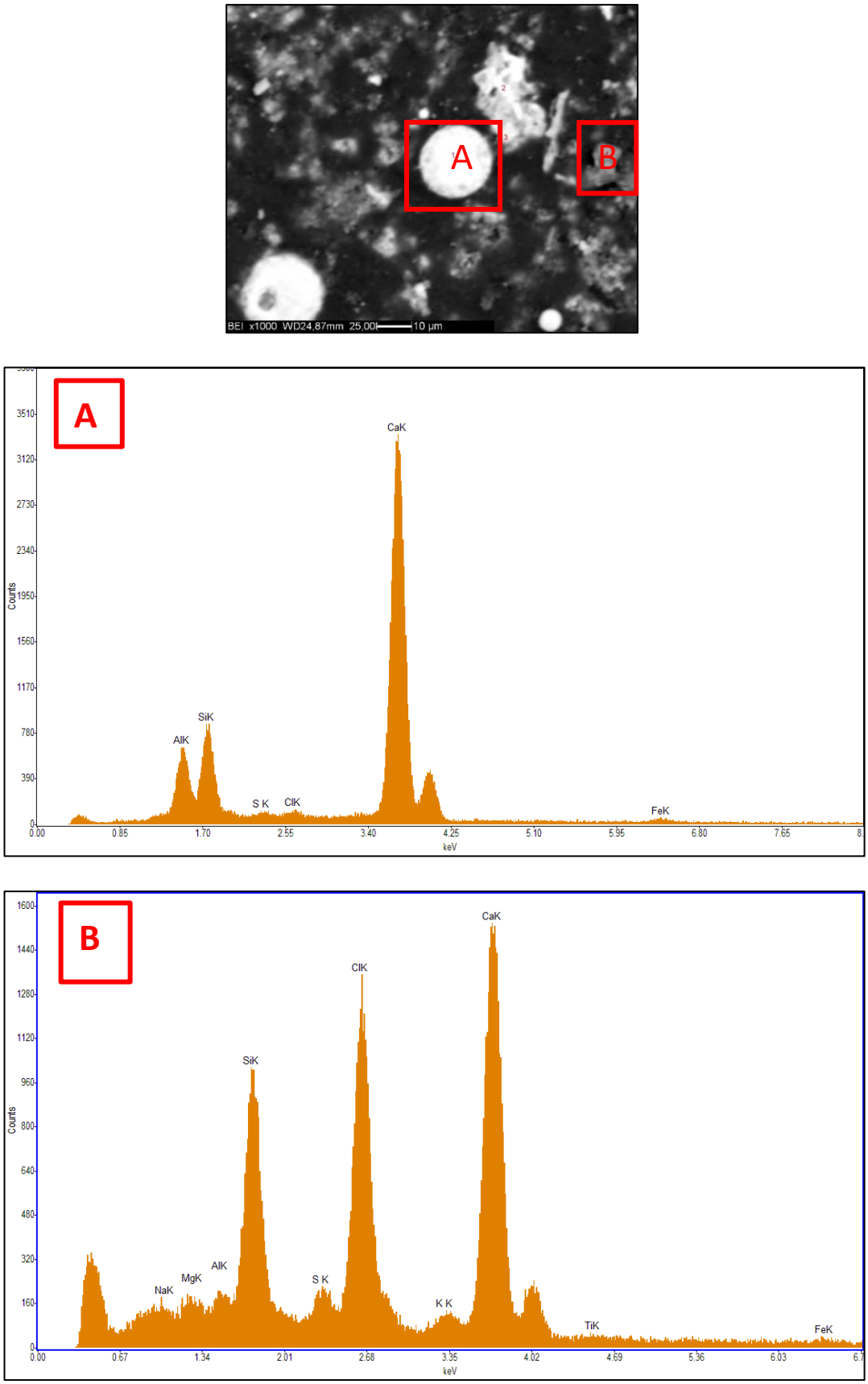

***Fig. 65**: Rounded particles (A) of fly ash surrounded by irregular grains. EDX analyses revealed that the particle (A) is composed by Ca, Al and Si (Probably gehlenite). EDX image on an irregular grain (B) detected the presence*

of a Silicate-Ca associated with great amount of Cl. To be noted that the gehlenite particle does not present Cl, whereas the B point presented it at significant amount.

4.2.1 HYDRATION OF OPC-MSWIFA

Fig. 66 reports the XRPD pattern obtained at the beginning of hydration – T0 (green pattern), after 24 hours (red pattern), after 14 days (orange pattern) and after 60 days (purple pattern).

At T0 the following phases were detected: Zinc chlorate Hydroxide, C_3S, portlandite, calcite, anhydrite, halite and sylivite. Balonis et al. (2010) conducted hydration tests on a binary system composed of Cl and OPC in presence and absence of calcite for ascertaining how the system evolved. They observed that the formation of Kuzel's salt [$(Ca_4Al_2(SO4)_{0.5}(Cl)(OH)_{12}$] occurred just in the system without calcite, whereas Friedel's salt [$Ca_2Al(OH)_6Cl\bullet\ 2H_2O$] predominated in the calcite-containing system by virtue of its greater stability with respect to Kuzel's salt that was not even formed. Furthermore, whilst in the former case sulfate ions were released provoking an increasing of the ettringite concentration, in the latter calcite concentration grew.

In our system although calcite was present at remarkable concentration (8.7 wt.%), Kuzel' salt was observed after 24 h (visible for its main peak at d-spacing = 8.32 Å). The overlapping of the diffraction peak produced by Zinc chlorate hydroxide, at the same d-spacing value, did not affect the reliability of our data since we may expect that Zinc chlorate hydroxide dissolved, once the hydration started. In accordance with what previously stated though, the formation of Kuzel's salt was unexpected, given the presence of calcite. However, we should also consider the high complexity of our system, which showed other phases than those reported by Balonis et al. (2010), particularly anhydrite. Furthermore, as reported in SEM images, the Fly ash sample presented a high heterogeneity itself. Given the high concentration of Cl and calcite, the Friedel's salt formation was expected as several studies reported its formation (Wan et al., 2018; Qian et al., 2008; Polettini et al., 2001). However, no peak corresponding at d-spacing of 10.7 Å, which is the characteristic position of the Friedel's salt peak, was detected. In addition to this, neither the precursor of Kuzel's salt nor of Friedel's salt, namely monosulphate and monocarboalluminate, respectively, were observed to be formed.

After 14 days a significant increase of the Kuzel's salt was observed together with the ettringite formation. Furthermore, we observed an increase of the portlandite peak, which

was not expected as suggested to be consumed by the Pozzolanic reaction forming C-S-H (**reaction 17** and **18** section 1.6). This is symptom that after 14 days no pozzolanic reaction occurred and that the hydration of both OPC and MSWIFA was still occurring, precipitating portlandite and C-S-H. This latter phase is not directly detectable by the presence of diffracted Bragg peak because of their amorphous structures (Contessi et al. 2019) but, it formed by reaction of C_3S with water forming portlandite, and indeed C-S-H (**reaction 12**, section 1.6). Additionally, a contribution to the portlandite peak may be given by MSWIFA presence, as it was found in a XRPD analysis reported in **Fig. 56** (green pattern). This observation agrees with Mangialardi et al. (1999) stating that the partial substitution of OPC with MSWIFA results in delaying both the initial and final setting of the cementitious mixtures. Our results partially agree with those reported by Kan et al. (2019) considering a system containing 20 % MSWIFA with 80 % OPC observed that after 14 days portlandite was still forming even though in presence of Friedel's salt, this latter did not find in our system though. Noteworthy it is also the thaumasite detection. This latter is reported to be formed in the presence of sulfate and carbonate when there is high humidity and low temperature conditions (St. John et al. 1998, Marsh, 2002).

After 60 days, the complete dissolution of the Kuzel's salt together with a significant increase of the halite and sylvite peaks were observed. The formation of this latter phases could be provoked by the dissolution of Kuzel's salt that have released Cl ions in the pore solutions. These have combined with Na and K ion to form halite and sylvite, respectively. Furthermore, a remarkable increase of thaumasite peaks was appreciated. Concerning the portlandite, all the peaks underwent a drastic reduction except for its main one (d = 4.90 Å) in which an unknown phase overlapping thereof may be supposed to be present. A drastic reduction of the ettringite contribution was also detected. Hence, after 60 days, after thaumasite was formed. Thaumasite precipitation explained the reason why ettringite decreased, as the prior formation of ettringite seemed to be needed, as a seeding agent (Crammond and Nixon, 1993). Thaumasite formation is reported to cause a drastic reduction of the strength as capable to decompose C-S-H, thus destroying the binding capacity of the cement paste (Taylor, 1997). According to what previously stated, thaumasite formation would explain the fact that after 60 days the sample did not harden as it may be seen in **Fig. 67** in which the demoulded sample after 60 days is reported. The sample showed inconsistency under the mechanical strength viewpoint. Thus, such a great amount of MSWIFA substituting OPC revealed to be detrimental. In addition, thaumasite formation further worsened the mechanical performances. Considering the presence of certain heavy metals such as Zn, Pb,

and As, at remarkable concentrations, the setting time was expected to show a marked delay as all the above-mentioned elements are considered retarders for the Portland cement hydration (Spence and Shi, 2004). Therefore, further work is needed for elucidating the reason why the MSWIFA play a so detrimental role in the hydration of OPC.

Singh and Kumar (2017) reported an increased strength as the curing period increased, reporting though a final UCS (unconfined compressive strength) of 0.700 MPa after 28 days, for MSWIFA treated with 8 % of OPC. The strength enhancement may be due to the time-dependency of pozzolanic reactions and stabilisation of cement, though not achieving good mechanical performances, symptom that probably either other binders than OPC or different s/w ratios must be taken into account.

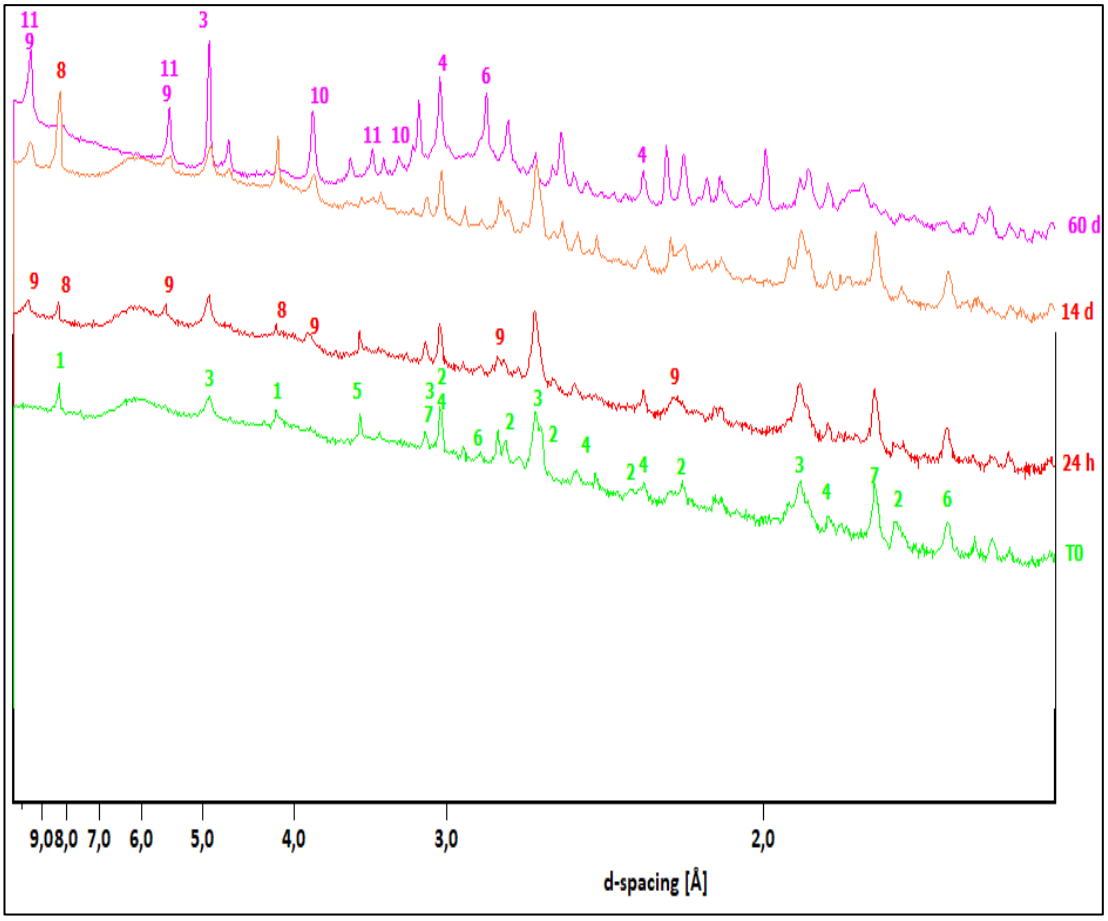

***Fig. 66**: Kinetic XRPD analysis of the system consisting of 80 % MSWIFA and 20 % OPC analysed at T 0, 24 h, 8 d and 60 d after hydration. 1: Zinc chlorate Hydroxide, 2: C_3S, 3: Portlandite, 4: Calcite, 5: Anhydrite, 6: Halite, 7: Sylvite 8: Kuzel's salt 9: Ettringite 10: $CaSO_4$, 11: Thaumasite*

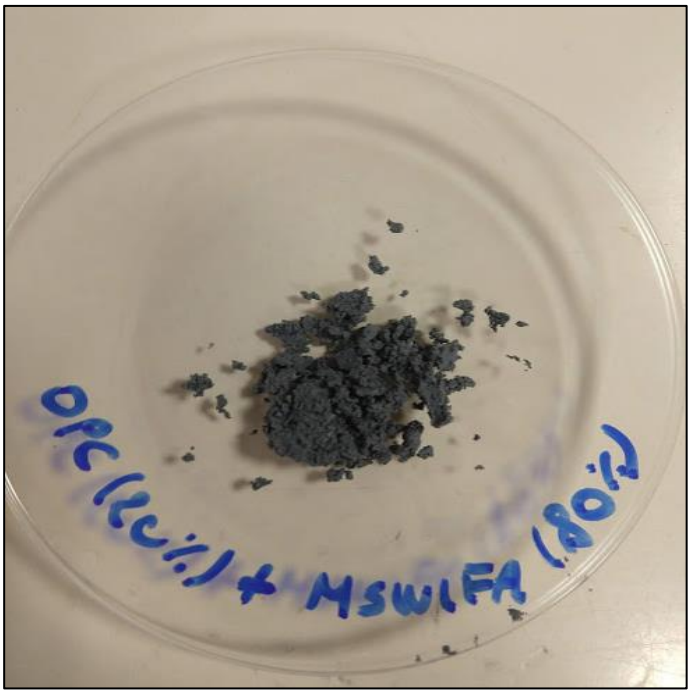

***Fig. 67**: Demoulded OPC-MSWIFA sample after 60 days of curing.*

4.2.2 HYDRATION OF CAC-MSWIFA

The diffractograms obtained via kinetic analysis performed on the binary system MSWIFA-CAC 70 (80:20) are reported in **Fig. 68**. The two reported diffractograms represent the initial conditions at the starting of hydration (red line) and the final result (black line) after 24 hours of hydration. Then a further analysis was carried out after 55 days (blue pattern). The system at the beginning was characterized by the presence of monocarboaluminate, that may be formed via reaction between the calcite contained in the MSWIFA and the CAC's anhydrous phases (**reaction 10 and 11** section 1.5.2). The latter reaction entails the gibbsite formation, not detected though, because of its amorphous structure. After approximately 5 hours monocarboaluminate disappeared and both ettringite and Friedel's salt were formed. Friedel's salt formation agreed with Macìas et al. (1996) results. C_2AH_8, CAH_{10} and C_3AH_6 were not observed, in accordance to Luz and Pandofelli (2012), as both calcite and anhydrite presence inhibited their formation.

After 55 days of hydration, the system presented a significant increase of the Friedel's salt peaks together with the ettringite and calcite peaks. Furthermore, portlandite peaks almost disappeared. A high contribution given by halite and sylvite was also observed. This means that after 55 days the system was still reacting, highlighting another time that the presence

of both Cl and heavy metals worked as retarders on the CAC 70 setting time. Calcite increasing together with portlandite lowering might be due to the occurrence of the carbonation reaction (**reaction 19**).

$Ca(OH)_2 + CO_2 \rightarrow CaCO_3$ (**19**)

According to Malviya and Chaudhary (2006), ettringite may be carbonated forming Calcite according to **reaction 20.** However, a decrease of the ettringite peak was not observed and this reaction has probably not occurred.

$3CaO \cdot Al_2O_3 \cdot 3CaSO_4 \cdot 32H_2O + 3CO_2 \rightarrow 3CaCO_3 + 3(CaSO_4 \cdot 2H_2O) + Al_2O \cdot XH_2O + 26 - XH_2O$ (**20**)

In addition to this, portlandite lowering may be also interpreted as due to the pozzolanic reaction between $Ca(OH)_2$, and the silica available from the MSWIFA, whereas the increase of calcite was probably due to the substitution of the CO_3^{2-} ions contained in the monocarboalluminate structure operated by Cl ions to form Friedel's salt (increased as well). As regards to the halite and sylvite presence, these were not expected as formation of Friedel's salt should have taken the dissolved chlorides ions from the solution. By comparing these results with those obtained for the Bagnolo Mella soil, it is clear how the matrix to be treated drastically affect the overall chemistry of the system. Even though the formation of Friedel's salt should ensure a hardening by virtue of its capacity to fill the voids, the sample has not developed strength even after 55 days (**Fig. 69**). This may be because of the absence of both gibbsite and hexagonal CAC hydrated phases after 55 days, and also for the presence of salts combined with metal at high concentrations, which delay the hydration conversions, working as retarders.

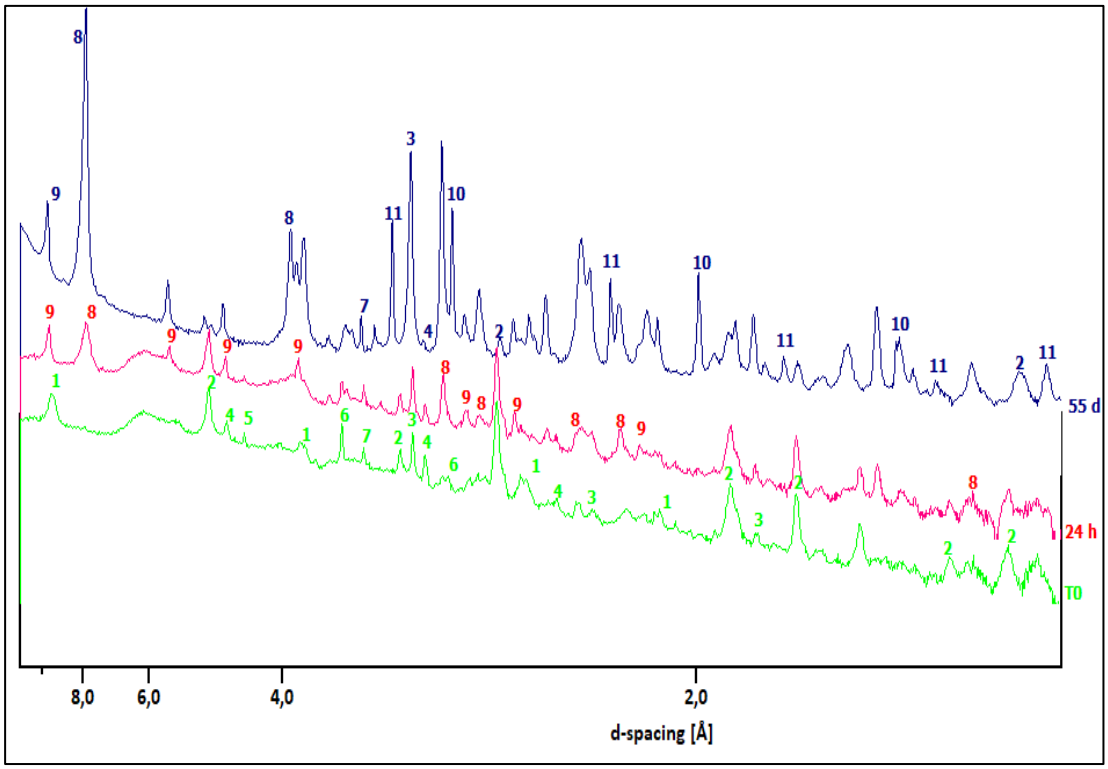

Fig. 68: *Diffraction patterns of CAC+MWIFA system at different curing time. At the beginning monocarboqluminate was already formed and the transformation thereof in Friedel's salt via reaction with Cl ions has been observed. In addition, ettringite was formed along with Friedel's salt. Slight increase of the calcite peaks was observed. 1: Monocarbonate, 2: Portlandite 3: Calcite 4: CA 5: CA_2 6: Anhydrite 7: Quartz 8: Friedel' salt 9: Ettringite, 10: Halite, 11: Sylvite*

Fig. 69: *Demoulded CAC70-MSWIFA sample after 55 days of curing at ambient temperature.*

4.2.3 BINARY HYDRATION OF GGBS-MSWIFA

As regards to the mix containing GGBS and MSWIFA, **fig. 70** reports the three diffractograms obtained at T0 (green line), after 24 hours (red line) and after 48 days (blue line) of curing. The detected phases in the initial pattern were portlandite, calcite and anhydrite. Over time, a progressive decrease of the anhydrite concentration along with the ettringite formation was observed. The formation of this latter compound entailed the reaction between anhydrite and the aluminium coming from the GGBS, which is usually abundant (Taylor, 1997). This indicated that GGBS could be activated not only by portlandite but also by chloride and sulfate contained in MSWIFA (Wan et al., 2018). In performing a similar experiment by using different mixing ratios of MSWIFA and GGBS, Wan et al. (2018) observed similar results at time 0, and in addition the formation of Friedel's salt after 3 days of hydration was also observed. Comparing these results with those obtained by treating MSWIFA with OPC, a total dissolution of the salts was obtained with GGBS.

Significant compositional variations were reported for the sample analysed after 48 days of curing time. In fact, a significant amount of Friedel's salt was formed together with a remarkable lowering of the portlandite peak and a calcite rise.

The lowering of the portlandite peaks was likely due to the formation of the Friedel's salt, through C_4AH_{13} formation, according to **reaction 20** (Suryavanshi et al.,1996) along with the pozzolanic reaction.

$$3CaO \cdot Al_2O_3 + Ca(OH)_2 + 12H_2O \rightarrow 4CaO \cdot Al_2O_3 \cdot 13\ H_20 \quad (\mathbf{20})$$

As C_4AH_{13} is metastable, it is suggested to foster an ion exchange between the -OH groups and the free chloride, forming the Friedel's salt. However, this hypothesis would not explain the formation of $CaCO_3$. This latter could have formed either via carbonation reaction of C-S-H (Taylor, 1997), or via carbonation of the portlandite.

The formation of Friedel's salt and ettiringite has surely allowed a beneficial effect on the mechanical properties of the sample. **Fig. 71** shows the sample moulded after 48 days. It is possible to observe how the sample has hardened and presumably developed good mechanical strength (not tested).

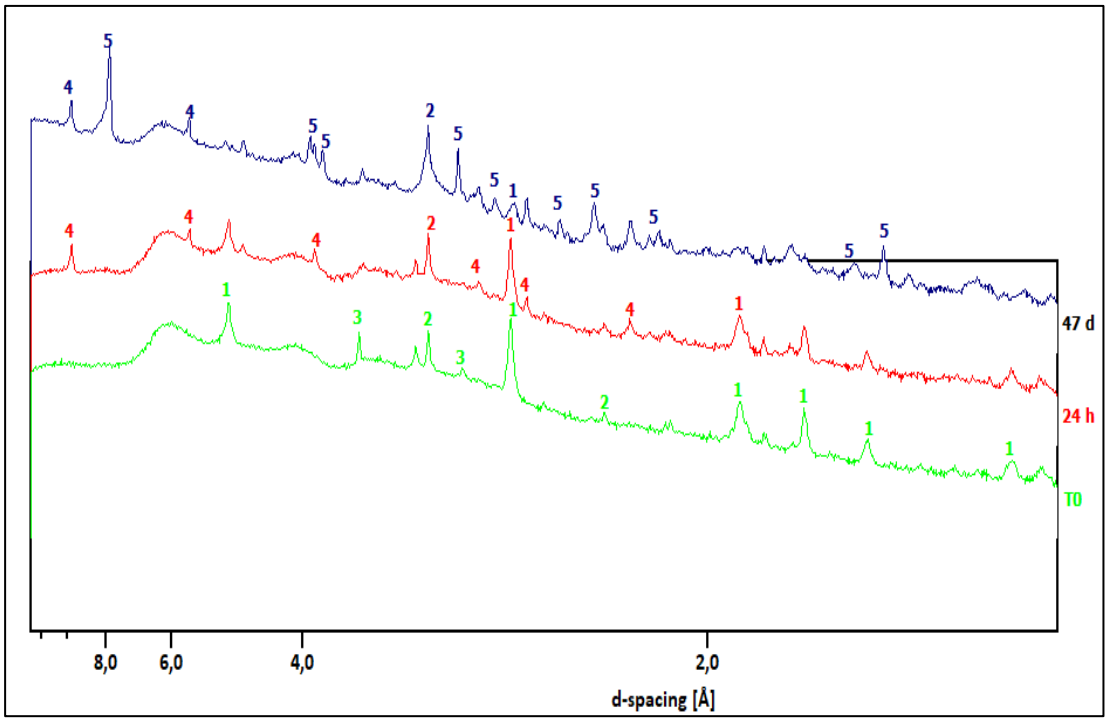

***Fig. 70**: Initial (green line), 24h (red line) and 48 days diffractograms obtained by performing a XRPD kinetic analysis on the recipe containing 46% GGBS, 50 % FA, 2.36 % $Na_2(CO_3)$ and 1.64 % $Ca(OH)_2$. A rather simplified pattern characterized the initial diffractogram that present 3 phases, namely: 1) Portlandite 2) Calcite 3) Anhydrite. Chlorine phases were dissolved as no peaks related to them were detected. After 24 h all the anhydrite was consumed because of Ettringite (4) formation. After 48 days Friedel's salt was formed.*

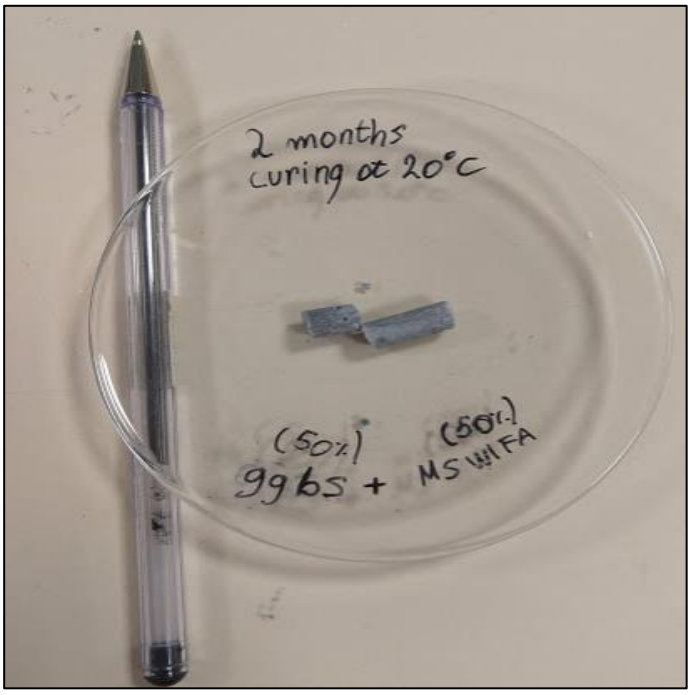

***Fig. 71**: 50% GGBS-50% MSWIFA monolithic sample demoulded after 48 days curing at ambient temperature. The sample hardened rapidly after 1 day of hydration.*

5. CONCLUSIONS AND FUTURE RESEARCH

The high-performance solidification/stabilisation (HPSS) method applied to two different materials, that is, a lead-bearing soil and MSWIFA, was assessed in this thesis.

Concerning the stabilisation of the contaminated soil of the former agrarian consortium of Bagnolo Mella, the calculation of the enrichment factor revealed that the soil was heavily contaminated by different heavy metals, with special concern for lead and selenium.

When stabilized with CAC 70, no significant differences were observed between samples cured at different temperatures and no significant variations of the temporal trend of the specimens mineralogy were observed during the studied period, meaning that the reactions happened in the first stages of hydration and then the system rather remained stable over time.

Conversion reactions occurred only in the reference sample (sample 4) containing CAC 70. Indeed, both gypsum and calcite hindered the formation of hydrogarnet in the other samples. Regardless, its formation did not provoke a decrease in terms of mechanical strength, as the formation of hydrogarnet was limited and, probably, balanced by a greater gibbsite production. CAC 70 reacted differently depending on the matrix to which the cement was added.

Regarding strength behaviour, the reference samples showed good mechanical performances. When CAC 70 was mixed with soil, more voids were generated and not always filled by hydrated cement products. This significantly impinged upon the mechanical strength, which decreased by as much as 50 % as average. Additionally, lead presence did not affect the hardening of the cement. The chemical reactions occurring in the two soil-containing systems were different. When gypsum was not present, the formation of monocarboaluminate was observed together with CAH_{10}, whereas the C_2AH_8 formation was prevented by calcite presence. When sulphate occurred in the sample along with calcite and CAC, the reactions were shifted towards ettringite formation, while neither monocarboaluminate nor monosulphate were formed.

Concerning the leaching tests, for all the elements showing an amphoteric behaviour a growth of concentration at lower pH values was observed. When the sample was exposed to milliQ water no changes of the final pH were observed because of the buffering effect yielded by cement, whereas when exposed at acid pH, a drastic drop of pH was observed, probably

due to the ettringite destabilisation. Within the pH range whereby ettringite is stable, CAC 70 showed good retention performances, as most of the considered elements showed concentrations also under the LOD in some cases. This could be interpreted as a beneficial effect given by ettringite for its good retention properties, at least for lead, as attested by SEM/WDS analyses. Concerning selenium, ettringite have an excellent affinity at basic pH when selenate might be present. Better results might be obtained combining CAC 70 with OPC or other binders forming C-S-H that shows better affinity with selenate, as reported by Contessi (2019), or using calcium solfoaluminate cements (CSA). In this latter case, Paysson et al. (2005) demonstrated excellent retention effectiveness using CSA for immobilising zinc nitrate and sulfate, lead nitrate, cadmium chloride, and chromium chloride.

A geochemical model is necessary in order to assess the speciation of the heavy metals in the cement matrix when leaching occurs and to ascertain what phase participates in the metal sorption/desorption process. Also, considering the soil presence, it is particularly important to determine if this latter has a role on binding heavy metals and, in particular, oxyanions. For this purpose, Leach XS combined ORCHESTRA (system for speciation and transport modelling framework) could be used (Van der Sloot et al., 2010; Engelsen et al., 2010). Additionally, as the total concentration of a contaminant has little correlation to its leachability, which depends on the chemical species present, X-ray absorption near edge structure (XANES) analysis may help to determine the binding mechanisms of heavy metals in the ettringite structure. These techniques provide information about oxidation state, symmetry, and identity of the coordinating ligand environment, and possible solid phases (Caporale and Violante, 2016; Spence and Shi, 2004).

Concerning the MSWIFA project, the stabilisation capacity of different binders was assessed. Initially, the considered sample was analysed in different days via XRPD and it showed a great penchant to hydrate with the formation of new phases. The sample possessed a high number of volatile elements such as Zn, Na, S, Cl and K. Metals were not involved in any mineralogical phase, meaning that they were just dispersed in the matrix even if at notable concentration.

From a qualitative viewpoint the binder that shows better properties was the GGBS, as also reported by Shy and Kan (2009). The GGBS system was the only one having a cylindrical shape after being demoulded. This was due to the capacity of the GGBS to fill the pore providing hydration channels that can be filled by other hydration products. The salts contained in the MSWIFA quickly dissolved in the matrix and ettringite, Friedel's salt and C-S-H formed. However, we need to take into account that higher binder quantity was used in this case,

with respect to the OPC and CAC 70 samples, thus providing a higher solidification performance.

On the other hand, both OPC and CAC 70 did not seem to be the right binders to treat this material, as no hardening was occurred. In particular, with OPC, the system developed thaumasite, that irreversibly jeopardized the setting process. Instead, with CAC 70 the system was probably interested either by carbonatation process which consumes portlandite and C-S-H. Other investigations by changing the proportions of the two binders with respect the MSWIFA have to be assessed.

More research is needed to obtain details about leaching from stabilised fly ashes as several heavy metals and oxyanions may be present. On the other hand, this study revealed that MSWIFA considerably delayed the cement hydration and that the pozzolanic reaction may occur after several weeks. Additionally, other studies (Shi and Kan, 2009; Gao et al., 2008; Du et al., 2018) reported that because of what above-mentioned, MSWIFA has a low cementitious potential. Furthermore, an acidic fly ash leaching, capable to extract heavy metals, might be tested prior to the stabilisation/solidification with cement, as reported by Schlumberger et al. (2007). This process irremediably increases the final cost associated with the treatment of this material with the risk to not be sustainable. Regardless, Mangialardi (2002) reported that after the washing process, an amount of 25 % of OPC cement was sufficient to obtain a stabilised material. Essential for the understanding of the leaching process is also the type of particles that host metals. Finally, as seen for the Bagnolo Mella case, leaching models are needed to predict heavy metals leaching from MSWIFA, knowing the binding forms of heavy metals and the specimens controlling the metal leaching.

6. REFERENCES

Adriano, D. C. (2001). Trace elements in terrestrial environments (2nd ed.). New York: Springer.

Agency for Toxic Substances and Disease Registry (ATSDR) (2000). Toxicological profile for Polychlorinated Biphenyls (PCBs). Atlanta, GA: U.S. Department of Health and Human Services, Public Health Service.

Akhter H., Butler L.G., Branz S., Cartledge F.K., Tittlebaum M.E. (1990). Immobilization of As, Cd, Cr and Pb-containing soils by using cement or pozzolanic fixing agents, J. Hazard. Mater. 24: 145-155.

Al-Tabbaa A, Evans CW (1996) In-situ treatment of contaminated ground using soil mixing. Ground Eng 29:37

Antemir A., Hills C.D., Carey P.J., Magni M.C., Polettini A. (2010). Investigation of 4- year-old stabilised/solidified and accelerated carbonated contaminated soil. J. Hazard Mater. 181 (1): 543-555.

Antonovič V., Kerienė J., Boris R., Aleknevičius M. (2013). The effect of temperature on the formation of the hydrated calcium aluminate cement structure, Procedia Eng. 57: 99-106.

Arthur E.L., Rice P.J., Rice P.J., Anderson T.A., Baladi S.M., Henderson K.L., Coats J.R. (2005) Phytoremediation—an overview, Crit. Rev. Plant Sci. 24: 109–122.

ASTM C618. (2003). Standard specification for coal fly ash and row or calcinated natural pozzolanas for use in concrete. American Society for testing and materials. West Conshohocken, PA, USA: ASTM International.

ASTM G200-09(2014). Standard Test Method for Measurement of Oxidation-Reduction Potential (ORP) of Soil, ASTM International, West Conshohocken, PA, www.astm.org.

Aubert J.E, Husson B., Vaquier A. (2004). Use of municipal solid waste incinerator fly ash in concrete. Cem. Concr. Res. 34: 957-963.

Baird, C. and Cann, N. (2012), Environmental Chemistry. 5th Edition, W. H. Freeman and Company, New York.

Balonis M., Lothenbach B., Saout G.L., Glasser F.P., (2010). Impact of chloride on the mineralogy of hydrated Portland cement systems. Cement Concrete Res. 40: 1009-1022.

Barnes P., Bensted J. (2002). Structure and Performance of Cements, CRC Press, Boca Raton.

Baur I., Johnson A.C. (2003). The solubility of selenate-Aft (3CaO·Al2O3· 3CaSeO4·37.5H2O) and selenate-AFm (3CaO·Al2O3·CaSeO4·xH2O), Cement Concrete Res. 33: 1741-1748.

Bayuseno A.P., Schmahl W.W., (2011). Characterization of MSWI fly ash through mineralogy and water extraction. Resour. Conserv. Recycl. 55: 524-534.

Bayuseno A.P., Schmahl W.W., Müllejans Th. (2009). Hydrothermal processing of MSWI Fly Ash-towards new stable minerals and fixation of heavy metals. Journal of Hazardous Materials 167: 250-259.

Bensted, J. (1993). High alumina cement—present state of knowledge. Zement-Kalk-Gips 46: 560–566.

Bigham J.M., Nordstrom D.K. (2011). Iron and aluminum hydroxysulfates from acid sulfate waters. Rev. Mineral. Geochem. 40: 351–403. https://doi.org/10.2138/rmg.2000.40.7.

Bizily S.P., Rugh C.L., Summers A.O. (1999). Phytoremediation of methylmercury pollution: merB expression in Arabidopsis thaliana confers resistance to organomercurials. Proc. Natl. Acad. Sci. USA; 96(12): 6808-13.

Bizzozero J., Scrivener K.L. (2015). Limestone reaction in calcium aluminate cement calcium sulfate systems, Cem. Concr. Res. 76: 159-169.

Borda M.J., Sparks D.L. (2008). Mobility of trace elements in soil environments. In: Violante A., Huang P.M., Gadd G.M., editors. Biophysicochemical processes of metals and metalloids in soil environments. Hoboken: Wiley; pp. 97–168.

Buelt J. L. and Thompson L. E. (1992). The In-situ Vitrification Integrated Program: Focusing on an Innovative Solution on Environmental Restoration Needs, Battelle Pacific Northwest Laboratory, Richland, Wash, USA.

Caporale A. G., Violante A. (2016). Chemical Processes Affecting the Mobility of Heavy Metals and Metalloids in Soil Environments. Curr Pollution Rep 2: 15–27.

Chandler A. J., Eighmy T. T., Hartlén J., Hjelmar O., Kosson D. S., Sawell S. E., Van der Sloot H. A., Vehlow J. (1997). Municipal Solid Waste Incinerator Residues. Studies in Environmental Science 67, the international Ash Working Group. Elsevier. ISBN 0-444-82563-0

Chilton K., Schwarz P, Godwin K. (2008). Final Report verifying the Social, Environmental, and Economic Promise of Brownfield Program s. https://www.epa.gov/sites/production/files/2015-09/documents/trta_report_2009.pdf

Chrysochoou M. and Dermatas D. (2006). Evaluation of ettringite and hydrocalumite formation for heavy metal immobilization: Literature review and experimental study, J. Hazard. Mater. 136: 20-33.

Cocke D. L., Mollah M. Y. A. (1993). The chemistry and leaching mechanism of hazardous substances in cementitious solidification/stabilisation systems. Chem. Microstructure Solidified Waste Forms 187-242.

Cong X., Kirkpatrick R.J. (1993). Hydration of calcium aluminate cements: a solid-state 27Al NMR study. J. Am. Ceram. Soc. 76: 409-416.

Contessi S. (2015). Influence of fly ash-based binders on the solidification/stabilization performance of heavy metals contamination in soils (Master's thesis).

Contessi S., Calgaro L., Dalconi M. C., Bonetto A., Bellotto M. P., Ferrari G., Marcomini A., Artioli G. (2020). Stabilization of lead contaminated soil with traditional and alternative binders. Journal of Hazardous Materials 382 120990. DOI: https://doi.org/10.1016/j.jhazmat.2019.120990.

Crammond N. J., Nixon P. J. (1993). Deterioration of concrete foundation piles as a result of thaumasite formation. Proceedings of the 6th International Conference on Durability of Building Materials and Components. Vol. 1. Japan.

Cussino L., Negro A. (1980). Hydration du ciment alumineux en présence d'agrégat siliceux et calcaire, 7th International Congress on the Chemistry of CementParis.

Damidot D., Glasser F.P. (1992). Thermodynamic investigation of the CaO–Al2O3–CaSO4–H2O system at 50 ◦C and 85 ◦C, Cement Concrete Res. 22: 1179–1191.
Damidot D., Glasser F.P. (1993). Thermodynamic investigation of the CaO–Al2O3–CaSO4–K2O–H2O system at 25 ◦C, Cement Concrete Res. 23: 1195–1204.

Decreto Legislativo del 3 aprile 2006, n. 152. "Norme in materia ambientale". Pubblicato nella Gazzetta Ufficiale n. 88 del 14 aprile 2006 - Supplemento Ordinario n. 96.

Derie R. (1996). A new way to stabilize fly ash from municipal incinerators. Waste Manag. 16: 711-716.

Dewar, J. D., and R. Anderson (1992). "Manual of Ready-Mix Concrete." Blakie Academic Professional, an imprint of Chapmen and Hell, UK.

Dijkstra J.J., Meeussen J.C.L., Comans R.N.J. (2004). Leaching of heavy metals from contaminated soils: an experimental and modeling study, Environmental Science & Technology 38 (16): 4390–4395.

during the hydrothermal treatment process. Journal of Soils and Sediments 18 (4): 1701-1719

Eighmy T.T., Eusden J.D., Krzanowski J.E., Domingo D.S., Stempfli D., Martin J.R, Erickson P.M. (1995). Comprehensive Approach toward Understanding Element Speciation and Leaching Behavior in Municipal Solid Waste Incineration Electrostatic Precipitator Ash. Environ Sci Technol. 29(3): 629-46. DOI: 10.1021/es00003a010.

Engelsen C.J, Van der Sloot H.A., Wibetoe G. Justnes H., Lund W., Stotenberg-Hansson E. (2010). Leaching characterisation and geochemical modelling of minor and trace elements released from recycled concrete aggregates. Cement and Concrete Research 40: 1639–1649.

Environment Agency (2010). Waste acceptance at landfills-Guidance on waste acceptance procedures and criteria. https://assets.publishing.service.gov.uk/government/uploads/system/uploads/attachment_data/file/296422/geho1110btew-e-e.pdf

Environmental Protection department of Hong Kong (2019). Integrated Waste Management Facilities; Available online:https://www.epd.gov.hk/epd/english/environmentinhk/waste/prob_solutions/WFdev_IWMFtech.html

Federal Remediation Technologies Roundtable Annual Summary of Activities (FRTR) (2012) (EPA-542-F-12-027).

Fentiman, C.H. (1985). Cem. Concr. Res. 15, 622.

Fernandez M. A. Martinez, L. Segarra, M. Garcia, J. C., Espiell F. (1992). Behaviour of heavy metals in the combustion gases of urban waste incinerators. Environ. Sci. Technol. 26: 1040- 47.

Frelih-Larsen, A., C. Bowyer, S. Albrecht, C. Keenleyside, M. Kemper, S. Nanni, S. Naumann, R., D. Mottershead, R. Landgrebe, E. Andersen, P. Banfi, S. Bell, I. Brémere, J. Cools, S. Herbert, A. Iles, E. Kampa, M. Kettunen, Z. Lukacova, G. Moreira, Z. Kiresiewa, J. Rouillard, J. Okx, M. Pantzar, K. Paquel, R. Pederson, A. Peepson, F. Pelsy, D. Petrovic, E. Psaila, B. Šarapatka, J. Sobocka, A.-C. Stan, J. Tarpey, R. Vidaurre (2016). 'Updated Inventory and Assessment of Soil Protection Policy Instruments in EU Member States.' Final Report to DG Environment. Berlin: Ecologic Institute.

Gabarrón M., Babur O., Soriano-Disla J.M., Faz A., Acosta J. A. (2018). Composition and risk assessment of roasted pyrite ash from fertiliser production. Chemosphere 209: 277-285. https://doi.org/10.1016/j.chemosphere.2018.06.109.

Gabrisovii A., Havlica J., and Sahu S., (1991). Stability of calcium sulphoaluminate hydrates in water solutions with various ph values, Cement and Concrete Research, 21: 1023

Gadd, G. M. (1990). Heavy metal accumulation by bacteria and other microorganisms. Experientia, 46: 834-840.

Gilardoni S., Fermo P., Cariati F., Gianelle V., Pitea D., Collina E., Lasagni M. (2004). MSWI Fly Ash Particle Analysis by Scanning Electron Microscopy-Energy Dispersive X-ray Spectroscopy. Environ. Sci. Technol. 38: 6669-75.

Gong Y., Zhao D., Wang Q. (2018). An overview of field-scale studies on remediation of soil contaminated with heavy metals and metalloids: Technical progress over the last decade. Water research 147: 440-460. DOI: https://doi.org/10.1016/j.watres.2018.10.024

Gosselin C. (2009). Microstructural Development of Calcium Aluminate Cement Based Systems with and without Supplementary Cementitious Materials, Faculte Sciences et Techniques de l'ingenieur, Ecole Polytechniqe Federale de Lausanne, Lausanne, CH, 2009.

Gougar, M.L.D., Scheetz, B.E., Roy, D.M. (1996). Ettringite and C-S-H Portland cement phases for waste ion immobilization: a review. Waste Manag. 16 (4): 295-303.

Guemiza K., Coudert L., Metahni S., Mercier G., Besner S., Blais J. F. (2017). Treatment technologies used for the removal of As, Cr, Cu, PCP and/or PCDD/F from contaminated soil: A

review. Journal of Hazardous Materials 333: 194-214 DOI: http://dx.doi.org/10.1016/j.jhazmat.2017.03.021

Guirado F., Galì A S., Chinchòn B J.S. (1998). Thermal Decomposition of Hydrated Alumina Cement (CAH10). Cement and Concrete Research 28 (3): 381-390.

Gupta V.K., Ali I., Saini V.K., Van Gerven T., Van Bruggen B.D., Vandecasteele C. (2005). Removal of dyes from wastewater using bottom ash. Ind. Eng. Chem. Res. 44: 3655-64.

GWRTAC (1997). Remediation of Metals-Contaminated Soils and Groundwater. Carnegie Mellon University Department of Civil and Environmental Engineering Pittsburgh, PA.

Hamelink J.L., Landrum P.F., Harold B.L., William B.H. (1994). Bioavailability: physical, chemical, and biological interactions. CRC, Boca Raton, FL

Haying Z., Youcai Z., Jingyu Q. (2007). Study on use of MSWI fly ash in ceramic tile. J Hazard. Mater 141: 106-114.

He P.J., Zhang H., Zhang C.G., Lee D.J. (2004). Characteristics of air pollution control residues of MSW incineration plant in Shanghai. J. Hazard. Mater. 166: 229-237.

Hong K.J., Tokunaga S., Kajiuchi T. (2002). Evaluation of remediation process with plant-derived biosurfactant for recovery of heavy metals from contaminated soils. Chemosphere 49(4): 379-87.

Huber F., Laner D., Fellner J. (2018). Comparative life cycle assessment of MSWI fly ash treatment and disposal. Waste Management 73: 392-403.

ISPRA (2019). Siti Di Interesse Nazionale.

Ito R., Dodbiba G., Fujita T., Ahn J. W. (2008). Removal of insoluble chloride from bottom ash for recycling. Waste Manage. 1317-1323.

Izquierdo M., Querol X., Vazquez E. (2011). Procedural uncertainties of Proctor compaction tests applied on MSWI bottom ash. Journal of Hazardous Materials 186(2): 1639-44.

Izumikawa C. (1996). Metal recovery from fly ash generated from vitrification process for MSW ash. Waste Manag. 16: 501-507.

Jacob A., Stucki S., Kuhn P. (1995). Evaporation of Heavy Metals during the Heat Treatment of Municipal Solid Waste Incinerator Fly Ash. Environ. Sci. Technol. 29 (9) 2429-36. DOI: https://doi.org/10.1021/es00009a040

Jensen T.R., Christensen A.N., Hanson J.C. (2005). Hydrothermal transformation of the calcium aluminum oxide hydrates $CaAl_2O_4 \cdot 10H_2O$ and $Ca_2Al_2O_5 \cdot 8H_2O$ to $Ca_3Al_2(OH)_{12}$ investigated by in situ synchrotron Xray powder diffraction, Cem. Concr. Res. 35: 2300-2309.

Jiang Y., Xi B., Li X., Zhang L., Wei Z. (2009). Effect of water-extraction on characteristics of melting and solidification of fly ash from municipal solid waste incineration. J. Hazard. Mater. 161: 871-877.

Kakali G., Tsivilis S., Aggeli E., Bati M. (2000). Hydration products of C3A, C3S and Portland cement in the presence of $CaCO_3$. Cement and Concrete Research 30: 1073-77.

Kan L., Zhang L., Shi H. (2019). Hydration Kinetics of Municipal Solid Wastes Incineration (MSWI) Fly Ash-Cement. Journal of Wuhan University of Technology-Mater. Sci. Ed. 34(3): 596-603. DOI https: //doi. org/10.1007/s11595-019-2093-z.

Karamanov A., Pelino M., Hreglich A. (2003). Sintered glass-ceramics from municipal solid waste-incinerator fly ashes-part I: the influence of the heating rate on the sinter-crystallisation, J. Eur. Ceram. Soc. 23: 827–832.

Khan S., Cao Q., Zheng Y. M., Huang Y. Z., Zhu Y. G. (2008). Health risks of heavy metals in contaminated soils and food crops irrigated with wastewater in Beijing, China. Environmental Pollution 152 (3): 686–692.

Kikuchi R. (2001). Recycling of municipal solid waste for cement production: Pilot scale test for transforming incineration ash of solid waste into cement clinker. Resour. Conserv. Recycl. 2001, 31: 137-147.

Kim H.S., Kim J.M., Oshikawa T., Ikeda K. (2003). Production and properties of Glass-ceramic from Incinerator Fly ash. In material Science Forum: Kim H.S., Park S.Y., Lee S.W., Eds; Elsevier: Gyungpodae, Korea, pp: 180-185.

Kirby C.S., Rimstidt J.D. (1994). Interaction of municipal solid waste ash with water, Environ. Sci. Technol. 28: 652–660.

Kirk, G. J. D. (2004). The biogeochemistry of submerged soils. Chichester: Wiley.

Klöppel H., Fliedner A., Kördel (1997). Behaviour and ecotoxicology of aluminium in soil and water - Review of the scientific literature. Chemosphere 35 (1-2): 353-363.

Kocaba V. (2009). Development and evaluation of methods to follow microstructural development of cementitious systems including slags, École Polytechnique Fédérale de Lausanne, p. 181.

Komonweeraket K., Cetin B., Benson C.H., Aydilek A.H., Edil T.B. (2015). Leaching characteristic of toxic constituents from fly ash mixed soils under the influence of pH,Waste Manag. 28: 174–184.

Komonweeraket, K., Cetin, B., Aydilek, A.H., Benson, C.H., Edil, T.B. (2015). Effects of pH on the leaching mechanisms of elements from fly ash mixed soils. Fuel 140, 788-802. https://doi.org/10.1016/j.fuel.2014.09.068.

Kumarathasan P., McCarthy G.J., Hassett D.J., Pflughoeft-Hassett D.F. (1990). Fly-ash and coal-conversion by products; characterization, utilization and disposal VI, Mater. Res. Soc. Symp. Proc. 178: 83-104.

Kuo S, Heilman P. E., and Baker A. S. (1983). Distribution and forms of copper, zinc, cadmium, iron, and manganese in soils near a copper smelter. Soil Science, 135 (2): 101–109.

Kuzel H. J., Baier H. (1996). Hydration of calcium aluminate cements in the presence of calcium carbonate, Eur. J. Mineral. 8: 129–141.

Lam C. H. K., Ip A. W. M., Barford J. P., McKay G. (2010). Use of Incineration MSW Ash: A review. Sustainability 2010 2: 1943-1968.

Langton C. A. (1989). Slag-based materials for toxic metal and radioactive waste stabilization, Proceedings of 3rd International Conference on the Use of Fly Ash, Silica Fume, Slag and Natural Pozzolans in Concrete, ACI SP-114, American Concrete Institute, Farmington Hills, MI, 1989, 1697.

Laporte-Saumure M., Martel R., Mercier G. (2010) Evaluation of physicochemical methods for treatment of Cu, Pb, Sb, and Zn in Canadian small arm firing ranges backstop soils, Water, Air Soil Pollut. 213: 171-189.

Le Forestier L.L., Libourel G. (1998). Characterization of flue gas residues from municipal solid waste combustors. Environmental Science and Technology 32: 2250-6.

Le Saoût, G. B., Lothenbach P. Taquet H., Fryda, F. Winnefeld (2018). Hydration of calcium aluminate cement blended with anhydrite. Adv. Cem. Res. 30 (1): 24–36. https://doi.org/10.1680/jadcr.17.00045.

Lea F.M. (2004). Lea's Chemistry of Cement and Concrete, 4th edition, Elsevier.

Li M., Xiang J., Hu S., Sun L. S., Su S., Li P. S., Sun X. X. (2004). Characterization of solid residues from municipal solid waste incinerator. Fuel 83: 1397-1405.

Li M., Xiang J., Hu S., Sun L.S., Su S., Li P.S., et al. (2004). Characterisation of solid residues from municipal solid waste incinerator. Fuel 83:1397-405.

Liu A., Ren F., Lin W.Y., Wang J.Y. (2015). A review of municipal solid waste environmental standards with a focus on incinerator residues. Int. J. Sustain. Built. Environ. 4: 165-188.

Luz A.P., Pandolfelli V.C. (2012). $CaCO_3$ addition effect on the hydration and mechanical strength evolution of calcium aluminate cement for endodontic applications, Ceram. Int. 38: 1417-1425.

Ma G.F., Onitsuka K., Negami T. (2007). Utilizations of incineration ash from municipal solid waste as admixtures for road embankment materials. Geothech. Eng. 38: 87-94.

Machner A., Maciej Z., Ben Haha M., Kjellsen K., Geiker M., De Weerdt K. (2018). Limitations of the hydrotalcite formation in Portland composite cement pastes containing dolomite and metakaolin. Cement and Concrete. Research. 105.10.1016/j.cemconres.2017.11.007.

Macias A., Kindness A., Glasser F.P. (1996). Corrosion behaviour of steel in high alumina cement mortar cured at 5, 25 and 55 C: Chemical and physical factors, J. Mater. Sci. 31 (9): 2279-89.

Mallampati S.R., Mitoma Y., Okuda T., Simion C., Lee B.K. (2015). Dynamic immobilization of simulated radionuclide 133 Cs in soil by thermal treatment/vitrification with nanometallic Ca/CaO composites. J. Environ. Radioact. 139: 118– 124.

Malviya R., Chaudhary R. (2006). Leaching behaviour and immobilization of heavy metals in solidified/stabilized products. J. Hazard Mater. 137: 207-217. DOI: https://doi.org/10.1016/j.envpol.2019.03.124.

Manahan S. E. (2010). Environmental chemistry. 9th Edition, CRC Press Taylor & Francis Group. ISBN 978-1- 4200-5920-5.

Mangialardi T. (2003). Disposal of MSWI fly ash through a combined washing-immobilisation process. J. Hazard. Mater. 98: 225-240.

Marsh, B. (2002). Update on thaumasite sulfate attack on concrete. BRE.

McLaughlin M. J., Zarcinas B. A., Stevens D.P., Cook N (2000). Soil testing for heavy metals. Communications in Soil Science and Plant Analysis 31 (11–14): (1661–1700)

Mehta P.K., Monteiro P.J. (2006). in: Concrete: Microstructure, Properties, and Materials, McGraw-Hill, New York, pp. 216–217

Mercier G., Duchesne J., Blackburn D. (2001). Prediction of metal removal efficiency from contaminated soils by physical methods, J. Environ. Eng. 127: 348-358.

Midgley, H.G. (1984). Clay Minerals 19, 857.

Midgley, H.G. and Pettifer, K. (1971). The microstructure of hydrated super sulphated cement, *Cem. Concr. Res.,* 1(1): 101-104.

Mudd G.M., Weaver T.R., Kodikara J. (2004) Environmental geochemistry of leachate from leached brown coal ash J Environ Eng, 130 (12): 1514-1516

Mulder E. (1996). Pre-treatment of mswi fly ash for useful application. Waste Manag. 16: 181-184.

Mulligan C.N., Yong R.N., Gibbs B.F. (2001). Remediation technologies for metal-contaminated soils and groundwater: an evaluation. Eng. Geol. 60: 193-207.

Navarro-Blasco I., Duran A., Sirera R., Fern"andez J.M., Alvarez J.I. (2013). Solidification/ stabilization of toxic metals in calcium aluminate cement matrices. J. Hazard Mater. 260: 89-103.

Nishida K., Nagayoshi Y., Ota H., Nagasawa H. (2001). Melting and stone production using MSW incinerated ash. Waste Manag. 21: 443-449.

Ohbuchi A., Koike Y., Nakamura T. (2019). Quantitative phase analysis of fly ash of municipal solid waste by X-ray powder diffractometry/Rietveld refinement. Journal of Material Cycles and Waste Management https://doi.org/10.1007/s10163-019-00838-0.

Pandey B., Kinrade S.D., Catalan L.J.J., (2012). Effects of carbonation on the leachability and compressive strength of cement-solidified and geopolymer solidified synthetic metal wastes. J. Environ. Manage. 101: 59–67.

Pandey S.P and Sharma R.L. (2000). The influence of mineral additives on the strength and porosity of OPC mortar. Cement and Concrete Research 30 (1): 19-23. DOI: https://doi.org/10.1016/S0008-8846(99)00180-5.

Parfitt R.L., Giltrap D.J., Whitton J.S. (2008). Contribution of organic matter and clay minerals to the cation exchange capacity of soils. Communications in Soil Science and Plant Analysis 26: 1343-1355.

Park H., Jeong Y., Jun Y., Jeong J.H., Oh J.E. (2016). Strength enhancement and pore-size refinement in clinker-free CaO-activated GGBFS systems through substitution with gypsum, Cem. Concr. Compos. 68: 57–65.

Peng J.F., Song Y.H., Yuan P., Cui X.Y., Qiu G.L (2009). The remediation of heavy metals contaminated sediment. Journal of Hazardous Materials 161: 633–640.

Peng W., Li X., Xiao S., Fan W. (2018). Stabilization and separation of heavy metals in incineration fly ash

Pérez A. P., Eugenio N. R. (2018). Status of local soil contamination in Europe: Revision of the indicator "Progress in the management Contaminated Sites in Europe, EUR 29124 EN, Publications Office of the European Union, Luxembourg, ISBN 978-92-79-80072-6, doi:10.2760/093804, JRC107508.

Pérez-López R., Sáez R., Álvarez-Valero A.M., Nieto J.M., Pace G. (2009).

Perkins, R.B., Palmer, C.D. (2000). Solubility of $Ca_6[Al(OH)_6]_2(- CrO_4)_3 26H_2O$, the chromate analog of ettringite, 5–75 °C. Appl. Geochem. 15: 1203–1218.

Polettini A., Pomi R., Sirini P., Testa F., (2001). Properties of Portland cement-stabilised MSWI fly ashes. Journal of Hazardous Materials 88: 123-138.

Qian G.R., Shi J., Cao Y.L., Xu Y.F., Chui P.C. (2008). Properties of MSW fly ash-calcium sulfoaluminate cement matrix and stabilization/solidification on heavy metals, J. Hazard. Mater. 152 (1): 196-203.

Qingjie G., Jun D.J., Yunchuan X., Qingfei W., Liqiang Y. (2008). Calculating Pollution Indices by Heavy Metals in Ecological Geochemistry Assessment and a Case Study in Parks of Beijing. Journal of China University of Geosciences 19 (3):230-241.

Quina M.J., Bordado J.C., Quinta-Ferreira R.M. (2008). Treatment and use of air pollution control residues from MSW incineration: An overview. Waste Manag. 28: 2097-2121.

Rashid S., Turrillas X., Bensted J., Barnes P. (1994). Cem. Concr. Sci. Abs. (Oxford), 29.

Raskin I., (1995). Phytoremediation e a novel strategy for the removal of toxic metals from the environment using plants. Biotechnology 13: 468-478.

Rawlings R.D, Wu J.P, Boccaccini A.R. (2006). Glass-ceramics: Their production from wastes-A review. J. Mater. Sci. 41: 733-761.

Rössler, M., and Odler, I. (1989). Relationship between pore structure and strength of set gypsum pastes. Zement-Kalk-Gips 42, 96–100, 419–4424.

Sakai S.I. and Hiraoka (2000). Municipal solid waste incinerator residue recycling by thermal processes. Waste Manag. 20: 249-258.

Scanferla P., Ferrari G., Pellay R., Volpi Ghirardini A., Zanetto G., Librato G. (2009). An innovative stabilization/solidification treatment for contaminated soil remediation: demonstration project results. J Soils Sediments 9:229–236. DOI: 10.1007/s11368-009-0067-z.

Scrivener K. and Capmas A. (1998) Calcium aluminate cement, in Lea's Chemistry of Cement and Concrete (ed. P.C.Hewlett), Arnold, London, pp. 709–778.

Shi H. S., Kan L.L (2009). Leaching behaviour of heavy metals from municipal solid wastes incineration (MSWI) fly ash used in concrete. Journal of Hazardous Materials 164 (2-3): 750-754.

Shi H.S., Kan L.L. (2009). Characteristics of municipal solid wastes incineration (MSWI) fly ash–cement matrices and effect of mineral admixtures on composite system. Constr Build Mater 23:2160-2166

Shim Y.S., Kim Y.K., Kong S.H., Rhee S.W., Lee W.K. (2003). The adsorption characteristic by heavy metals by various particle sizes of MSWI bottom ash. Waste management. 23: 851-857.

Shim Y.S., Rhee S.W., Lee W.K. (2005). Comparison of leaching characteristics of heavy metals from bottom and fly ashes in Korea and Japan, Waste Manage. 25: 473–480.

Singh D., Kumar A. (2017). Geo-environmental application of municipal solid waste incinerator ash stabilized with cement. Journal of Rock Mechanics and Geotechnical Engineering 9: 370-375.

Soares, M.A.R., Quina, M.J., Quinta-Ferreira, R.M., (2015). Immobilisation of lead and zinc in contaminated soil using compost derived from industrial eggshell. J. Environ. Manag. 164, 137–145.

Spence R. D., Shi C. (2004). Stabilization / solidification of hazardous, radioactive, and mixed wastes. CRC Press. ISBN 1-56670-444-8.

Spuller C., Weigand H., Marb C. (2007). Trace metal stabilisation in a shooting range soil: mobility and phytotoxicity, J. Hazard. Mater. 141: 378–387. DOI: https://doi.org/10.1016/j.jhazmat.2006.05.082

St. John D.A., Poole A.W., Sims I. (1998). Concrete Petrography; A handbook of investigative techniques. Arnold, London, UK.

Stegemann J. A., and Shi C. (1997). Acid resistance of different monolithic binders and solidified wastes, in Waste Materials in Construction: Putting Theory in Practice, Studies in Environmental Science 71, Elsevier Science B.V., Amsterdam, 803.

Stegemann, J.A. and Buenfeld, N.R. (2002). Prediction of leachate pH for cement paste containing pure metal components, Journal of Hazardous Materials 90, 169.

Stern B. N (2010). Essentiality and Toxicity in Copper Health Risk Assessment: Overview, Update and Regulatory Considerations. Journal of Toxicology and Environmental Health, Part A 73: 114-127.

Surico F., Peli G., Zeno L., Scattolin M., Scanferla P., Rinaldo D. (2003). The remediation of the Conterie in Murano (Venice). Proceedings of the Second International Conference on Remediation of Contaminated Sediments (Venice, 30th September–3rd October 2003). ISBN 1-57477- 143-4. Battelle Press, Columbus, OH.

Suryavanshi A.K., Scantlebury J.D., Lyon S.B. (1996). Mechanism of Friedel's salt formation in cements rich in tri-calcium aluminate, Cement Concrete Res. 26: 717–727.

Swartzbaugh J.T., Weisman A., Gabrera-Guzman D. (1990). The use of electrokinetics for hazardous waste site remediation. Journal of Air and Waste Management Association. 40(12): 1670-7.

Taylor, H.F.W. (1997). Cement Chemistry, 2nd edn, Thomas Telford Publishing, London.

Tessier A., Campbell P. G. C., Blsson M. (1979). Sequential extraction procedure for the speciation of particulate trace metals. Analytical Chemistry 51 (7): 844–851.

Thurman E.M. (1985). Organic geochemistry of natural water. Springer Netherlands. DOI 10.1007/978-94-009-5095-5

Tokunaga S., Hakuta T. (2002). Acid washing and stabilization of an artificial arsenic-contaminated soil. Chemosphere, 2002; 46(1): 31-8.

Triano J.R., Frantz G.C. (1992). Durability of MSW fly-ash concrete. J. Mater Civ. Eng. 4: 369-384.

United Nations, Department of Economic and Social Affairs, Population Division (2019). World Population Prospects 2019: Ten Key Findings.

Van der Sloot H. A., Seignettte P.F.A.B., Meeussen J.C.L., Hjelmar O., Kosson D.S. (2008). A database, speciation modelling and decision support tool for soil, sludge, sediments, wastes and construction products: LeachXS™- Orchestra. In: Venice Symposium, Venice 2008.

Verkleji J.A.S (1993). The effects of heavy metals stress on higher plants and their use as biomonitors. In: Markert B (ed) Plant as bioindicators: indicators of heavy metals in the terrestrial environment. VCH, New York, NY, pp. 415–424.

Violante A. (2013). Elucidating mechanisms of competitive sorption at the mineral/water interface. In: Sparks DL, editor. Adv Agr; pp. 111–76.

Violante A., Pigna M., Cozzolino V., Huang P.M. (2012). Impact of soil physical, chemical and biological interactions on the transformation of metals and metalloids. In: Huang P.M., Li Y., Sumner M.E. Handbook of soil sciences. Resource management and environmental impact, Chapter 8. Boca Raton: CRC Press, Taylor and Francis Group.

Vithanage M., Chandrajith R., Weerasooriya R. (2007). Role of natural red earth in arsenic removal in drinking water – comparison with synthetic gibbsite and goethite. Trace Metals and other Contaminants in the Environment 9: 587-601. https://doi.org/10.1016/S1875-1121(06)09022-5

VROM (1999). Ministry of Spatial Planning, Housing and the Environment. Building Material Decree, http://www2.minvrom.nl/Docs/internationaal/BMD_broch.pdf.

Wan S., Zhou X., Zhou M., Han Y., Chen Y., Geng J., Wang T., Xu S., Qiu Z., Hou H. (2018). Hydration characteristics and modelling of ternary system of municipal solid wastes incineration fly ash-blast furnace slag-cement. Construction and Building Materials 180: 154–166.

Wang Y., Ni W., Suraneni P. (2019). Use of Ladle Furnace Slag and Other Industrial By-Products to Encapsulate Chloride in Municipal Solid Waste Incineration Fly Ash. Materials 12: 925

Wang, K.S., Chiang, K.Y., Lin, K.L., Sun, C.J., (2001). Effects of a water-extraction process on heavy metal behaviour in municipal solid waste incinerator fly ash. Hydrometallurgy 62: 73-81.

Wasay S., Barrington S., Tokunaga S. (1998). Remediation of soils polluted by heavy metals using salts of organic acids and chelating agents, Environ. Technol. 19: 369-79.

Weibel G., Eggenberger U., Schlumberger S., Mäder U. K. (2017). Chemical associations and mobilization of heavy metals in fly ash from municipal solid waste incineration Waste Management 62: 147-159.

Weibel G., Eggenberger U., Schlumberger S., Mäder U.K., (2017). Chemical associations and mobilization of heavy metals in fly ash from municipal solid waste incineration. Waste Manag. 62: 147-159. https://doi.org/10.1016/j.wasman.2016.12.004.

WHO/FAO/IAEA (1996). Trace Elements in Human Nutrition and Health. World Health Organization, Geneva, pp. 6-10.

Wittbrodt P. R., Palmer C. D. (2005). Reduction of Cr(VI) by soil humic acids. European Journal of Soil Science 47:151-162.

Wojciech G.P. (1990). The Effect of Limestone Fillers on sulfate Resistance of High Alumina Cement Compositers. Calcium Aluminate Cements, E & FN Spon, London, 241-255.

Wu, L.H., Luo, Y.M., Christie, P., Wong, M.H. (2003). Effects of EDTA and low molecular weight organic acids on soil solution properties of a heavy metal polluted soil. Chemosphere 50, 819-822.

Xu L., Wang P., Zhang G. (2012). Formation of ettringite in Portland cement/calcium aluminate cement/calcium sulfate ternary system hydrates at lower temperatures. Constr. Build Mater.31:347-52.

Yao Z., Li J., Xie H., Yu C. (2012). Review on remediation technologies of soil contaminated by heavy metals. Procedia Environ. Sci. 16: 722– 729.

Youcai Z.,Song L., Guojian L. (2002). Chemical stabilization of MSW incinerator fly ashes, J. Hazard. Mater. B95: 47–63.

Zhang M., Reardon E.J. (2003). Removal of B, Cr, Mo, and Se from wastewater by incorporation into hydrocalumite and ettringite, Environ. Sci. Technol. 37 (13): 2947-2952.

Zhang X., Xia H., Li Z., Zhuang P., Gao B. (2010). Potential of four forage grasses in remediation of Cd and Zn contaminated soils," Bioresource Technology 101 (6): 2063-2066

Zhang X.Z., Chang W.Y., Zhang T.J. (2000). Nanostructure of calcium silicate hydrate gels in cement paste. Journal of the American Ceramic Society 83 (10): 2600–2604.

Zhu F., Takaoka M., Oshita K., Takeda N. (2009). Comparison of two types of municipal solid waste incinerator fly ashes with different alkaline reagents in washing experiments. Waste Manag. 29: 259-264.

7. APPENDIX

7.1 APPENDIX A: CHEMICAL ANALYSIS OF THE SOIL

Table A.1: *Concentrations expressed in mg/Kg s.s of the elements analysed in the contaminated soil of Bagnolo Mella via ICP-MS. Concentrations are compared with the Italian legislation limit given by the D.Lgs 152/06.*

Parameter	Concentration (mg/Kg s.s)	D.Lgs 152/06 Col. A (mg/Kg s.s)	Parameter	Concentration (mg/Kg s.s)	D.Lgs 152/06 Col. A (mg/Kg s.s)
Al	10170±1030		**Mn**	805±92	
As	383±24	20	**Mo**	4.66±0.54	
Ba	300±16		**Ni**	31.8±1.3	120
Be	0.85±0.11	2	**Pb**	40430±3210	100
Cd	2.38±0.22	2	**Sb**	41.0±3.3	10
Co	42.3±2.1	20	**Se**	362±28	3
Cr	45.2±4.1	150	**Sn**	76.3±12.9	
Cu	311±21	120	**Tl**	1.90±0.22	1
Fe	144170±15830		**V**	47.3±5.0	90
Hg	8.27±0.47	1	**Zn**	500±62	150

Table A.2: *Concentrations expressed in mg/Kg s.s of the elements analysed in the uncontaminated soil of Bagnolo Mella using an ICP-MS.*

Parameter	Concentration (mg/Kg s.s)	Parameter	Concentration (mg/Kg s.s)
Al	13700	**Mn**	3214
As	34.61	**Mo**	15.7
Ba	133	**Ni**	22.18
Be	1.86	**Pb**	247.74
Cd	0.64	**Sb**	3.94
Co	13.54	**Se**	0.88
Cr	90.9	**Sn**	3.96
Cu	76.49	**Tl**	0.86
Fe	35718.65	**V**	78.97
Hg	0.34	**Zn**	172.87

7.2 APPENDIX B: SEM IMAGES OF THE SOIL

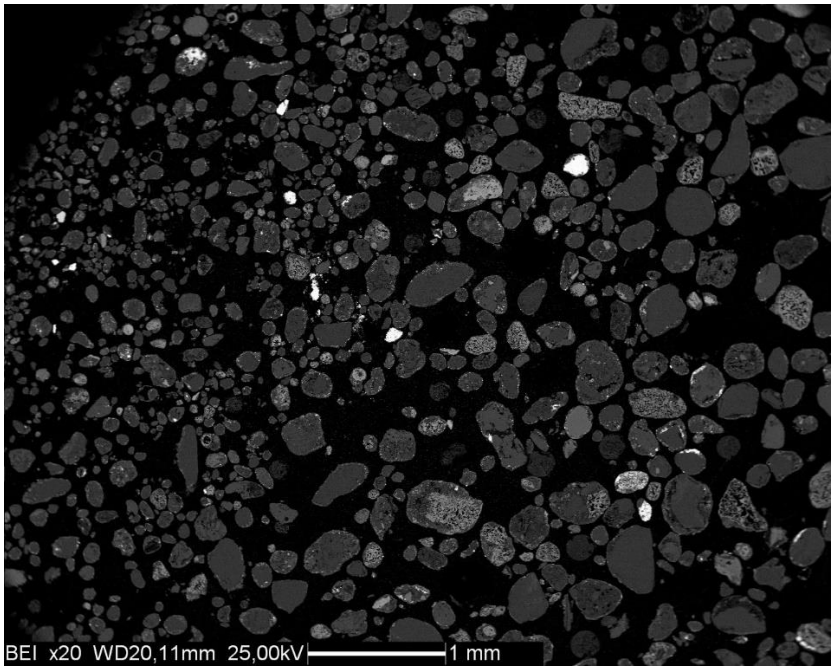

Figure B.1: *BEI-SEM image of the contaminated soil in which particle size distribution has been carried out.*

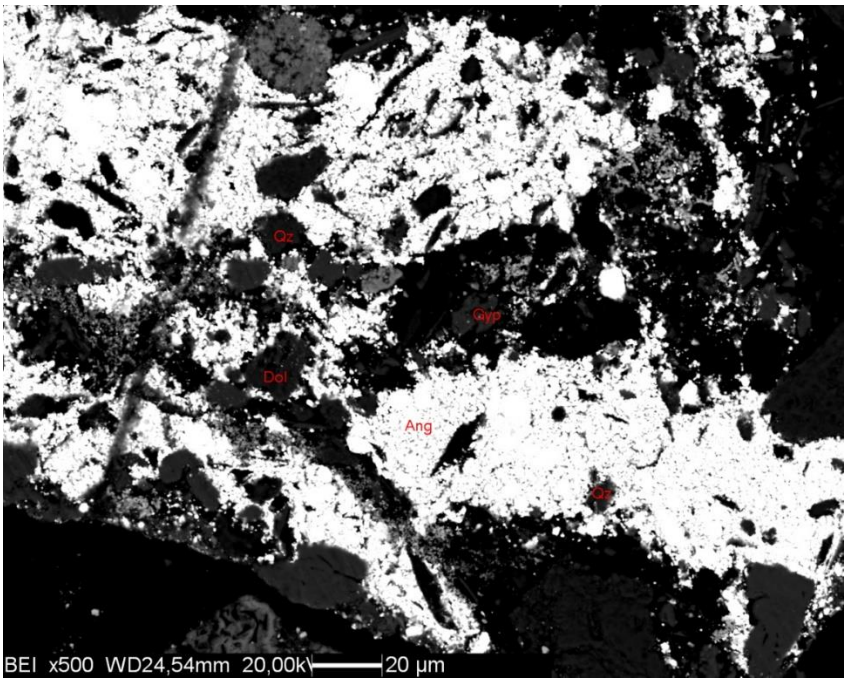

Figure B.2: *BEI-SEM image of a spot having a high presence of Anglesite.*

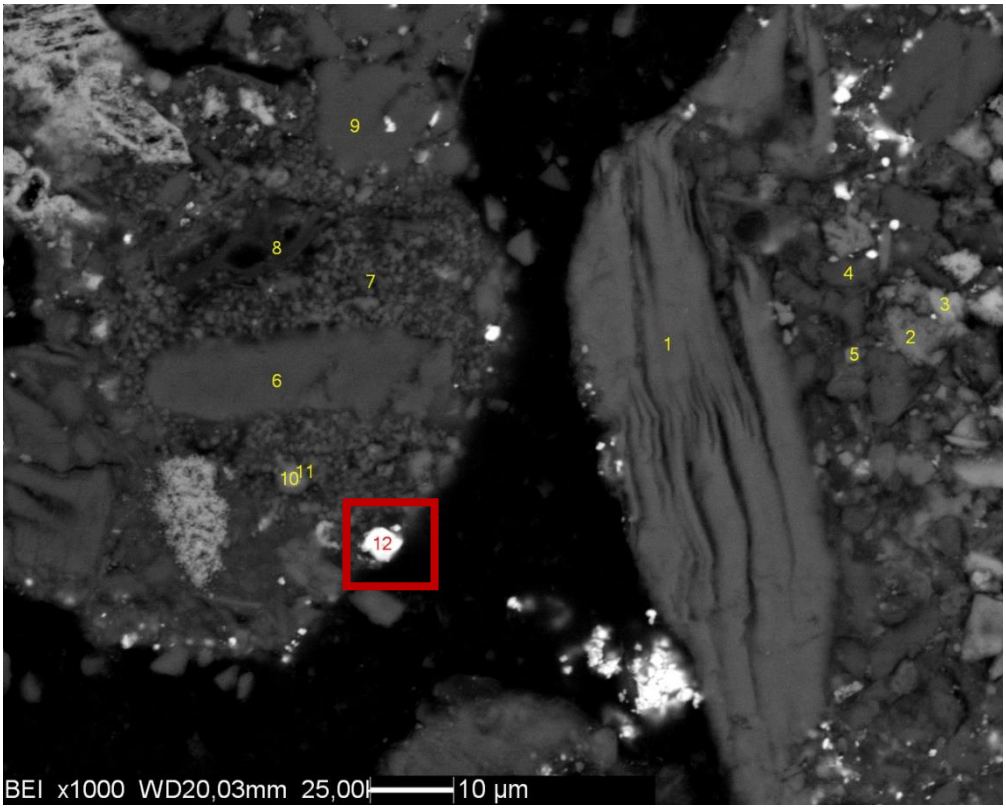

***Figure B.3**: BEI-SEM image of a portion of the contaminated soil sample*

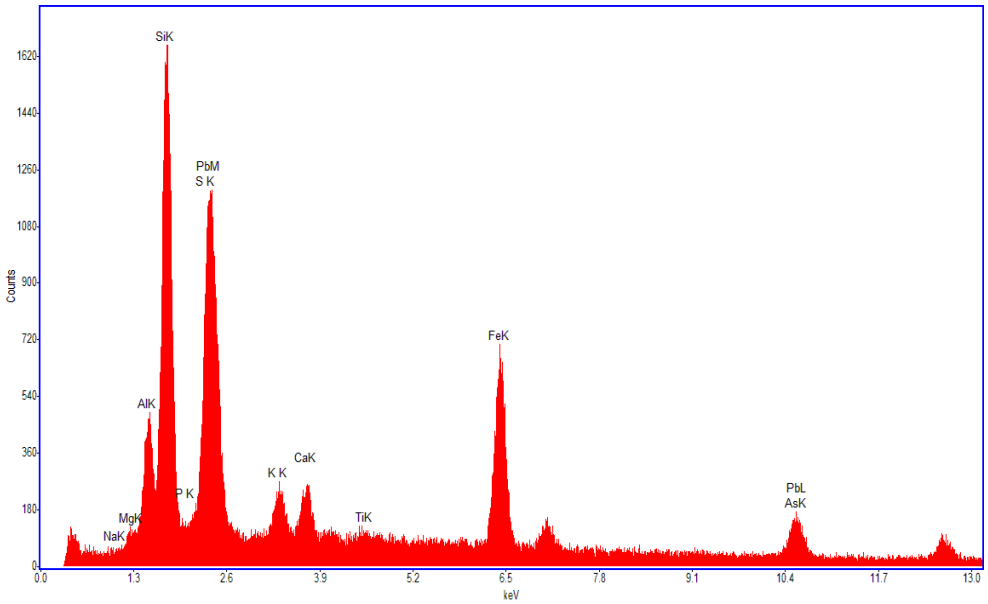

***Figure B.4:** SEM-EDX analysis realized on the particle 12 of the Fig. B.3. Presence of Pb and Fe was observed. According to the XRPD analysis the peaks are probably given by anglesite and hematite..*

7.2 APPENDIX C: XRPD ANALYSIS

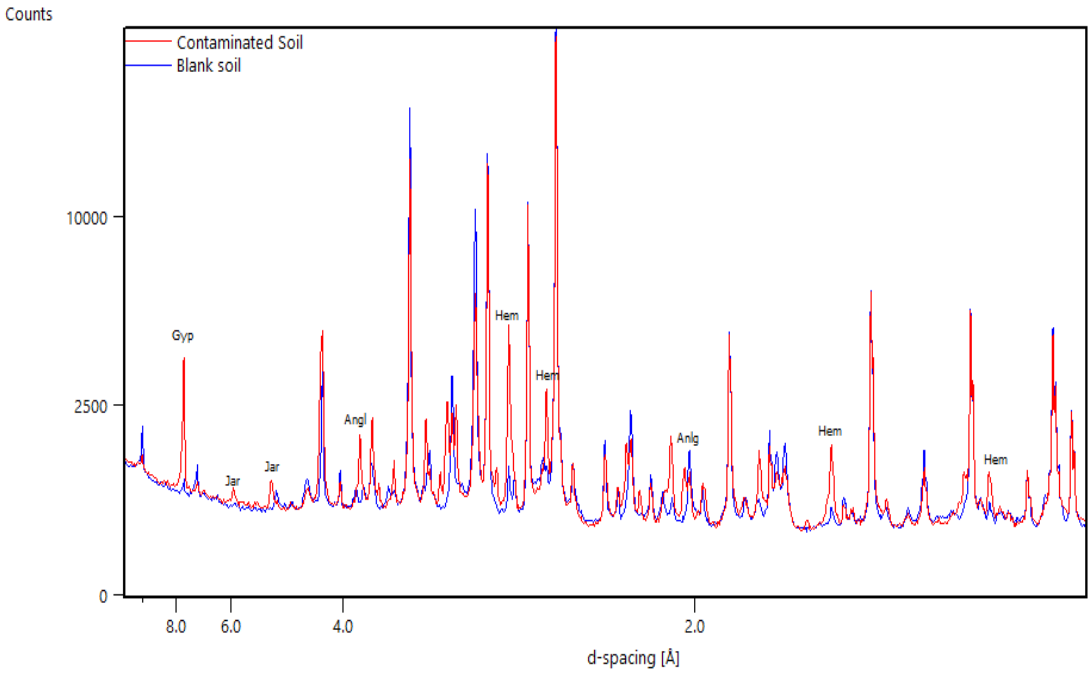

Figure C.1: *XRPD pattern of both contaminated and uncontaminated (blank) soils.*

Table C.1: *Quantification of the mineral phases in the contaminated soil.*

N	Mineral phase	Original (%)	Error (%)
1	Amorphous Content	20.72	0.52
2	Dolomite	18.99	0.10
3	Quartz	15.68	0.08
4	Hematite	12.94	0.07
5	Gypsum	8.99	0.05
6	Albite	7.72	0.04
7	Calcite	5.26	0.03
8	Jarosite	2.81	0.01
9	Anglesite	2.78	0.01
10	Muscovite	2.55	0.02
11	Clinochlore	1.57	0.01

***Table c.2**: Quantification of the mineral phases in the uncontaminated soil.*

N	Mineral phase	Original (%)	Error (%)
1	Dolomite	28.44	0.16
2	Amorphous Content	25.35	0.56
3	Quartz	19.93	0.11
4	Albite	8.584	0.048
5	Calcite	7.415	0.041
6	Clinochlore	4.459	0.025
7	Muscovite 2M-1	3.65	0.020
8	Hematite	2.119	0.012

***Table c.3**: Weight fractions (wt. %) of mineral phases in sample 4 cured at 20 °C.*

	Sample 4 Mineralogical phase	Days 7	Error %	Days 14	Error %	Days 21	Error %	Days 28	Error %	Days 35	Error %
1	**Amorphous Content + ukn**	**40.5**	**0.5**	**43.1**	**0.5**	**43.4**	**0.5**	**41.0**	**0.5**	**42.7**	**0.5**
2	**CA**	**14.9**	**0.1**	**14.1**	**0.1**	**14.3**	**0.1**	**14.5**	**0.1**	**15.3**	**0.1**
3	**CA2 Grossite**	**20.6**	**0.1**	**18.3**	**0.1**	**18.4**	**0.1**	**17.2**	**0.1**	**17.4**	**0.1**
4	**CAH10**	**12.0**	**0.1**	**13.4**	**0.1**	**12.0**	**0.1**	**9.9**	**0.1**	**7.7**	**0.0**
5	**Gibbsite**	**11.8**	**0.1**	**10.7**	**0.1**	**11.7**	**0.1**	**17.2**	**0.1**	**16.8**	**0.1**
6	Quartz	<1	0.002	<1	0.002	<1	0.002	<1	0.001	<1	0.001

***Table c.4:** Weight fractions (wt. %) of mineral phases in sample 3 cured at 20 °C.*

	Sample 3 Mineralogical phase	Days 7	Error %	Days 14	Error %	Days 21	Error %	Days 28	Error %	Days 35	Error %
1	**Afm solid solution**	**5.53**	**0.04**	**5.29**	**0.05**	**6.93**	**0.04**	**6.60**	**0.06**	**6.32**	**0.05**
2	**Amorphous Content + ukn**	**17.3**	**0.7**	**22.1**	**0.9**	**18.1**	**0.7**	**17.2**	**1.0**	**22.6**	**0.8**
3	**CA**	**13.0**	**0.1**	**11.6**	**0.1**	**12.7**	**0.1**	**15.7**	**0.1**	**14.4**	**0.1**
4	**CA2 Grossite**	**15.4**	**0.1**	**12.0**	**0.1**	**11.1**	**0.1**	**12.6**	**0.1**	**11.9**	**0.1**
5	**Ettringite**	**18.2**	**0.1**	**16.3**	**0.2**	**16.4**	**0.1**	**14.3**	**0.1**	**16.9**	**0.1**
6	**Gibbsite**	**26.1**	**0.2**	**28.5**	**0.3**	**31.3**	**0.2**	**28.9**	**0.3**	**23.0**	**0.2**
7	**Gypsum**	**4.01**	**0.03**	**3.61**	**0.03**	**3.10**	**0.02**	**4.45**	**0.04**	**4.72**	**0.04**
8	Quartz	<1	0.0	<1	0.0	<1	0.0	<1	0.0	<1	0.0

***Table c.5:** Weight fractions (wt. %) of mineral phases in sample 2 cured at 20 °C.*

N	Sample 2 Mineralogical phase	Days 7	Error %	Days 14	Error %	Days 21	Error %	Days 28	Error %	Days 35	Error %
1	Albite	4.72	0.03	4.33	0.03	4.48	0.03	4.27	0.03	4.22	0.03
2	**Amorphous Content + ukn**	**16.7**	**0.6**	**21.3**	**0.7**	**23.6**	**0.6**	**19.8**	**0.7**	**21.1**	**0.7**
3	**CA**	**2.22**	**0.01**	**2.89**	**0.02**	**2.50**	**0.02**	**1.13**	**0.01**	**1.59**	**0.01**
4	**CA2 Grossite**	**4.85**	**0.03**	**3.88**	**0.03**	**3.02**	**0.02**	**2.15**	**0.02**	**2.32**	**0.02**
5	**CAH10**	**2.31**	**0.01**	**3.80**	**0.02**	**3.21**	**0.02**	**4.71**	**0.03**	**3.61**	**0.02**
6	Calcite	11.7	0.1	12.3	0.1	11.0	0.1	11.0	0.1	11.1	0.1
7	Clinochlore	4.04	0.02	2.31	0.02	1.29	0.01	1.79	0.01	1.24	0.01
8	Dolomite	20.5	0.1	19.4	0.1	20.0	0.1	20.4	0.1	20.9	0.1
9	**Gibbsite**	**10.2**	**0.1**	**10.3**	**0.1**	**10.1**	**0.1**	**12.7**	**0.1**	**12.6**	**0.1**
10	**Hydrotalcite**	**<1**	**0.00**	**1.64**	**0.01**	**1.64**	**0.01**	**1.68**	**0.01**	**1.22**	**0.01**
11	**Monocarbonate**	**7.34**	**0.03**	**5.25**	**0.03**	**6.10**	**0.04**	**7.21**	**0.05**	**6.87**	**0.05**
12	Muscovite	1.01	0.01	<1	0.00	<1	0.00	<1	0.01	<1	0.00
13	Quartz	13.7	0.1	12.6	0.1	12.7	0.1	12.4	0.1	12.6	0.1

Table c.6: *Weight fractions (wt%) of mineral phases in sample 1 cured at 20 °C.*

N	Sample 1 Mineralogical phase	Days 7	Error %	Days 14	Error %	Days 21	Error %	Days 28	Error %	Days 35	Error %
1	Albite	2.00	0.01	1.66	0.01	1.70	0.01	2.36	0.02	2.87	0.02
2	**Amorphous Content + ukn**	**19.8**	**0.7**	**26.5**	**0.8**	**22.5**	**0.7**	**20.5**	**0.8**	**18.2**	**0.8**
3	**CA**	**4.09**	**0.03**	**3.70**	**0.03**	**3.89**	**0.03**	**4.53**	**0.04**	**4.91**	**0.04**
4	**CA2 Grossite**	**7.32**	**0.05**	**5.26**	**0.04**	**4.68**	**0.03**	**6.30**	**0.05**	**7.04**	**0.06**
5	Calcite	2.50	0.02	3.99	0.03	3.51	0.02	3.76	0.03	3.95	0.03
6	Clinochlore	<1	0.01	1.06	0.01	<1	0.01	<1	0.01	<1	0.01
7	**Dolomite**	**15.8**	**0.1**	**13.9**	**0.1**	**13.7**	**0.1**	**14.4**	**0.1**	**14.6**	**0.1**
8	**Ettringite**	**10.3**	**0.1**	**9.6**	**0.1**	**10.2**	**0.1**	**9.5**	**0.1**	**9.4**	**0.1**
9	**Gibbsite**	**12.0**	**0.1**	**11.3**	**0.1**	**18.0**	**0.1**	**13.3**	**0.1**	**11.5**	**0.1**
10	**Gypsum**	**1.72**	**0.01**	**1.45**	**0.01**	**1.38**	**0.01**	**<1**	**0.01**	**1.56**	**0.01**
11	Hematite	8.8	0.1	8.6	0.1	8.6	0.1	9.2	0.1	9.0	0.1
12	Jarosite	2.96	0.02	2.16	0.02	0.24	0.00	1.96	0.02	2.10	0.02
13	Muscovite	1.79	0.01	<1	0.01	<1	0.00	2.38	0.02	3.34	0.03
14	Quartz	10.2	0.1	9.9	0.1	10.2	0.1	10.2	0.1	10.6	0.1

Table c.7: *Weight fractions (wt. %) of mineral phases in sample 4 cured at 40 °C.*

N	*SAMPLE 4* Phase Name	14 days	Error %	21 days	Error %	28 days	Error %	35 days	Error %
1	**Amorphous Content + ukn**	**47.1**	**0.4**	**46.0**	**0.4**	**37.8**	**0.5**	**44.5**	**0.4**
2	**CA**	**11.1**	**0.1**	**11.7**	**0.1**	**15.8**	**0.1**	**11.6**	**0.1**
3	**CA2 Grossite**	**13.1**	**0.1**	**13.7**	**0.1**	**20.5**	**0.1**	**13.3**	**0.1**
4	**CAH10**	**3.73**	**0.02**	**3.05**	**0.01**	**7.57**	**0.04**	**3.26**	**0.02**
5	**Gibbsite**	**21.2**	**0.1**	**21.2**	**0.1**	**16.6**	**0.1**	**22.5**	**0.1**
6	**Hydrogarnet**	**3.43**	**0.02**	**4.01**	**0.02**	**1.56**	**0.01**	**4.74**	**0.02**
7	Quartz	<1	0	<1	0	<1	0	<1	0

Table c.8*: Weight fractions (wt. %) of mineral phases in sample 3 cured at 40 °C.*

N	*SAMPLE 3* Phase Name	14 days	Error %	21 days	Error %	28 days	Error %	35 days	Error %
1	**Afm solid solution**	**9.4**	**0.1**	**9.7**	**0.1**	**7.2**	**0.0**	**6.0**	**0.0**
2	Amorphous Content + ukn	21.9	0.8	19.4	0.9	17.5	0.6	30.7	0.7
3	**CA**	**11.1**	**0.1**	**13.5**	**0.1**	**15.9**	**0.1**	**11.3**	**0.1**
4	**CA2 Grossite**	**10.0**	**0.1**	**10.5**	**0.1**	**14.7**	**0.1**	**8.6**	**0.1**
5	**Ettringite**	**16.3**	**0.1**	**13.3**	**0.1**	**12.2**	**0.1**	**17.3**	**0.1**
6	**Gibbsite**	**28.4**	**0.2**	**29.4**	**0.3**	**26.7**	**0.0**	**24.0**	**0.2**
7	**Gypsum**	**2.57**	**0.02**	**3.72**	**0.03**	**5.67**	**0.03**	**1.95**	**0.01**
8	Quartz	<1	0	<1	0	<1	0	<1	0

***Table c.9**: Weight fractions (wt. %) of mineral phases in sample 2 cured at 40 °C*

N	*SAMPLE 2* Phase Name	14 days	Error %	21 days	Error %	28 days	Error %	35 days	Error %
1	Albite	4.60	0.03	4.18	0.02	4.14	0.02	4.33	0.02
2	Amorphous Content + ukn	21.4	0.6	23.0	0.5	21.2	0.5	20.5	0.5
3	**CA**	**1.75**	**0.01**	**1.57**	**0.01**	**2.25**	**0.01**	**1.05**	**0.01**
4	**CA2 Grossite**	**2.17**	**0.01**	**1.63**	**0.01**	**3.53**	**0.02**	**1.63**	**0.01**
5	**CAH10**	**2.15**	**0.01**	**2.65**	**0.01**	**2.40**	**0.01**	**2.44**	**0.01**
6	Calcite	10.7	0.1	10.5	0.1	11.7	0.1	11.2	0.1
7	Clinochlore	3.30	0.02	1.45	0.01	0.76	0.00	1.74	0.01
8	Dolomite	20.7	0.1	20.4	0.1	20.2	0.1	21.1	0.1
9	**Gibbsite**	**12.2**	**0.1**	**11.6**	**0.1**	**11.5**	**0.1**	**13.4**	**0.1**
10	**Hydrotalcite**	**2.414**	**0.013**	**<1**	**0**	**<1**	**0**	**<1**	**0**
11	**Monocarbonate**	**5.69**	**0.03**	**8.69**	**0.04**	**7.56**	**0.04**	**8.79**	**0.04**
12	Muscovite	<1	0	<1	0	1.07	0.01	<1	0
13	Quartz	12.3	0.1	12.8	0.1	13.1	0.1	12.6	0.1

***Table c.10**: Weight fractions (wt. %) of mineral phases in sample 1 cured at 40 °C.*

N	*SAMPLE 1* Phase Name	14 days	Error %	21 days	Error %	28 days	Error %	35 days	Error %
1	Albite	2.28	0.02	2.03	0.02	2.35	0.02	2.32	0.02
2	Amorphous Content + ukn	20.6	0.8	25.9	0.7	21.3	0.7	20.5	0.8
3	**CA**	**3.74**	**0.03**	**4.09**	**0.03**	**4.56**	**0.03**	**4.79**	**0.03**
4	**CA2 Grossite**	**5.14**	**0.04**	**4.96**	**0.04**	**6.11**	**0.04**	**6.01**	**0.04**
5	Calcite	4.14	0.03	3.43	0.03	3.65	0.03	3.97	0.03
6	Clinochlore	<1	0	<1	0	<1	0	<1	0
7	**Dolomite**	**14.6**	**0.1**	**13.7**	**0.1**	**14.3**	**0.1**	**14.7**	**0.1**
8	**Ettringite**	**10.4**	**0.1**	**8.9**	**0.1**	**10.3**	**0.1**	**10.6**	**0.1**
9	**Gibbsite**	**16.2**	**0.1**	**13.9**	**0.1**	**13.4**	**0.1**	**13.4**	**0.1**
10	**Gypsum**	**1.78**	**0.01**	**1.25**	**0.01**	**1.62**	**0.01**	**1.37**	**0.01**
11	Hematite	8.6	0.1	8.8	0.1	9.3	0.1	8.8	0.1
12	Jarosite	<1	0	1.35	0.01	1.29	0.01	1.46	0.01
13	Muscovite	<1	0	<1	0	1.06	0.01	1.00	0.01
14	Quartz	10.1	0.1	9.9	0.1	10.1	0.1	10.2	0.1